AN ABSTRACT OF THE THESIS OF

Ghawamedin Bayan for the degree of Doctor of Philosophy

in Chemical Engineering presented on July 11, 1980

Title: MASS TRANSFER IN A MULTIPLE STAGE CROSSCURRENT PACKED COLUMN

Abstract approved: Redacted for Privacy

Dr. Charles E. Wicks

A cascade crosscurrent column, packed with Pall rings, was employed for ammonia absorption from ammonia-rich air phase by contacting with water. Absorption efficiency was presented as the percentage of NH_3 removed as well as the volume of a transfer unit.

A review of the literature concerning the theoretical and experimental investigation of mass transfer in the crossflow columns was presented.

Information extracted from the tracer studies along with the mass transfer results confirmed the existence of two distinct regions; the transition between the two regions could be visually observed in the column.

A decrease in the absorption efficiency was observed due to the expansion of the packing section. Upon reduction in the number of baffles, the absorption efficiency decreased further. It was also concluded that the mixing activities in the packing and on the baffles after the transition compensated for the loss of efficiency due to the dead space, created by the criss-crossing of the liquid.

Based on the experimental results and visual observations in the crosscurrent column, the bypass model for the region prior to the transition and the zero bypass model for the region after the transition were proposed. The models were successful in predicting the experimental data.

Correlations were developed that adequately predicted the percentage bypass in the column, with original packing, expanded packing and expanded packing with six baffles, for the operating conditions investigated in this work.

Favorable pressure drop results, obtained by other investigators, combined with the results of this work suggested the cascade crosscurrent packed column to be an attractive alternative to the conventional towers for the ammonia-air-water system.

Mass Transfer in a Multiple Stage Crosscurrent Packed Column

by

Ghawamedin Bayan

A THESIS

submitted to

Oregon State University

in partial fulfillment of
the requirements for the
degree of

Doctor of Philosophy

Completed July 1980

Commencement June 1981

APPROVED:

Redacted for Privacy

Head of Department of Chemical Engineering and Professor in charge of major

Redacted for Privacy

Dean of Graduate School

Date thesis is presented July 11, 1980

Typed by Cheryl E. Curb for Ghawamedin Bayan

ACKNOWLEDGEMENTS

I wish to express my sincere appreciation to Dr. Charles E. Wicks, my major advisor, for his invaluable advice, constructive criticisms and continual encouragement during the course of this study.

I would like to thank Dr. Thomas Fitzgerald for his guidance and advice in conducting the tracer studies, and Dr. Robert Mrazek for his helpful suggestions and for his "picking a G."

Many thanks are due to the Chemical Engineering Department of Oregon State University, Dr. Charles E. Wicks, Head, for financial support in the form of a Graduate Teaching Assistantship and also for use of its facilities. The financial support and services of the Oregon State Computer Center, which enabled me to accomplish the numerical analysis of this work, is acknowledged.

I am deeply grateful to the faculty members and staff of the Chemical Engineering Department who have assisted me in this work.

I would also like to acknowledge my gratitude to a number of friends. In particular, Mrs. Vi Campbell for her help and occasional arguments, and Larry Lahm for his suggestions in accomplishing the least square fit analysis.

Finally, I wish to thank my wife, Terri, and my family for whom I have a great deal of love, for their understanding and constant moral support.

TABLE OF CONTENTS

LIST OF FIGURES

LIST OF FIGURES (Cont.)

LIST OF FIGURES (Cont.)

LIST OF TABLES

LIST OF TABLES (Cont.)

MASS TRANSFER IN A MULTIPLE STAGE CROSSCURRENT PACKED COLUMN

I. INTRODUCTION

The occurrence of mass transfer between a gas and liquid is of fundamental importance in a variety of industrial operations and research activities. One of the greatest area of concentration in this diffusional field is gas absorption. In gas absorption a soluble vapor is absorbed from its mixture with an inert gas into a liquid in which the solute gas is more or less soluble. The absorption of ammonia from a mixture of ammonia and air by means of liquid water is a typical example. Sometimes a solute is removed from a liquid by bringing the liquid into contact with an inert gas; such an operation, the reverse of gas absorption, is called desorption or gas stripping. The removal of pollutants from plant discharge streams by absorption and the stripping of gases from wastewater are two applications of this diffusional process. Due to growing environmental concerns the gas absorption has become more important in recent years.

A common apparatus used in gas absorption, and also in certain other operations, is the packed tower. Generally, three different flow patterns are used for gas-liquid contact operations: countercurrent, cocurrent and crosscurrent flow.

The vast majority of commercial packed columns are operated countercurrently. The liquid phase falls downward due to gravity, while the gas phase moves upward through the column by an imposed pressure gradient. The gas throughput in this type of operation is limited. Above a critical gas velocity the drag forces imposed on the liquid by the upflowing gas exceed the gravity forces and create an unstable, undesirable condition known as flooding.

One means of overcoming this throughput limitation of countercurrent operation is to operate the packed column cocurrently. In this operation the gas and liquid are introduced at the top of the column and flow cocurrently downward through the column due to a combination of gravity and applied pressure gradient. There is no flooding limit in this type of operation. However, from a mass transfer standpoint, cocurrent operation has a definite limitation relative to countercurrent operation. The overall concentration driving force and the number of equilibrium stages in cocurrent columns are smaller than in countercurrent column. This means it would take a much larger cocurrent column to do a certain mass transfer job than it would take with a countercurrent unit.

An alternative to the two conventional packed towers is the crosscurrent tower. This device is essentially operated on the countercurrent basis except the fact that the two existing phases, namely liquid and gas, flow perpendicular to each other. The crossflow columns enjoy the low pressure drop characteristic of cocurrent columns as well as the high mass transfer efficiency of countercurrent towers. The crossflow column also has a concentration driving force profile between that of the cocurrent and countercurrent towers. In such an operation, since the gas and liquid flow at right angles to each other, the concentrations of solute in both phases change in the direction of flow of the gas and liquid. Therefore, the mechanism of mass transfer in this equipment is considerably more complicated than that in countercurrent and cocurrent-flow devices. One of the unique features of the crosscurrent cascade is that it displays some of the fluid dynamic

characteristics of tray towers. At high gas rates, liquid accumulates on the baffles which make the withdrawal of samples very convenient. Vigorous mixing in the packing section as well as the bubbling activity on the baffles add up to the efficiency of this column. A cascade crosscurrent column can be visualized as a series of single-stage crossflow units interconnected to each other. Each packing section between the two baffles resembles a single-stage unit. The uniqueness of this cascade is due to having the option of adjusting the baffle spacing which would give the designer an additional design parameter. Due to the reasons mentioned above, the crosscurrent column can be considered an attractive alternative gas-liquid contactor.

Scientific research and technical literature has brought up to date the various activities related to gas absorption in the crossflow columns. These activities are presented in the literature survey section of this work.

The objective of this study is to thoroughly investigate the various parameters existing in the crosscurrent column and obtain an adequate understanding of the problem of mass transfer in this type of apparatus by taking pertinent experimental data. The final goal is to develop a conceptual model and correlations that would best describe the crosscurrent contactor and test the model against the experimental results.

II. LITERATURE SURVEY

Despite the importance of study of the multi-stage crossflow tower, reports on mass transfer problems in such units have scarcely been published. Available literature deals mostly with heat and mass transfer in cocurrent and countercurrent packed columns. For crossflow type, however, not enough attention has been centralized to understand the mass transfer phenomena in this industrially attractive piece of equipment.

Single-stage crossflow gas-liquid contactors have likely had their first application in water cooling (1). Theoretical and experimental analyses of crossflow cooling towers were performed on single-stage columns (2). Pittaway and Thibodeaux (3) used a single-stage crossflow packed tower to study the rate of oxygen desorption. These investigators showed that the device gave higher throughput rates and lower pressure drop than the conventional countercurrent flow device. Experimental runs were performed using 1/2-inch ceramic Rasching rings and correlations were developed to predict the liquid phase mass transfer coefficients as well as liquid holdup and angle of liquid deflection. Oza (4) studied the fluid dynamics of a single-stage crosscurrent packed tower. He developed an empirical correlation to predict the drift angle. The plots of predicted drift angle showed that the drift angle increased with increasing gas rate and either increased or decreased with increasing liquid rate.

The crossflow columns have also been employed in scrubbing particulates from air with gas absorption as a parallel benefit. Hanf (5)

presented a drawing of a crosscurrent packed scrubber. He found the crossflow column to yield lower pressure drop, compared to a countercurrent unit, when using the same gas and liquid mass flow rates. HEW Bulletin (6) described the crossflow column as a scrubber which operates with very low pressure drop and water requirements, both of which were about 40 percent of that required for the conventional countercurrent operation. Pittaway (7) reported that a single crossflow stage could be operated at loading conditions which would cause flooding in the conventional operation.

Thibodeaux (8) listed some advantages of the crossflow towers compared to countercurrent towers. He presented a trial and error procedure, suitable for use with digital computers, for calculating the approximate concentrations from such a tower if the inlet concentrations and H_{OG}, the overall height of a gas-phase transfer unit, were known. Wnek and Snow (9) presented a practical design method for the single-stage crossflow considering two applcations: cooling tower, and ammonia stripping with simultaneous cooling. They observed that the temperature change of the liquid across the width of the tower is small in comparison to that across its height. Roesler, Smith and Eilers (10) have developed a digital computer program for design of ammonia stripping and cooling towers for the single-stage crosscurrent configuration. Their numerical calculations were similar to the scheme described by Thibodeaux (8) and Baker and Shryock (11). Inazumi and Kageyama (12) presented a graphical technique to solve the heat and mass transfer related to the crossflow columns used in air-water operations of water-cooling, air humidification or dehumidification. Sherwood,

Pigford and Wilke (13) demonstrated the use of a ical technique for mass transfer design based upon the results of cow heat exchanger calculations. Their technique involved the use orrection factor to account for the crossflow conditions. Hayashi et al. (14) obtained experimental data of the concentration distribut;ide a wetted wall crossflow tower and a rod-like irrigation crossfwer packed with 3/4 inch Rasching rings. The experimental data wtained by absorbing ammonia from air into water. The authorsnted a numerical method based on the Zivi-Brand method and an anal solution based on the Nusselt solution of heat exchangers. Howeot enough experimental data were collected to conclusively verifyrossflow models and the proposed design procedures. Hayashi and (15) also conducted experiments on the absorption of carbon(diand ammonia in water with a similar column described above and ri values of mass transfer coefficients. Thibodeaux et al. (16) us concept of numbers of transfer units and volume of transfer uninique to study the efficiency of the crossflow column. Plots weloped to help design the column. They found that the efficiencie single-stage device to be intermediate between countercurrent current columns. They showed that as the number of stages increase efficiency approached to the countercurrent unit.

Gray et al. (17) constructed and obtained data cascade crosscurrent packed tower. This was considered tmultistage packed tower with gas flow directed across the towuse of baffles. Fluid dynamics were investigated and pressure drowere obtained.

Thibodeaux (18) and Golshani (19) collected extensive pressure drop data for a cascade crossflow column. Visual observations of the flow patterns were made and liquid hold-up data were collected. They both showed that the crossflow column could be operated at conditions which exceeded those possible in the conventional countercurrent units. They observed significantly lower pressure drop with the cascade crossflow. Thibodeaux raised the question of mass transfer efficiency which was not well understood in the column. Vigorous mixing as well as irrigated section of packing were observed. However, mass transfer data and a model to describe the behavior of the column were lacking. Zuehlsdorff (20) collected mass transfer data using the multistage packed column. He studied the overall mass transfer efficiency experimentally for three baffle arrangements and for the countercurrent column as well. He found the crosscurrent tower to be comparable to and at some conditions more efficient than the conventional countercurrent packed column in absorbing ammonia from air into water. He concluded that the crosscurrent column could process significantly higher flow rates with the same or better pressure drop and absorption efficiency than an equivalent packed volume in a countercurrent unit. Although his work was very informative in understanding the mass transfer efficiency in the cascade crossflow column, but the investigation was not thorough enough to establish the behavior of the column.

No one has yet tried to model the crossflow column and check the model against a set of experimental runs. The baffle spacing, liquid and gas flow rates, types of packing, bubbling action on the baffles as

well as the dry zones existing in the packing section right underneath each baffle have considerable effect on the overall mass transfer efficiency of the multistage crossflow column.

Thibodeaux (18) pointed out in his paper the fact that certain of the "open" plastic shapes, such as Tellerettes and Pall rings were more adaptable to crossflow than to countercurrent contacting. No mass transfer coefficients were available for the air-ammonia-water system using Pall rings as the packing material.

Leva (21) and Treybal (22) provided useful information in the form of discussions of packing characteristics and packed towers. Perry's Handbook (23) provided information on Henry's law constant and the gas-phase mass transfer coefficients.

III. EXPERIMENTAL EQUIPMENT AND PROCEDURE FOR ABSORPTION STUDY

The main pieces of equipment employed in this work were the multistage crossflow packed column along with the tracer equipment. Each equipment will be described separately in the following sections.

A. The Crosscurrent Packed Column

A diagram of the column is presented in Figure 1. The practical range of conditions and the operating procedures for this equipment are given by Zuehlsdorff (20). Briefly the column which is in the shape of a rectangular box was constructed of 0.5 inch plexiglass and metal, and was held together with screws. The joints were sealed with "Silicone Seal." In this device a central packed core was positioned in the column, held by screens from the sides and top and bottom. Several baffles were placed at regular intervals on the opposite sides of the central packed section and attached to the side walls. These baffles were used as gas deflectors. This internal arrangement of the column caused the liquid to move in a zig-zag manner through the packing.

The column was constructed of 13 mm clear plexiglass and had dimensions of 2.44 m (96 in) in height, 254 mm (10 in) in width and 127 mm (5 in) in depth. The side walls, with the dimensions of 127 mm by 2.44 m, were easily removable in order to change the baffle spacing. To facilitate the change of packing material, two 127 mm square access ports were placed immediately above and below the packed section. The top section of the column (508 mm) remained void to serve as a water droplet deentrainer where the bottom section (381 mm) of the column, which also remained void, was used as a liquid accumulator.

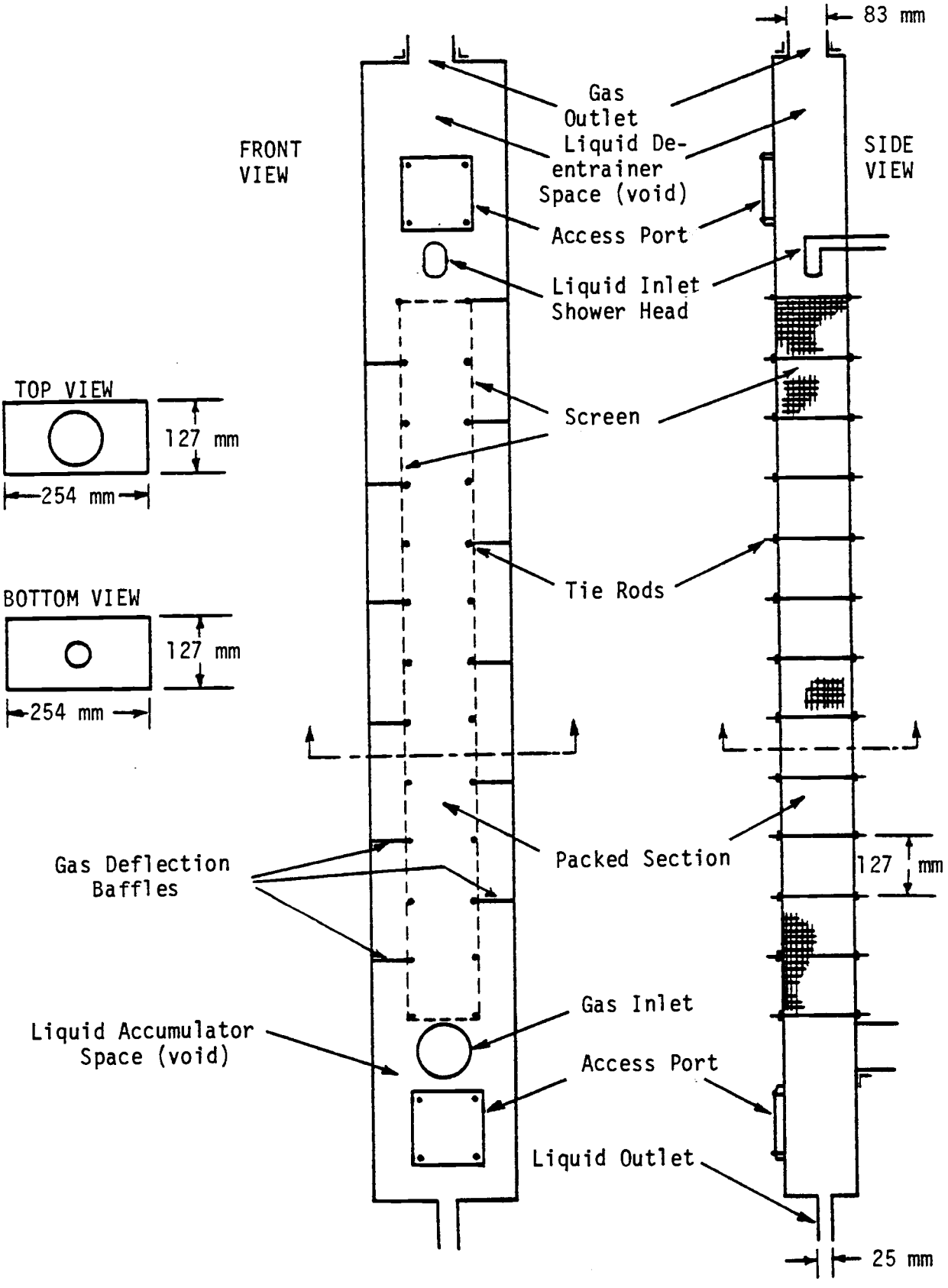

Figure 1. Multiple stage crosscurrent packed column.

The central packed section, with the dimensions of 127 mm by 127 mm cross section and 1.52 m (60 in) in height, was surrounded by plexiglass on two sides and screened on the other two sides and top and bottom. The screen, with the projected open area of 74 percent, was made of 0.88 mm stainless steel wire woven into a 6.35 mm (1/4 in) square mesh. Steel tie-rods, with the dimensions of 178 mm in length and 3 mm in diameter (7 in by 1/8 in), were used to support the packed section. These rods were placed at 127 mm intervals along the walls and wired to the screen. The packing material used for this study was 16 mm (5/8 in) polyethylene pall rings with 87 percent porosity.

Two different sizes of deflection baffles were made of 3 mm thick stainless steel plates. Baffles, having the dimensions of 127 mm by 64 mm, were used where the cross sectional area of the packed section was 127 mm by 127 mm. The baffles with dimensions of 127 mm by 51 mm were employed with the packing cross sectional area of 127 mm by 152 mm. Since the column dimensions were kept unchanged, the baffles has to be sized down in order to study the effect of packing expansion on the mass transfer. The baffles were gasketed with rubber to prevent any air and water bypass from the side walls. The baffles were attached to the side walls by two 64 mm long, 3 mm diameter rods which were tack-welded to the back of each baffle. These rods were, in turn, inserted into 6 mm deep holes on the side walls. Only two different baffle arrangements were used in this study (6 and 12 baffles).

Figure 2 shows a schematic diagram of the equipment arrangement. The gas phase was a mixture of air and ammonia, and water was employed as the liquid phase.

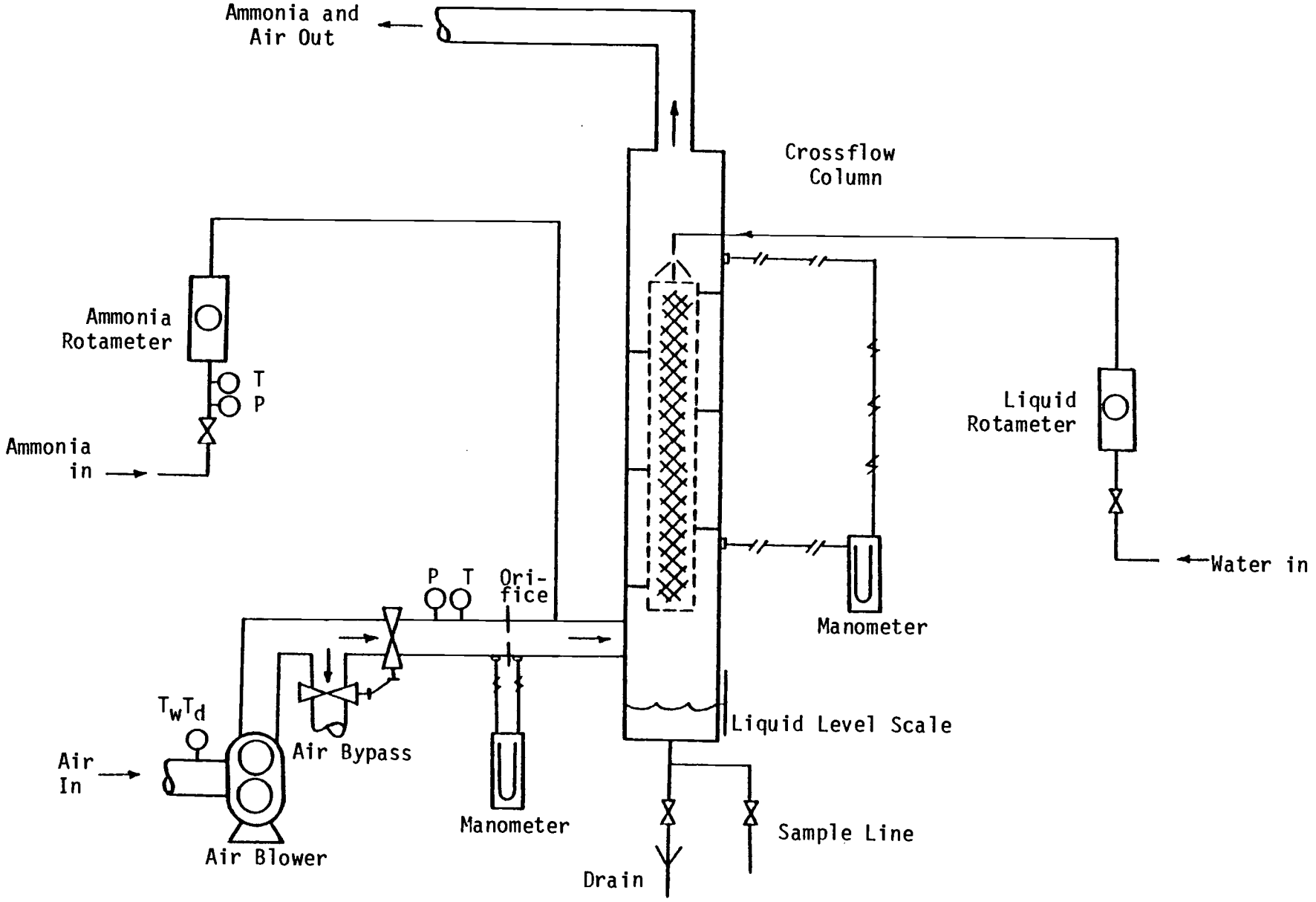

Figure 2. Schematic of Equipment Arrangement.

A Sutorbilt Horizontal California Series B positive displacement blower was used to pump the air to the system through an 83 mm inside diameter (3-1/4 in ID) PVC plastic pipe which was rated at 860 k Pa. The air flow rate was controlled by a bypass and a two-valve system located about 2.4 m upstream from the column. For safety purposes, the two vales were connected with a bar to eliminate the possibility of closing the two valves at the same time. Sharp-edged orifices (0.63 inch, 1.0 inch or 2.0 inch) were used to measure the air flow rates. These orifices were made for the appropriate flow range and installed with radius pressure taps according to ASME standards (24). Calibration of the orifices was performed using a Meriam Laminar Flow Meter, Model 50MC2-4F, along with a Meriam micromanometer. Pressure drop across the orifice as well as upstream pressure were measured by water manometers. A mercury thermometer was placed in the air pathway to measure the incoming air temperature.

The liquid, entering from the top of the column, was city water; its flow rate was measured by rotameters. Depending upon the flow rate desired, two different rotameters were used to supply a combined range of 82 to 8097 kilograms of water per second. The liquid flow meters were calibrated by the simple bucket and stopwatch method. That is, the flow through the meters was collected for a measured amount of time and a calibration chart was developed. The water was carried to the system through a galvanized 25 mm (1 in) Schedule 40 pipe. A plastic shower head distributed the water uniformly over the top of the packing.

Pressure taps and water manometers were used to obtain the pressure drop in the tower as well as the orifice pressure readings. The pressure taps were positioned in the column to account for 1.27 m (50 in) of packing height.

Figure 3 shows the scheme with which the manometers were used to measure the desired pressure readings for the experiment as well as necessary valve operations.

The anhydrous ammonia was supplied from a 68-kg capacity liquid storage tank and delivered through a stainless steel regulator as a gas. The ammonia flow rate was measured by a Gilmont Model F1500 rotameter. The calibration chart, supplied by the factory, was for air and water. A calibration chart for ammonia was developed by using the correlations provided by the factory. Pressure and temperture of the ammonia were measured just before the gas entered the rotameter by means of a mercury manometer and a metal thermometer, respectively. In order to prevent corrosion problems caused by ammonia, plastic tubing and nylon Swage locks were used to carry ammonia to the system. The ammonia was introduced to the gas stream about 1/3 meter before the mixed gas entered the column.

1. Test Conditions. All of the tests for this study have been conducted within the following range of conditions:

Molar liquid-to-gas ratio = 1.5, 2.0, 3.0 or 4.0

$$\frac{(\text{moles/min})}{(\text{moles/min})}$$

Gas flow rate = 72 kgmole/m^2 hr (14.76 lbmole/ft^2 hr) to

210.92 kgmole/m^2 hr (43.2 lbmole/ft^2 hr)

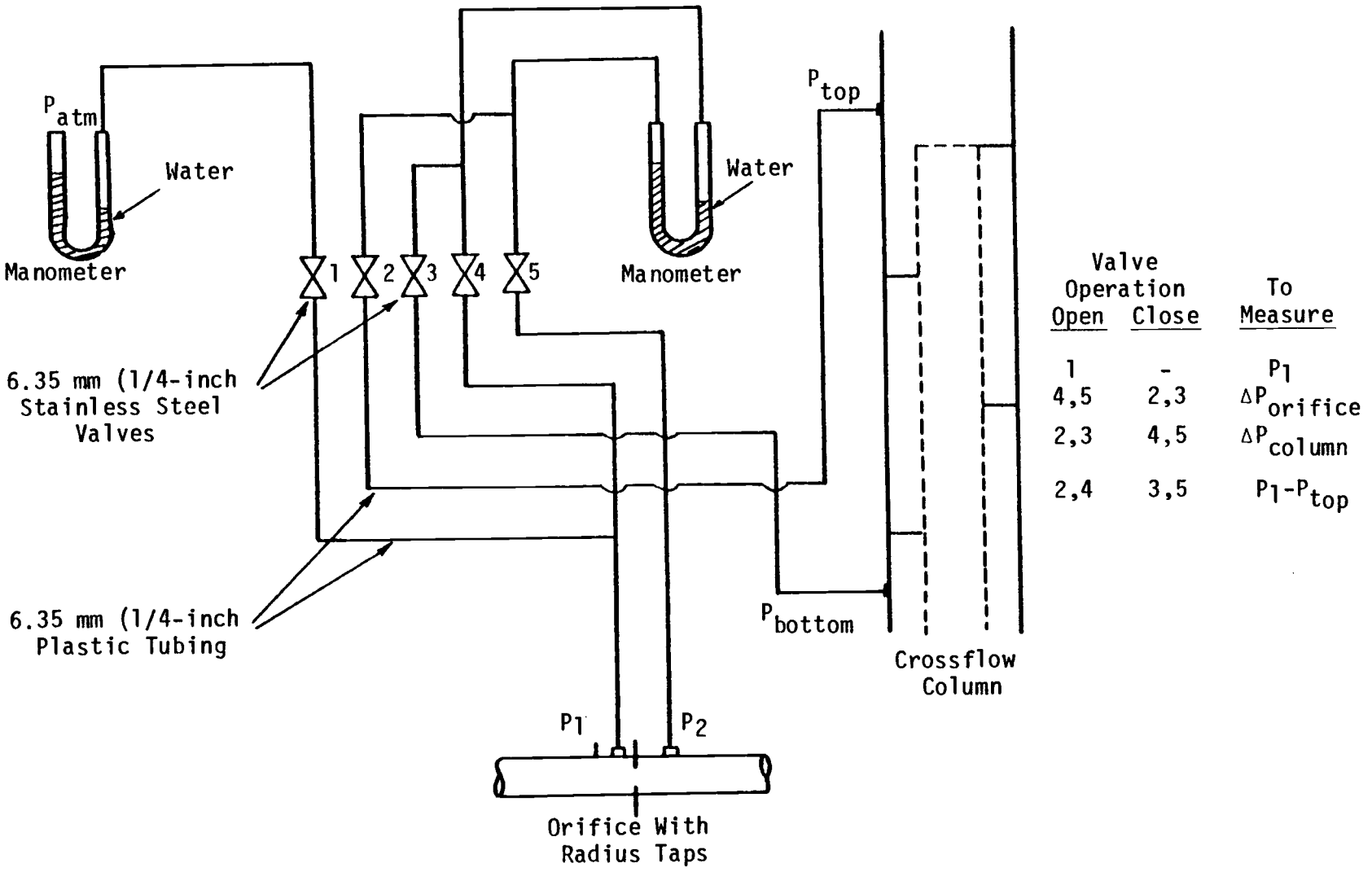

Figure 3. Schematic of Manometer System.

Liquid flow rate = 108.1 kgmole/m^2 hr (22.14 lbmole/ft^2 hr) to 843.68 kgmole/m^2 hr (172.8 lbmole/ft^2 hr).

2. Measurement of Concentration. The concentration of ammonia leaving in the liquid stream was measured by the titration method. Sulfuric acid was used to stop the reaction and sodium hydroxide was used to back titrate the unreacted acid in the solution. Bromocresol green was used as an indicator. Complete titration procedure is given by Zuehlsdorff (20).

B. Tracer Equipment

The tracer equipment consisted of a conductivity probe which was constructed in the Department of Chemical Engineering, a DC power supply (model 950) and a Hewlett Packard recorder model No. 7402A (serial No. 1421A01105). The necessary materials for construction of the probe and the platinizing process (will be described in later sections) were obtained from the Chemical Engineering Department and the Chemistry Stockroom at Oregon State University.

1. Probe Construction. A simple probe was designed and constructed for measuring the conductivity at a point; this probe, as shown in Figure 4, consisted of a 6.35 mm glass tube, two 0.508 mm platinum wire and teflon insulated wires. All exposed platinum wires were platinized in a standard platinizing solution until the surface of the platinum wire formed a cage around the point electrode. This wire shielded the point electrode so that voltage disturbances, such as batteries, are minimized.

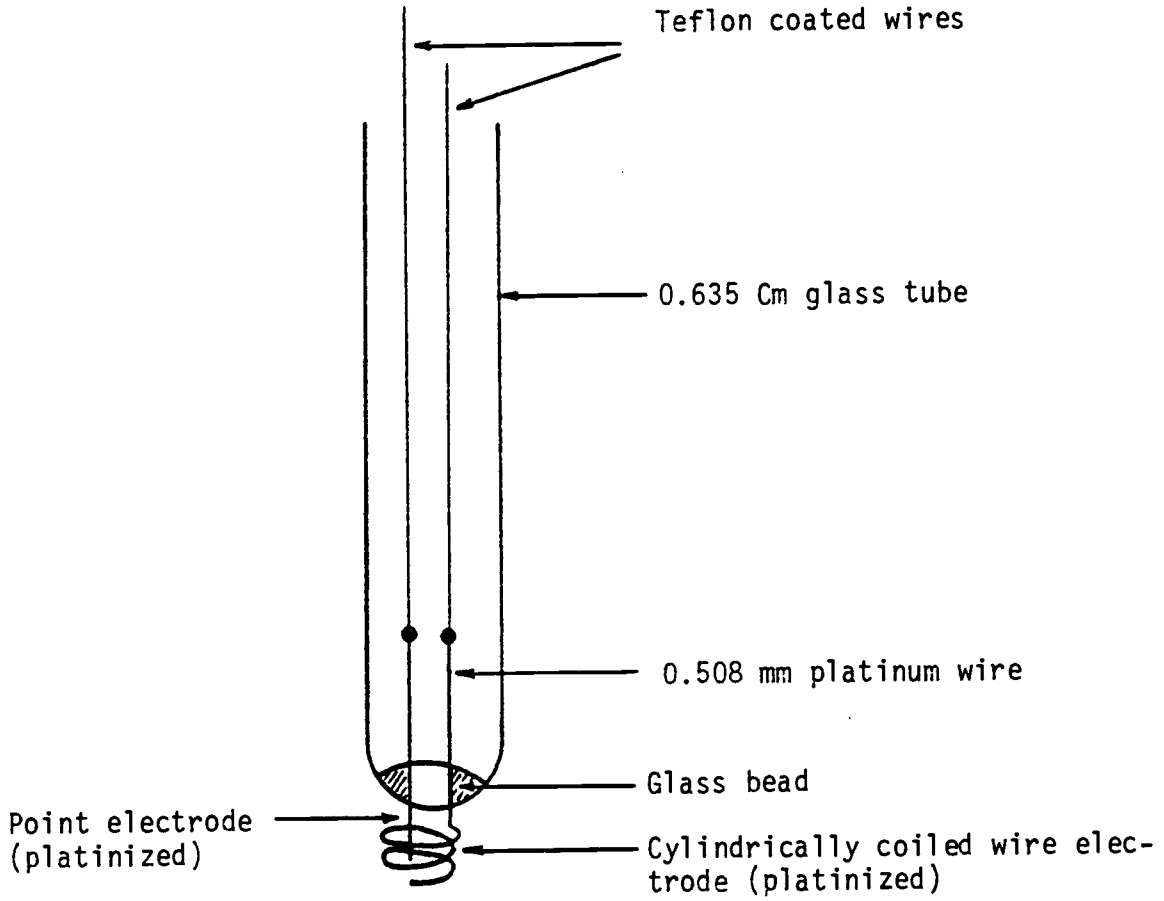

Figure 4. Structure of the Conductivity Probe.

2. Platinizing Process. As described in the previous section, the platinum wires used in the conductivity probe were platinized. The platinization process reduces polarization on the surface of electrode as well as reduction of the electrode-electrolyte impedance to very low value and thus assumes a better probe performance.

The conductivity probe used in this experiment measured the potential difference when ions were transformed through the water flowing in the column. This voltage difference is directly related to the concentration of the potassium chloride which was used as the tracer in this study.

The platinum wires used in the conductivity probe were platinized in the standard solution referred by Khang (25). This solution was found (26, 27) to consist of:

0.025 N HCl

3% (10% solution) platinum chloride

0.025% lead acetate

Lead acetate was added to the solution in small quantities to obtain a uniform coating of platinum black on the wires. Failure to include the lead acetate resulted in a strong deposit having a velvety black appearance (26). Experimental setup for the platinizing process is shown in Figure 5.

The electrode was first cleaned thoroughly and placed in the standard solution mentioned above. A direct current is passed through the solution via a large area platinum anode; the electrode, acting as the cathode, was blackened during the process.

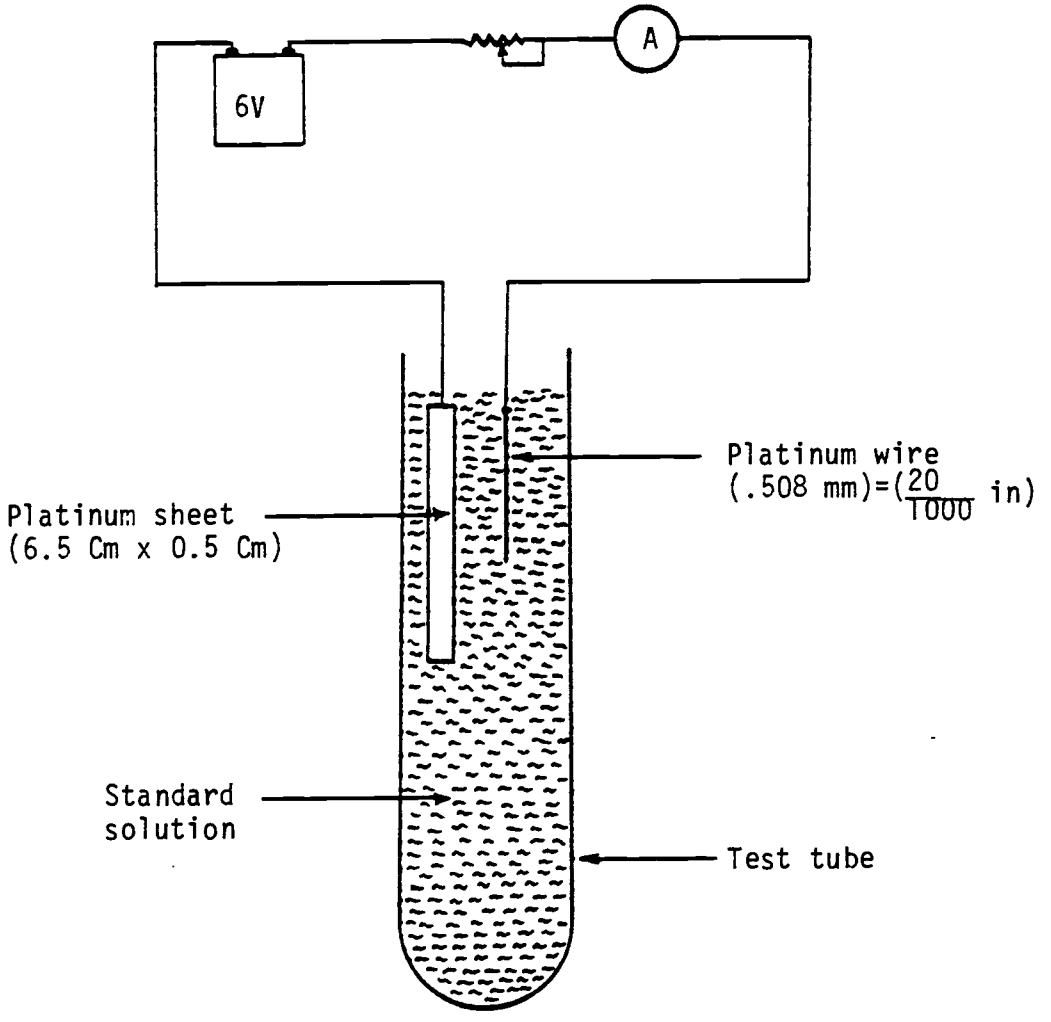

Figure 5. Experimental Setup for the Platinization Process.

3. Circuitry Set up for the Tracer Equipment. The conductivity probe was placed in the column and was connected to the strip chart as shown in Figure 6. Potassium chloride solution (10 gm KCl in 2000 cc H_2O) was used as the tracer material. Every time 20 cc of this solution was injected by a hypodermic syringe. The resistance R shown in the diagram is equivalent to the resistance offered by the KCl solution. This resistance was measured separately by an ohmeter.

C. Working Equations to Calculate Flow Rates

A theoretical development of the equations necessary to calculate the flow rates and desired concentrations were presented thoroughly by Zuehlsdorff (20). A summary of the equations is presented here.

1. Entering Air Flow Rate. As mentioned in the previous section, a sharp-edged orifice was employed to measure the inlet gas flow rate. The pressure drop across the orifice for a compressible gas is related to the gas flow rate

$$W = YKA_2\sqrt{2(P_1-P_2)\rho_1} \qquad (1)$$

where: A_2 = cross sectional area of the orifice opening

Y = expansion factor

$K = \frac{C}{\sqrt{1-\beta^4}}$, orifice coefficient

β = ratio of orifice diameter to pipe diameter

P_1, P_2 = pressures upstream and downstream from the orifice, respectively

ρ_1 = density of the ambient air at the upstream conditions.

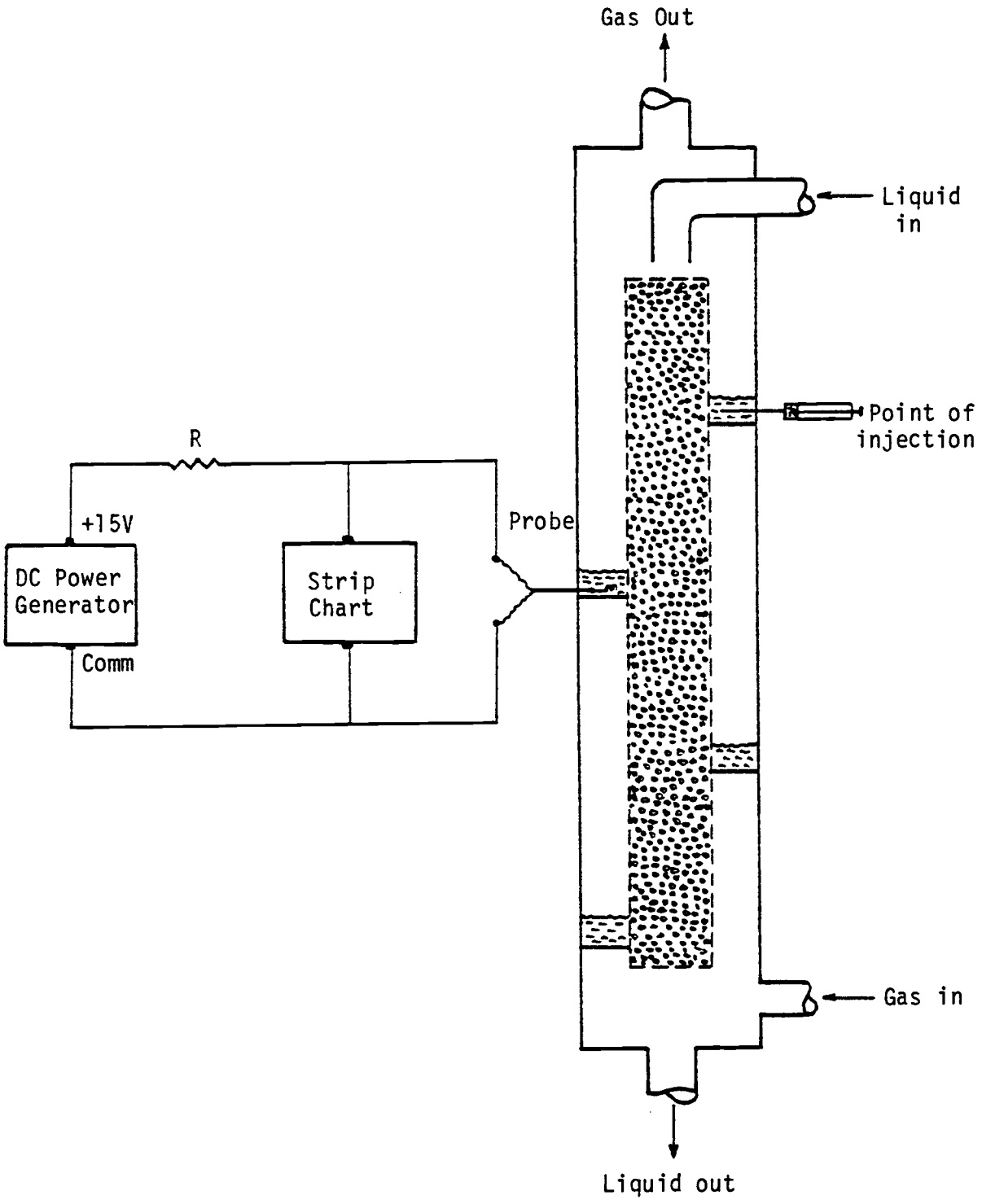

Figure 6. Circuitry Setup for the Tracer Experiment.

For the orifice dimensions and existing conditions in the system, the molar flow rate of incoming air can be obtained from the following equation.

$$\dot{m}_{air} = K_1\left[1.0-K_2\frac{\Delta P}{P_1}\right]\sqrt{\frac{P_1\Delta P}{\bar{M}\,T_1}} \qquad (2)$$

where:

$\dot{m}$ = molar flow rate, gmole/sec

P_1 = upstream pressure, Pa

ΔP = orifice pressure drop, Pa

T_1 = orifice upstream temperature, ^{o}K

$\bar{M} = \frac{28.97 + 18.01(1.609\ Z)}{1.0 + 1.609\ Z}$, average molecular weight of the gas stream, kg/kgmol

Z = humidity, kg H_2O/kg dry air

The constants K_1 and K_2 are given in Table 1 for the three orifice plates.

Table 1. The constants K_1 and K_2 used in calculating $\dot{m}_{air}$.

d, diameter mm	K_1	K_2	Operating Range, mole/s
16.0	1.779×10^{-3}	0.29321	0.159 - 0.393
25.40	4.50×10^{-3}	0.29510	0.393 - 1.172
50.80	20.721×10^{-3}	0.32871	0.975 - 4.891

2. Entering Water Flow Rate. Liquid flow rates in this work were measured by two different rotameters. The calibration charts are given by Zulhsdorff (20). Since the flow rates and % of scale have a linear relationship, the flow rate of water in moles/s can be obtained as follows:

$$\dot{m}_{H_2O,\ in} = F(\%\ \text{of scale}) \tag{3}$$

where:

F = 0.1574 for the small rotameter

F = 1.091 for the large rotameter

3. Entering Ammonia Flow Rate. Measurement of the ammonia flow rate was achieved by a rotameter. Calibration charts and development of working equations are given by Zuehlsdorff (20). For ammonia, at the operating conditions encountered in this work, the following equations were used to calculate the flow rate.

$$\dot{m}_{NH_3,\ in} = 1.528 \times 10^{-3} C_r R_d \sqrt{\rho} \left[2.0 + R_d/100\right] \tag{4}$$

ρ, the density of ammonia entering the system, in moles/s, can be obtained by

$$\rho = 1.291 \times 10^{-3} P_{NH_3}/(T_{NH_3} V) \tag{5}$$

where:

$$V = 0.6222 + 8.0 \times 10^{-5}(1.8T_{NH_3} - 499.67) + 6.0 \times 10^{-4}\left(15.0 - \frac{P_{NH_3}}{6894.75}\right) \tag{6}$$

R_d, the percent change in diameter ratio, is given by the following expression:

$$R_d = 1.0 + 0.263 \text{ (\% of scale)} \tag{7}$$

and Cr, the rotameter flow coefficient is calculated:

$$Cr = \frac{\sqrt{b^2 + 4ac} - b}{2a} \tag{8}$$

where:

$a = 3.08 \log (Rd) - 1.25$

$b = 3.83 - 1.17 \log (R_d)$

$c = \log(St) - 0.111 \log (R_d)$

St is called "stoke's number" and is defined as:

$$St = 2.829 \times 10^{-9} \rho R_d^3 / \mu^2 \tag{9}$$

and finally, μ, the viscosity of ammonia, in Pa·S is available for the operating temperature and pressure of the system (23, 28) and can be presented by the following expression:

$$\mu = 9.2 \times 10^{-6} + 2.0 \times 10^{-8}(1.8\, T_{NH_3} - 499.67) \tag{10}$$

4. Exit Air Flow Rate. Since the amount of water stripped by the air is negligible, a good approximation is:

$$\dot{m}_{air,\ in} \simeq \dot{m}_{air,\ out} \tag{11}$$

where:

$\dot{m} \equiv$ mole/s

5. Exit Water Flow Rate. By measuring T_{wb} and T_{db} (wet bulb and dry bulb temperatures) of the entering and leaving air the humidity, Z (kg H_2O/kg dry air) can be obtained. Then the amount of evaporated water is approximated by:

$$H_2O \text{ evaporated} = \dot{m}_{air,\ in}\ 1.609(Z_{out} - Z_{in}) \tag{12}$$

Thus, $$\dot{m}_{H_2O,\ out} = \dot{m}_{H_2O,\ in} - H_2O \text{ evaporated} \tag{13}$$

However, since H_2O evaporated was never over 0.2 percent of the liquid flow rate:

$$\dot{m}_{H_2O,\ out} \simeq \dot{m}_{H_2O,\ in} \tag{14}$$

where:

$\dot{m} \equiv$ mole/s

6. Exit Ammonia Flow Rate in the Liquid Stream. The titration method briefly described in section A-2 of this chapter was followed (see Ref. (20) for details). A sample of the exit liquid stream was quickly pipetted and the ammonia concentration was determined.

$$\dot{m}_{\substack{NH_3 \text{ out} \\ \text{liquid}}} = \frac{N_{H_2SO_4}\ V_{H_2SO_4} - N_{NaOH}\ V_{NaOH}}{1000\ V_{sample}}(18.01)(\dot{m}_{H_2O,\ out}) \tag{15}$$

where:

N = normality, kg equiv/m^3

$V_{H_2SO_4}$ = volume of H_2SO_4 used to trap the ammonia in the solution, m^3

V_{NaOH} = volume of NaOH required to neutralize the unreacted H_2SO_4 in the sample, m^3

V_{sample} = volume of the ammonia sample solution, m^3

7. Exit Ammonia Flow Rate in the Gas Stream. The exit ammonia flow rate in the exit gas stream can easily be obtained by subtracting the amount of ammonia leaving with the liquid stream from the total amount entering the column in the gas stream.

$$\dot{m}_{NH_3,\ out\ gas} = \dot{m}_{NH_3,\ in} - \dot{m}_{NH_3,\ out\ liquid} \qquad (16)$$

D. Operating Procedure

Preliminary operating procedure and the manner in which baffle spacing was adjusted as well as instruction to fill the packing section has been previously thoroughly explained (20). Solutions of sodium hydroxide and sulfuric acid of approximately 0.2 normal were prepared and titrated against a known standard solution to obtain exact normalities.

1. Procedure for Generating Required Data. After the preliminary operating procedures, the following steps were taken to generate necessary data for a run. Before recording any data, the following startup steps should be performed (20).

a. Open the liquid outlet valve.

b. Open manometer valves (1, 4 and 5).

c. Place the appropriate orifice plate in the system for the the desired flow range (beveled edge on the downstream side).

d. Turn on the air blower switch (located on the same floor) and open air control valve mechanism about one-third. Let the air run through the system until the inlet air temperature stabilizes.

e. Set the scale on the small water rotameter on ten.

f. Check the ammonia tank as well as the system for leaks. Production of a white cloud in the presence of concentrated hydrochloric acid solution is an indication of an ammonia leak.

Once the startup steps were performed, the operating gas and liquid rates were chosen. Knowing the desired liquid to gas ratio, and setting the air flow rate (using Eq. 2), one could then calculate the required liquid flow rate. From Eq. 3 an appropriate scale setting for the rotameter is determined. Allow 10 minutes for the flow patterns and liquid hold-up within the column to fully develop. The drainage liquid valve was adjusted so that from 50 mm to 100 mm of water was maintained in the bottom of the column. The ammonia flow rate was then set at about 2 percent of the air flow rate using the calibration curve at 283^{o}K and 103.4 K Pa given in Appendix A. The exact flow rate, however, should be calculated later using Eq. 4. Twenty (20) to 30 minutes was allowed for the column to reach equilibrium before taking any samples.

The barometric pressure in the immediate area was read in inches of mercury (P_{atm}). The flow rates as well as the temperature and pressures were checked frequently during the course of experiment to make sure drastic fluctuations have not occurred. Necessary adjustments were made, if needed. For each run, the following informations were recorded:

T_1 = temperature of the incoming air

P_1 = orifice upstream pressure

ΔP = pressure drop across the orifice

T_w, T_d = wet bulb and dry bulb temperatures of the inlet and exit gas stream

ΔP_{col} = pressure drop across the column

% of scale for water rotameter

% of scale for ammonia rotameter

T_{NH_3} = temperature of ammonia entering the system

P_{NH_3} = pressure of ammonia entering the system

After 20 to 30 minutes of operating the column in the manner described above, 10 ml of the liquid sample was quickly pipetted into 25 ml of 0.20 normal sulfuric acid. This excess acid will react with the ammonia solution and a portion of the acid will be left unreacted. Bromocresol green indicator was used to back titrate the solution with 0.2 normal sodium hydroxide. This way ammonia concentration in the liquid stream was obtained. The liquid in the bottom section of the column was drained and was allowed to refill to its original level. To complete the run, this sampling procedure was repeated until reasonable agreements between successive samples were obtained.

2. Procedure to Shut Down the Column. The following steps should be performed once the desired data were taken:

a. Close the ammonia tank valve and let the ammonia, still in the lines, out to the system.

b. Turn off the main water supply and drain all water lines.

c. Turn off the air blower switch and record the operating time in the maintenance notebook.

d. Close all the valves in the manometer system to prevent fluid evaporation (loss of manometer liquid).

IV. ANALYSIS OF ERRORS

The presentation of experimental results without careful consideration of the reliability of the data would be meaningless. It must be realized that the true value of many quantities can never be known because of unavoidable errors in measurements and calculations. Attempts were made to minimize the error due to poor equipment performance such as sudden fluctuations in the flow rates. However, it is important to specify the highest amount by which the quantity might be in error or to specify the value of some other parameters (standard error, probable error, etc.) from which the probability of the existence of an error of any given magnitude can be predicted.

The probable error is in a very common use in presenting the reliability of the experimental results. It represents an error of such magnitude that from the standpoint of probability, the true error is just as likely to be greater as it is to be less than this magnitude (29). If P represents the probable error of a quantity, F, then the quantity may be reported as $F \pm P$. This implies that if another measurement of the quantity were to be made by the same methods, the obtained value would lie in the range of $F \pm P$.

The experimental measurements fit into two categories--direct and indirect measurements. A direct measurement is made whenever the magnitude of the measured quantity is determined by direct observation from the measuring instrument. Instruments have errors associated with them. These errors are usually reported in operating manuals or on the scale increments of the instrument; estimated error is ordinarily one-half of the smallest division that is easily read on the instrument.

An indirect measurement results from a functional relationship between the indirect quantity and the quantities directly measured. The magnitude of the indirect quantity is determined through the errors associated with the direct quantities.

If the desired result, for which the experiment was carried out, be designated by F and the directly measured quantities (e.g., volume, barometer readings, temperatures, rotameter readings, etc.) be designated by q_i, the indirect quantity, F, can be determined by substituting the experimentally determined values of the quantities q_i into a formula which may be represented as,

$$F = f(q_1, q_2, \ldots, q_n) \tag{17}$$

The infinitesimal changes dq_i in the experimentally determined values of q_i will produce in F the infinitesimal change

$$dF = \frac{\partial F}{\partial q_1} dq_1 + \frac{\partial F}{\partial q_2} dq_2 + \ldots + \frac{\partial F}{\partial q_n} dq_n \tag{18}$$

And if the changes are finite rather than infinitesimal but are small enough that the values of the partial derivatives are not appreciably affected by the changes, the above expression can be written as,

$$\Delta F = \frac{\partial F}{\partial q_1} \Delta q_1 + \frac{\partial F}{\partial q_2} \Delta q_2 + \ldots + \frac{\partial F}{\partial q_n} \Delta q_n \tag{19}$$

Δq_i represents the probable errors in the quantities q_i. By assigning correct signs to the direct errors so that they will act to increase the value of ΔF, then ΔF will be the probable error for the indirect quantity.

The maximum probable error can also be estimated by first inserting the direct experimentally measured values into the analytical expression of the quantity F and then by increasing or decreasing the direct quantities by the probable error and reporting the calculation. The difference in the two quantities represents the maximum probable error for the indirect quantity F. It should be noted that the actual error in F might not be equal to the maximum error calculated since errors in the various measured quantities might offset each other.

The maximum probable errors for the direct and indirect measurements are tabulated and presented in Tables 2 and 3. The error is also reported as smallest and largest percentage of the measured quantity.

A careful evaluation of Tables 2 and 3 indicate that the accuracies of most values are reasonable and acceptable. The largest error is associated with the calculation of Y_{out}, X_{out}, % NH_3 removed and volume of a transfer unit (VTU). The quantities Y_{out} and X_{out} were obtained from $\dot{m}_{NH_3,out,gas}$ and $\dot{m}_{NH_3,out,liquid}$ which, in turn, were subtraction operations. The operation of subtraction is the source of great loss of accuracy (29). The inaccuracy of the above mentioned quantities in turn produced inaccuracies in % NH_3 removed and VTU calculations.

Table 2. Maximum Probable Error of Direct Measurement.

Measurement	Smallest Value	Largest Value	Maximum Probable Error	% Error	
				Largest	Smallest
d	16.00	50.80	± 0.05	0.3	0.1
D	--	82.55	± 0.25	--	0.3
Z	--	1.52	± 0.005	--	0.3
V	1.60	16.60	± 0.05	3.1	0.3
P_{atm}	100106.0	102950.0	± 68.0	0.1	0.1
T_1	315.65	337.15	± 0.50	0.2	0.1
P_1	101890.0	107455.0	±180.0	0.1	0.1
ΔP	299.0	6147.0	± 12.0	4.0	1.9
T_w	277.04	297.04	± 1.0	0.4	0.3
T_d	283.15	301.15	± 1.0	0.4	0.3
T_{NH_3}	275.37	292.04	± 0.50	0.2	0.2
P_{NH_3}	96802.0	107834.0	±200.0	0.2	0.2
% of scale water rotameter	8.33	38.00	± 0.5	6.0	1.3
% of scale NH_3 rotameter	10.0	45.0	± 0.5	5.0	1.1

Table 3. Maximum Probable Error of Indirect Quantities.

Quantity	Smallest Value	Largest Value	Maximum Probable Error	% Error	
				Largest	Smallest
β	0.194	0.615	$\pm$0.0025	1.3	0.4
C	0.57	0.61	$\pm$0.005	0.9	0.8
K_1	1.779×10^{-3}	20.721×10^{-3}	$\pm 0.235 \times 10^{-3}$	16.0	1.4
K_2	0.29321	0.32871	0.0036	1.2	1.1
A_2	201.1×10^{-6}	2027×10^{-6}	$\pm 4.0 \times 10^{-6}$	2.0	0.2
Z	0.0026	0.0215	$\pm$0.0002	7.7	0.9
μ	9.12×10^{-6}	9.72×10^{-6}	$\pm 1.8 \times 10^{-8}$	0.2	0.2
ρ	0.720	0.789	$\pm 2.0 \times 10^{-3}$	0.3	0.1
$\bar{M}$	28.678	28.924	$\pm$0.031	0.1	0.1
$\dot{m}_{air,in}$	2.335	6.767	$\pm$0.144	6.2	2.1
$\dot{m}_{H_2O,in}$	4.727	21.564	$\pm$0.288	6.1	1.3
$\dot{m}_{H_2O,out}$	4.705	21.564	$\pm$0.288	6.1	1.3
$\dot{m}_{NH_3,in}$	0.0292	0.1315	$\pm 1.44 \times 10^{-3}$	4.9	1.1
$\dot{m}_{NH_3,out,liquid}$	0.0196	0.1194	$\pm 1.8 \times 10^{-3}$	9.2	1.0
$\dot{m}_{NH_3,out,gas}$	6.739×10^{-3}	26.964×10^{-3}	$\pm 7.2 \times 10^{-4}$	10.7	2.7
Y_{in}	0.00863	0.0366	$\pm 3.0 \times 10^{-4}$	3.5	0.8
Y_{out}	0.00117	0.0387	$\pm 4.0 \times 10^{-4}$	34.1	1-0
X_{out}	0.00366	0.00887	$\pm 6.0 \times 10^{-4}$	16.4	6.8
% NH_3 removed	67.30	91.80	$\pm$4.0	5.9	4.4
VTU	0.0458	0.0786	$\pm$0.01	21.8	12.7

V. EXPERIMENTAL RESULTS AND DISCUSSIONS

Visual observations of the flow pattern and the quantitative measurements of flow rates and pressure drop on the crosscurrent packed column were discussed (18, 19) and the correlations for operating liquid buildup as well as liquid phase drift angle were developed (3). While pressure drop and gas-liquid contact observations were encouraging, the question of overall mass transfer efficiency of the column still remained unsolved. Zuehlsdorff (20) attempted to answer some of the questions raised concerning the mass transfer performance of the column. Although his results were informative in regard to understanding the mass transfer performance of the crosscurrent column, the interpretation of the experimental results were questionable. The overall absorption efficiency was plotted versus the gas rate and the resulted points were fitted by a straight line. This linear fit of data was questioned since for each set of data there existed one point which deviated from the proposed linear fit. By the visual observation, this point corresponded to the conditions where liquid began to build up on the baffles. It was thought that the system might experience a transition; transition being the turning point in the column from no liquid presence on the baffles to the appearance of a few drops of liquid on the baffles.

The purpose of this portion of work was to resolve this ambiguity in the system and to confirm experimentally whether this point was off due to experimental error and the following analytical analysis of the sample or whether there is a distinct trend in the system's behavior.

A set of experiments was designated to measure the overall absorption efficiency of the column around the suspected point. The experiments

were conducted in the multistage crosscurrent column according to the procedure described previously. Ammonia-air-water system was used. Entrance ammonia flow rate in the gas phase was set by a calibrated rotameter. The quantitative analysis of the ammonia content of the exit liquid system was determined by the titration method. The overall absorption efficiency which is defined as:

$$\% \text{ Absorption Efficiency} = \frac{Y_{in} - Y_{out}}{Y_{in}} \times 100 \qquad (20)$$

was calculated and the result are presented in Figure 7.

1. Discussion of Results

At low gas and liquid flow rates the experimental data fell on a curve until the turning point was reached. Up to this point no liquid was present on the baffles and it appeared that the liquid was flowing rather vertically downward. As the flow rates were increased further, liquid started to appear on the baffles. From this point on the absorption efficiency followed a different trend and the data points generated a new curve as the flow rates kept increasing. As shown in Figure 7, the system showed a transition at the suspected point. It seemed that prior to liquid buildup on the baffles gas would find less resistance to bypass the liquid and portion of the gas would flow around the baffles without coming into intimate contact with the liquid. It was not feasible to measure the percent bypass which appeared to be a function of gas and liquid rates.

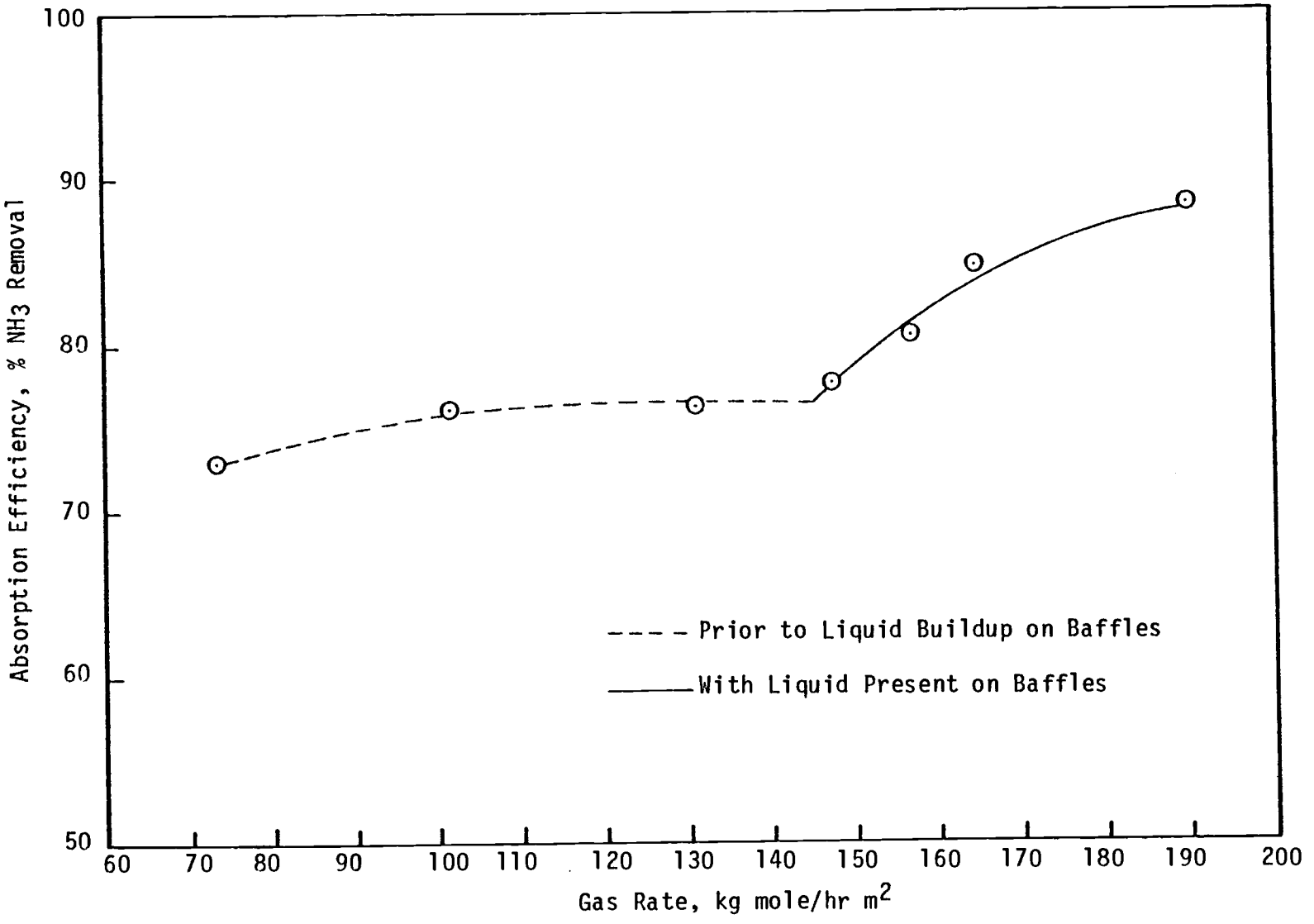

Figure 7. Absorption Efficiency as a Function of Gas Rate, for L/G = 2.0.

B. Tracer Study to Confirm the Visual Observation

To further confirm the visual observation regarding the liquid flow pattern in the column as the system goes through the transition, a series of tracer runs were designed and conducted. Experimental set up and operating procedure for the tracer study were discussed in the previous chapter. First the conductivity probe was placed on the top of one of the baffles and was connected to the recorder. Then 20 milliliters of KCl was injected from the position of the previous baffle. Attempts had been made to simulate an input impulse by minimizing the injection time. The results for various flow rates are shown in Figures 8, 9, and 10.

1. Discussion of Results. The tracer response to the input impulse for the flow conditions prior to the transition point is shown in Figure 8. No response was essentially obtained. However, as the gas and liquid flow rates were increased the recorder started to sense the existence of the tracer material as can be seen in Figure 9. As the flow rates were increased furthermore (still keeping L/G = 2.0) a more pronounced response was obtained. Figure 10 shows this behavior. This indicated that as the flow rates were increased the liquid tended to deviate its path. The water accumulated on the baffles did not make a desirable path for the gas to bypass anymore and thus the crossflow behavior developed.

A set of experiments was performed with the same probe, but this time positioned underneath the baffle above which the tracer was introduced. Results are shown in Figures 11, 12 and 13.

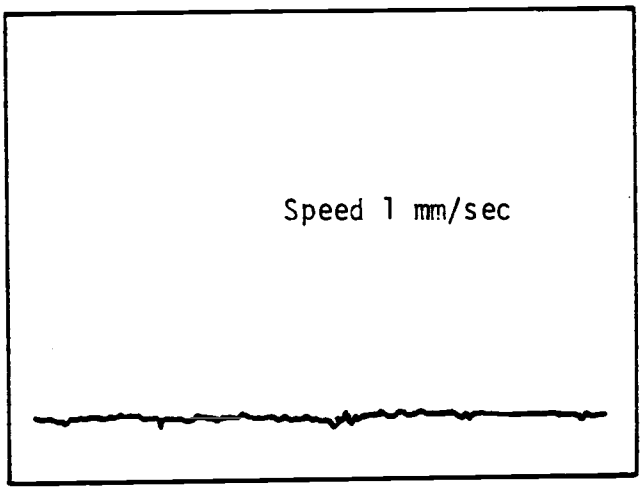

Figure 8. Tracer Output at Gas Rate of 131 kgmole/hr m^2; L/G = 2.0; Probe Location on the Baffle.

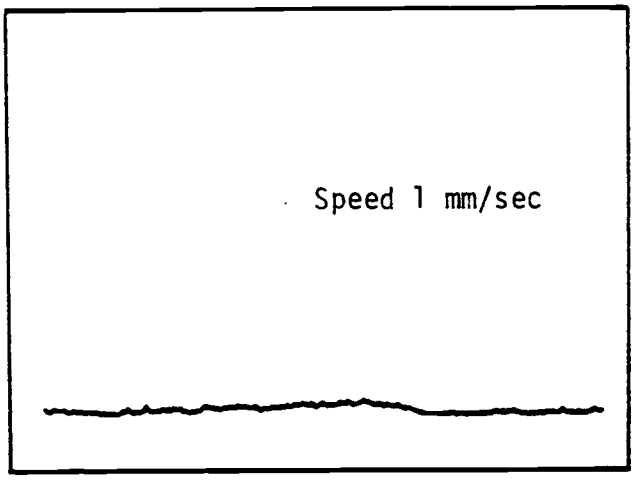

Figure 9. Tracer Output at Gas Rate of 148 kgmole/hr m^2; L/G = 2.0; Probe Location on the Baffle.

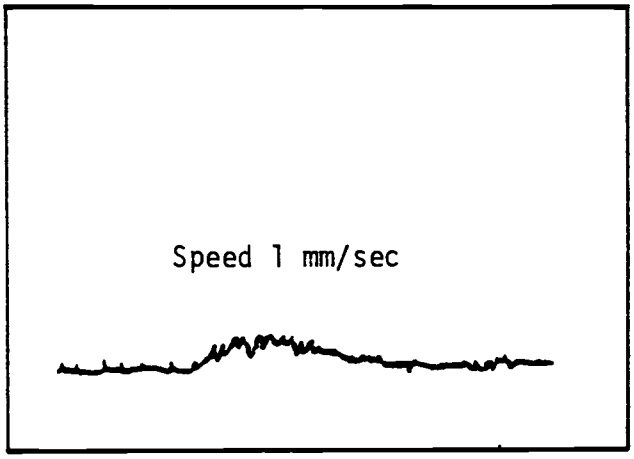

Figure 10. Tracer Output at Gas Rate of 189 kgmole/hr m^2; L/G = 2.0; Probe Location: on the Baffle.

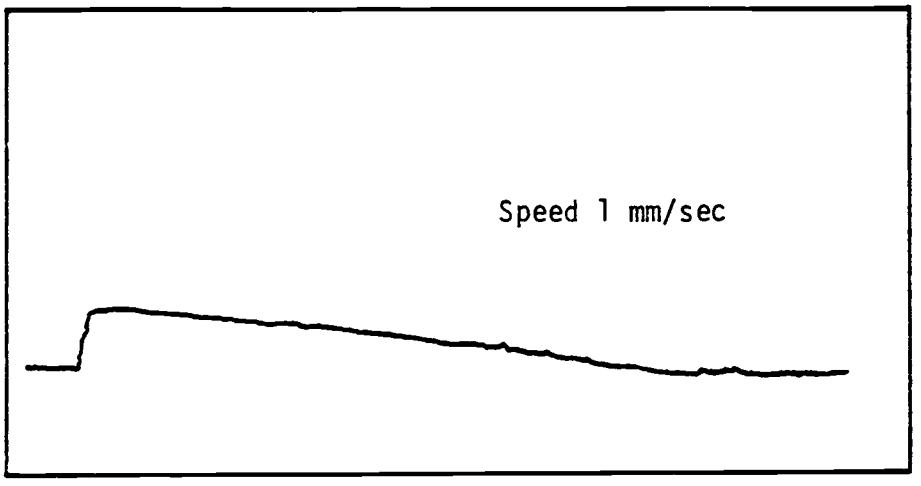

Figure 11. Tracer Output at Gas Rate of 131 kgmole/hr m^2; L/G = 2.0; Probe Location: Underneath the Baffle.

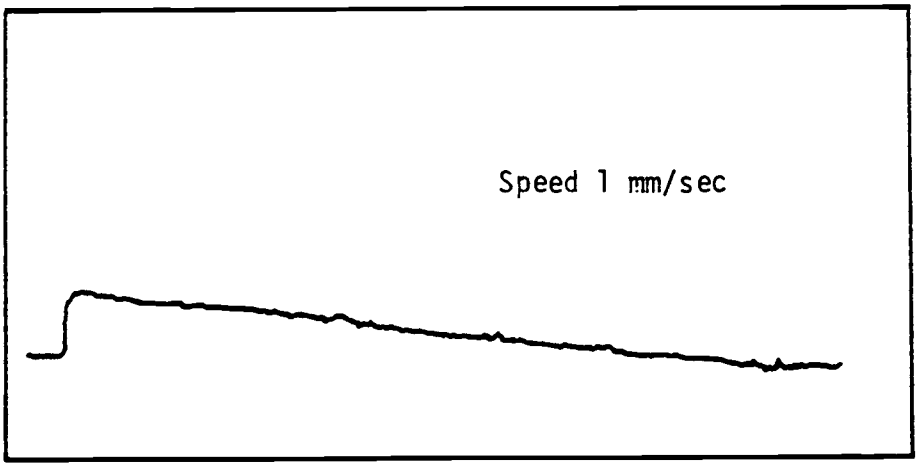

Figure 12. Tracer Output at Gas Rate of 148 kgmole/hr m^2; L/G = 2.0; Probe Location: Underneath the Baffle.

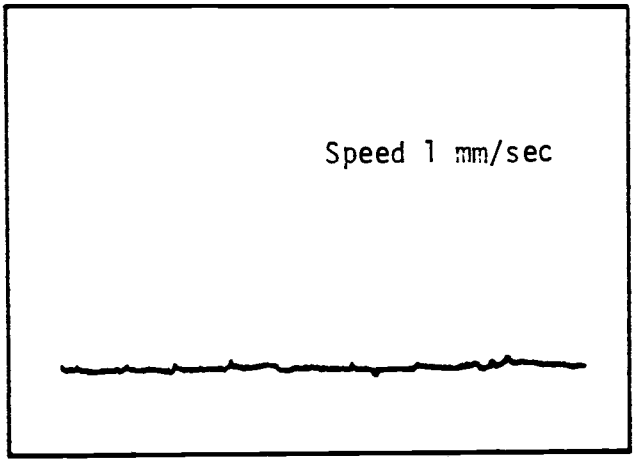

Figure 13. Tracer Output at Gas Rate of 189 kgmole/hr m^2; L/G = 2.0; Probe Location: Underneath the Baffle.

Figure 11 illustrates the response of the probe to the tracer at low gas and liquid flow rates. At this probe position the tracer was sensed by the probe; however, for the same flow conditions the probe on the next baffle did not register at all (see Figure 8). As the gas and liquid flow rates were increased the probe started to sense less tracer material and upon further increases in the flow rates the response of the probe vanished. This suggested that at the flowing conditions the tracer material must be carried to the next baffle which was indicative of a criss-cross flow. Comparison of Figures 12 and 13 with 9 and 10 confirms the above statement.

The tracer results presented above agreed well with the trend obtained from the absorption efficiency results presented in the previous section. Therefore, as a result of the above studies, the anticipated trend was confirmed. In other words, the system showed a distinct transition. Prior to the transition point the liquid flowed rather straight down the column instead of crossing. This behavior was observed visually and was confirmed by the tracer study. As the system passed the transition point, liquid started to deviate its path from more or less straight down the column to a zig-zag manner. This behavior was again observed visually and was further confirmed by the tracer study. It was difficult to pinpoint where the transition exactly occurred since the system was not very sensitive to small changes in flow rates. However, if the data points on each zone were extrapolated, the intersection of these two curves would represent the transition point.

C. Behavior of the Crosscurrent Column with Various Liquid-Gas Ratios

Once the trend of the system was established, an attempt was made to examine the system's behavior when liquid-to-gas ratios other than 2.0 were used. To accomplish this objective, the multistage crosscurrent packed column was employed and the same operating procedures described previously were used to generate the experimental points. The absorption efficiencies were calculated from the experimental data and were plotted as a function of the gas rate for L/G ratios of 1.5, 2.0, 3.0 and 4.0 with 12 baffles in the column. The results are presented in Figure 14.

Attempts had been made to generate each set of runs in the same gas rate range. In spite of equipment limitations the above task was more or less accomplished.

1. Discussion of Results. The system demonstrated exactly the same behavior with various L/G ratios as it was observed with L/G of 2.0. Again the transition occurred at different values of gas flow rate. As L/G ratio increased, the relative position of the transition point shifted in the direction of decreasing the gas rate, meaning that at a larger L/G ratio, the transition occurred at lower gas rate. This phenomena was due to the availability of liquid phase in the column at larger L/G ratios. In other words, increased liquid phase left less void space for the gas phase to flow through and caused the gas to exact more force on the liquid, resulting in the change of liquid phase flow direction. Therefore, the transition occurred earlier at larger L/G ratios. This is equivalent to what an increase in the gas rate would

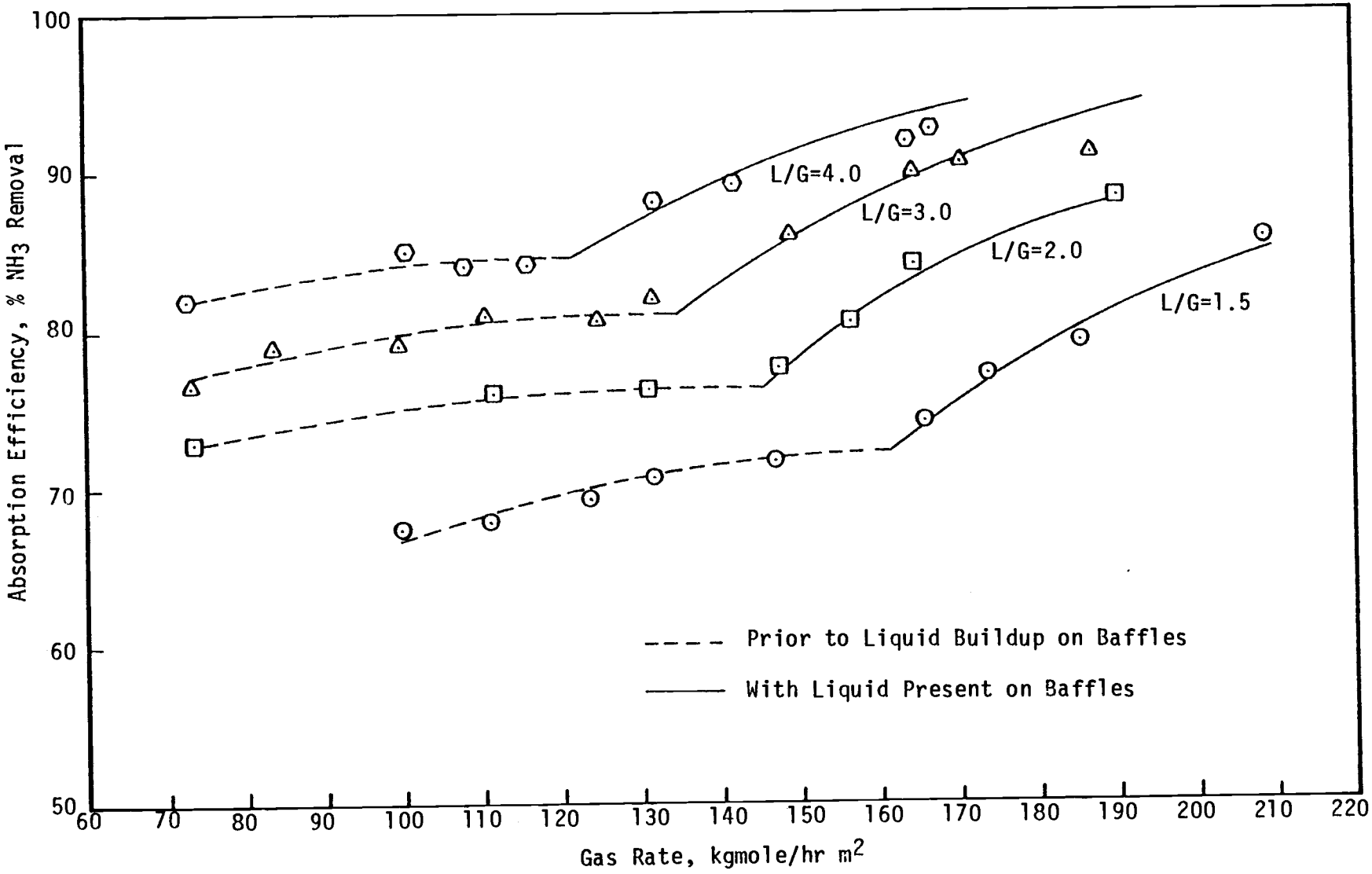

Figure 14. Absorption Efficiency as a Function of Gas Rate for Various L/G Ratios.

have caused, because increasing gas velocity would have increased the forces acting on the liquid, thus pushing it out of the packing section.

The absorption efficiency ranged between 67 to 93 percent removal for the operating conditions used in this set of runs. Increasing L/G ratio significantly improved the absorption efficiency of the column. The comparison of absorption efficiencies are shown in Figure 14.

An interesting result was deduced from the information presented in Figure 14. When L/G ratios were plotted on a semi-log plot against the gas rate at which the transition occurred, a linear relationship was obtained. As can be seen in Figure 15, the points fell very nicely on a straight line. This simple plot has a great value in designing the crosscurrent column because the location of the transition point can easily be predicted as long as the designer decides at what L/G ratio to operate the column (at least for the L/G values between 1.5 and 4.0 studied in this investigation). Higher efficiency in the region after the transition would encourage the designer to adjust the operating parameters in order to stay in the upper zone.

D. Effect of Intercore to Outer Wall Baffle Spacing on the Mass Transfer Efficiency

In order to understand the effect of the packed space to the open space (intercore to outer wall baffle spacing) the width of the packing section was expanded from 127 mm (5 inches) to 152.4 mm (6 inches), keeping the same column size and the same number of baffles. A set of runs was conducted with the expanded bed for L/G ratios of 2.0, 3.0 and

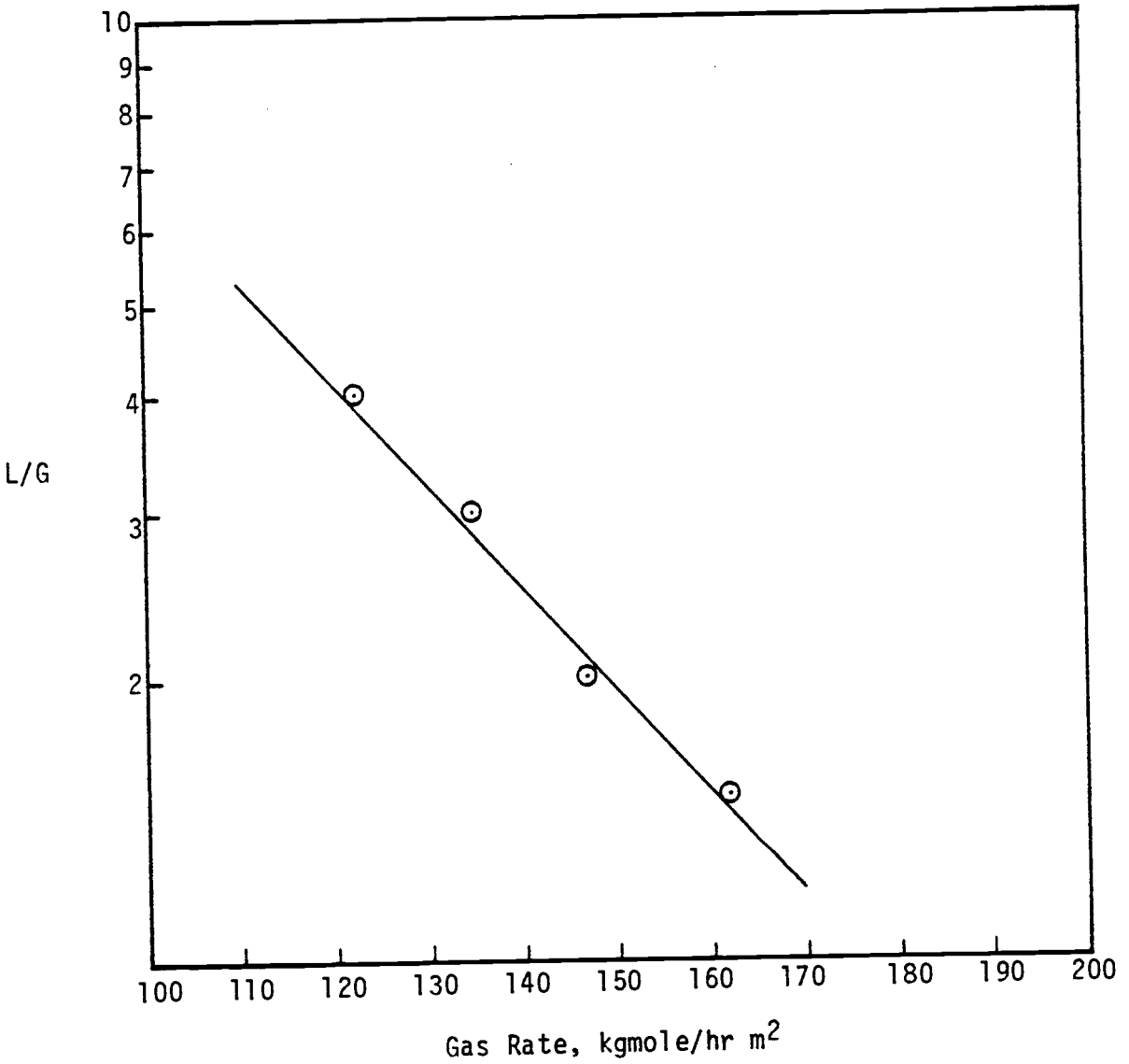

Figure 15. Liquid-to-Gas Ratio as a Function of Gas Rate at Transition Point.

4.0. The experimental data were converted to the absorption efficiency through Equation 20. The results are presented in Figures 16, 17 and 18.

1. Discussion of Results. The expanded bed also showed a transition. However, the location of the transition point occurred at slightly higher gas rate, compared to the original bed, for all L/G ratios.

A comparison of the absorption efficiencies between the expanded bed and the original bed for L/G = 2.0 is shown in Figure 16. The upper curve represents the original bed geometry and the lower curve belongs to the expanded bed. As can be seen from Figure 16, the mass transfer efficiency decreased considerably when the packing section of the bed was expanded. This was again due to having enough void space for the gas to flow through the bed without making any contact with the liquid. In other words, expansion of the packing section created more void space thus the absorption efficiency of the column decreased.

At L/G ratio of 3.0 the same behavior was observed. The mass transfer efficiency decreased. However, the gap between the absorption efficiency of the two beds narrowed. Figure 17 illustrates the results. Again the upper curve represents the original column where the lower curve describes the behavior of the expanded bed. Having higher liquid flow rate at the L/G = 3.0 forced the gas to contact the liquid more frequently thus the difference between the efficiencies decreased.

Further increase in L/G ratio to 4.0 created no appreciable difference between the two bed configurations. At L/G = 4.0 there was enough liquid available so that the gas did not feel the effect of the bed expansion as much as it did with lower L/G ratios. In other words, at L/G of 4.0 the liquid rate was high enough and well distributed

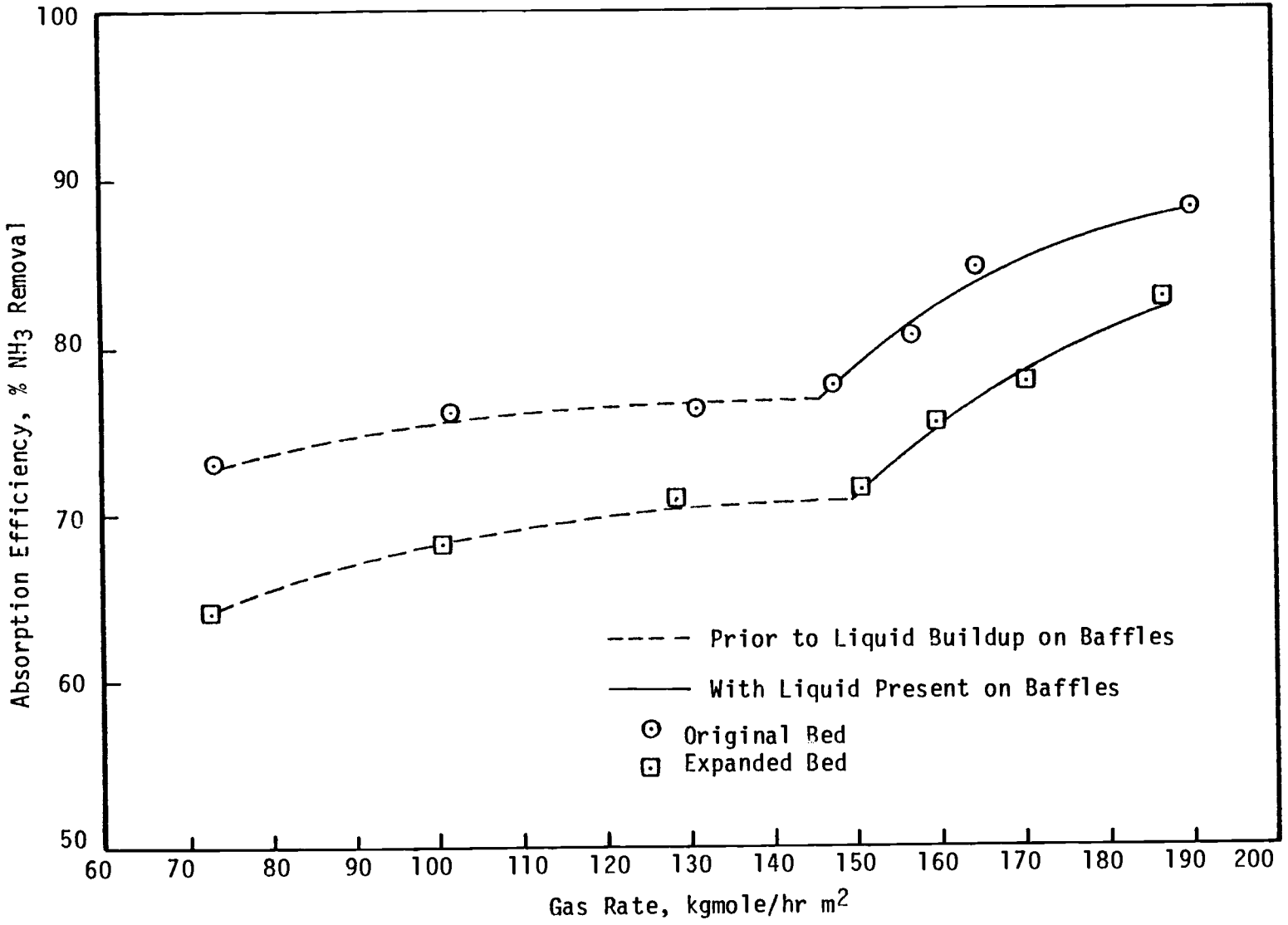

Figure 16. Comparison of Absorption Efficiency Between Original and Expanded Beds, for L/G = 2.0.

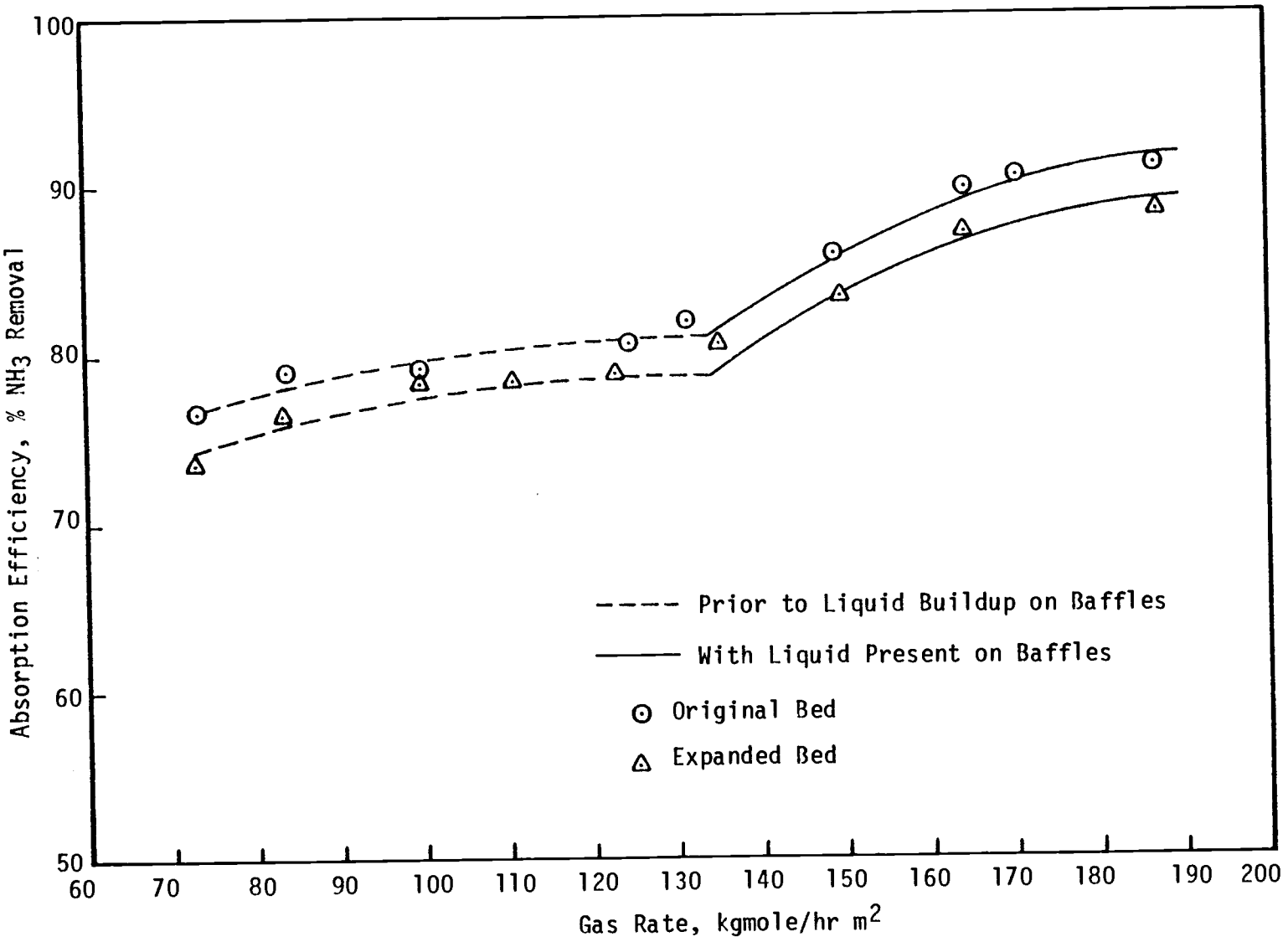

Figure 17. Comparison of Absorption Efficiency Between Original and Expanded Beds, for L/G = 3.0.

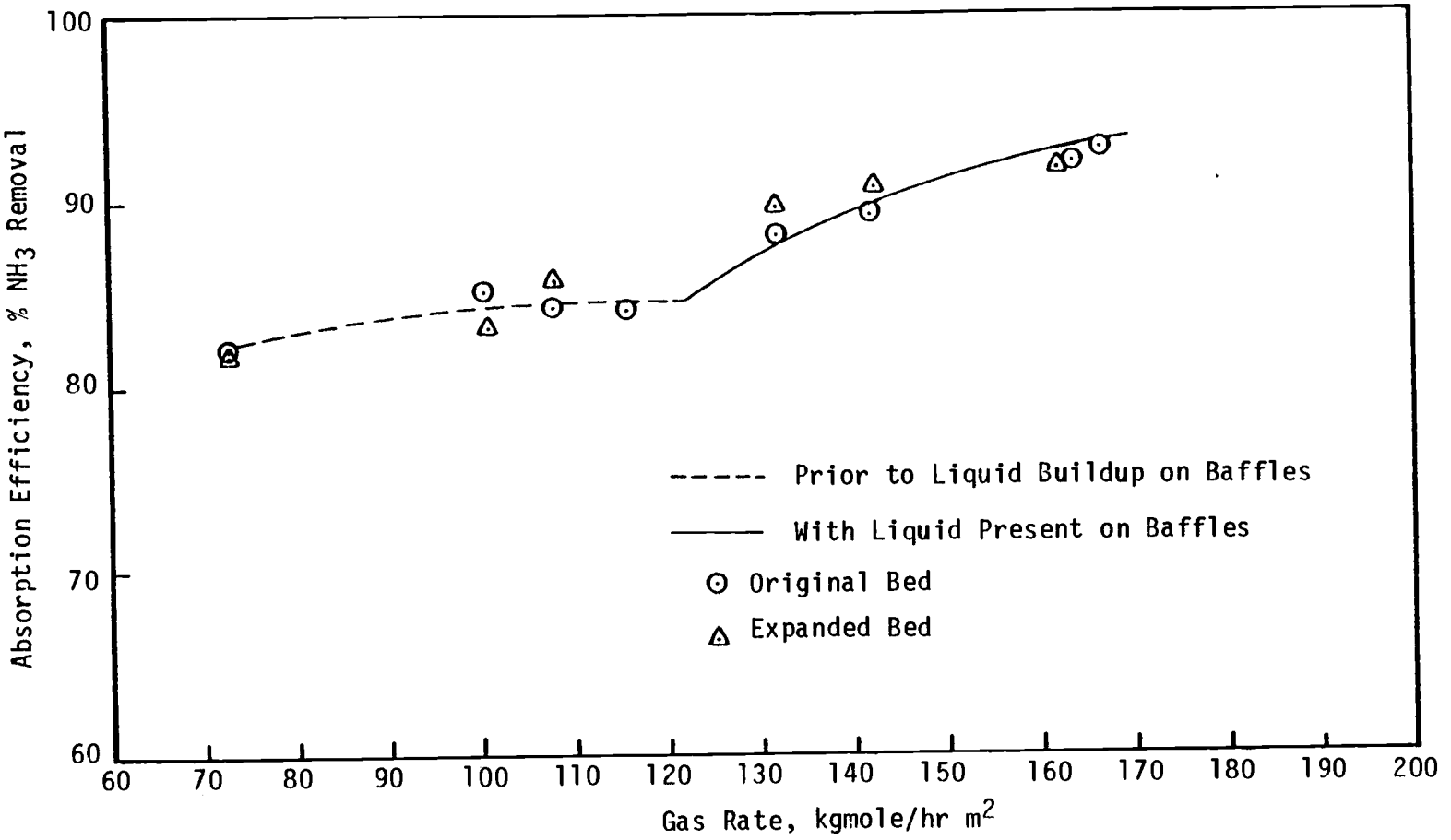

Figure 18. Comparison of Absorption Efficiency Between Original and Expanded Beds, for L/G = 4.0.

throughout the column to offer the same resistance to the gas in both bed geometries.

E. Effect of Dead Space Created in the Packing Section Due to the Crossflow Pattern on the Mass Transfer Efficiency

The movement of the gas phase across the liquid flow causes the liquid to move in the downstream direction of the gas flow at an angle of θ from the vertical. This phenomenon is called drift (7).

The drift of the liquid when the crossflow pattern is developed creates unirrigated packing sections immediately below each baffle. This situation is shown in Figure 19a. The dead space generated this way causes a major fraction of the packing to become void of liquid, thus ineffective for mass transfer. In these dead regions there is essentially no interphase contact. To understand the effect of dead space on the mass transfer efficiency the dead space should either be increased or decreased.

There are two methods to increase the dead space in the column. Either by expanding the packing section or by decreasing the number of baffles, as illustrated in Figure 19b.

In order to decrease the dead space the baffles may be taken out and total cross section of the column be filled with the packing material. This way there will be essentially no dead space in the column, as shown in Figure 19c.

Experimental runs were designed to generate the above three cases. The results are presented in Figures 16, 20, 21 and 22.

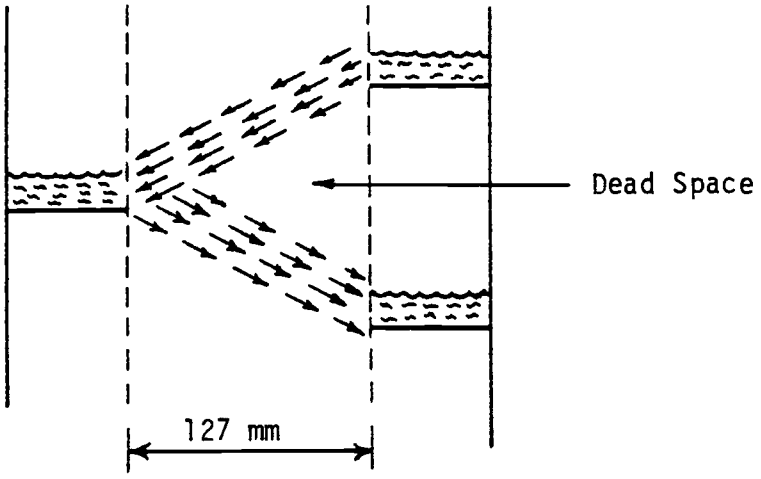

(a) Original Bed

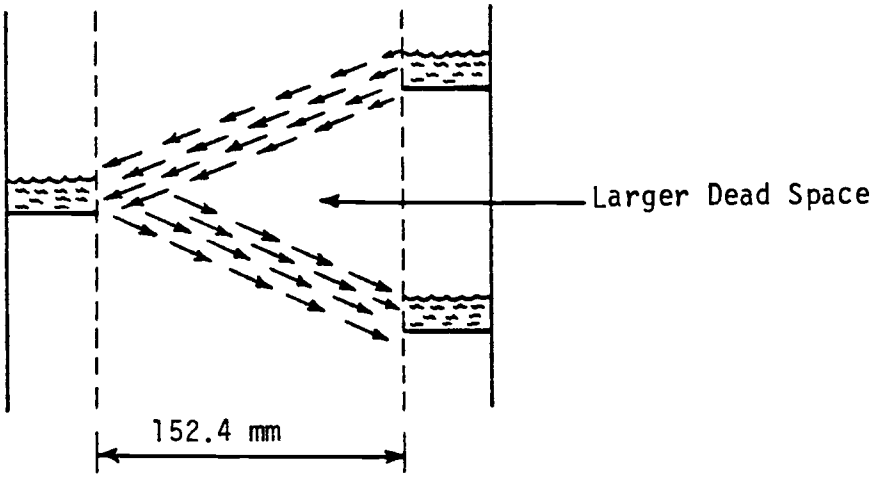

(b) Expanded Bed

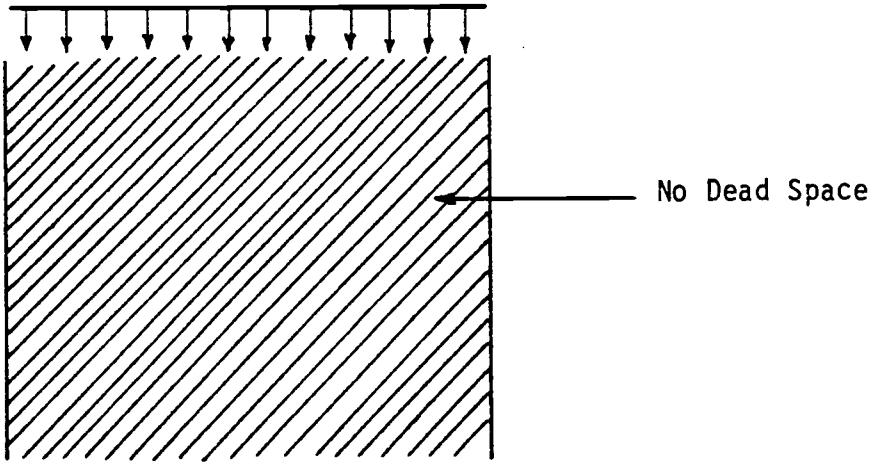

(c) Total Bed Cross Section Packed

Figure 19. Schematic Diagram Showing the Effect of Bed Expansion on Dead Space.

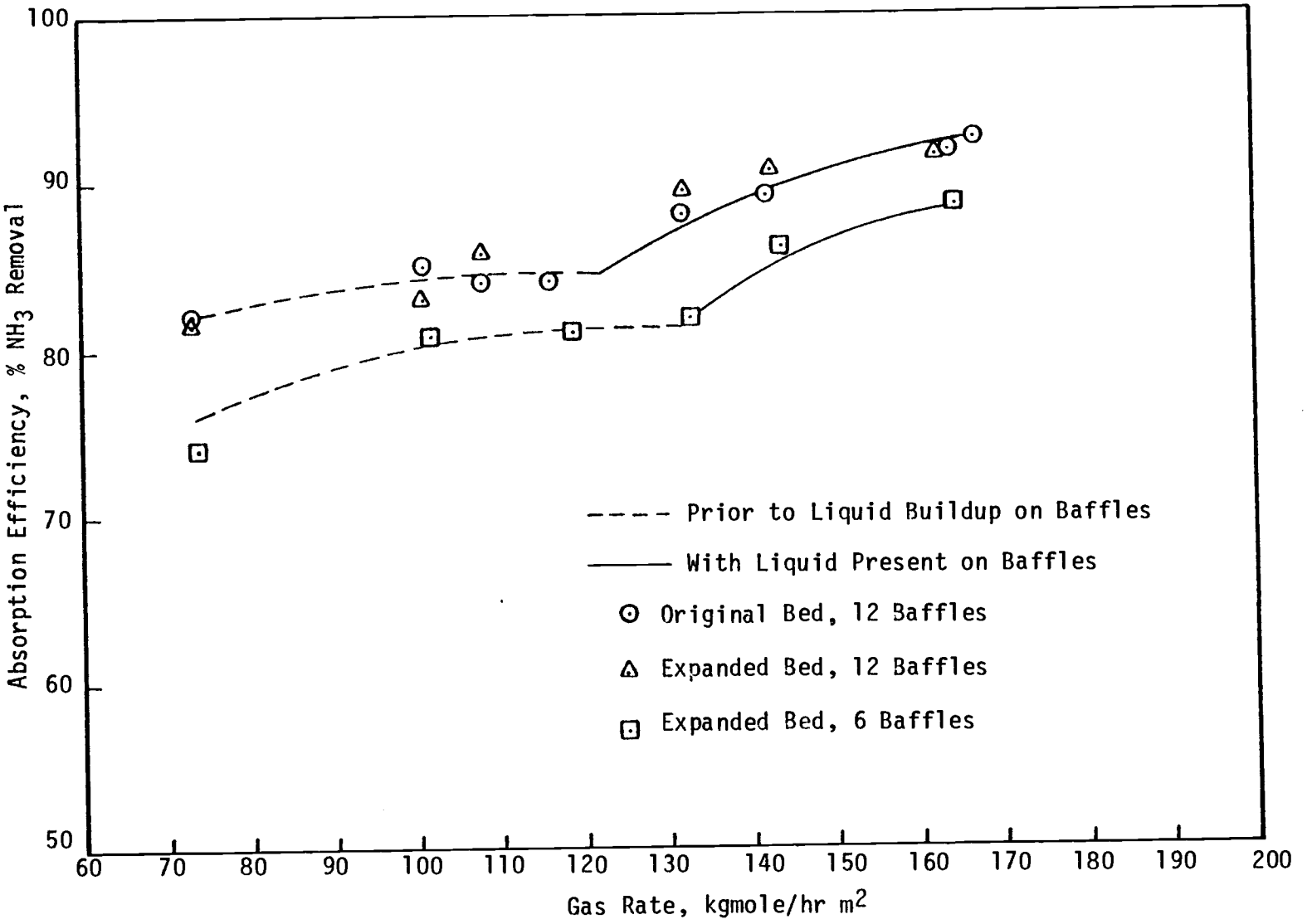

Figure 20. Effect of Dead Space, Created by Reduction in Number of Baffles, on Absorption Efficiency, for L/G = 4.0.

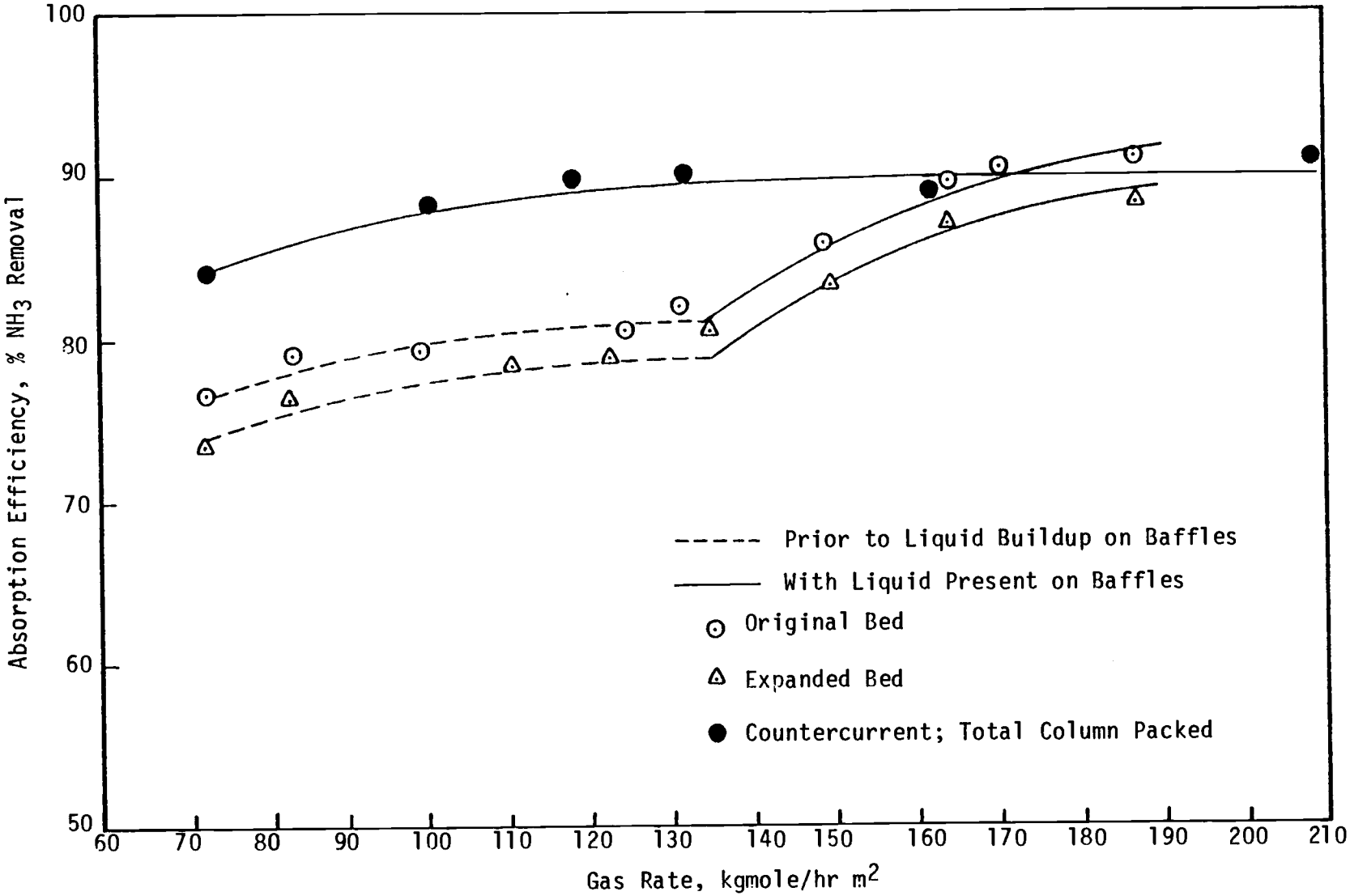

Figure 21. Comparison of Absorption Efficiency Among Various Bed Configurations, for L/G = 3.0.

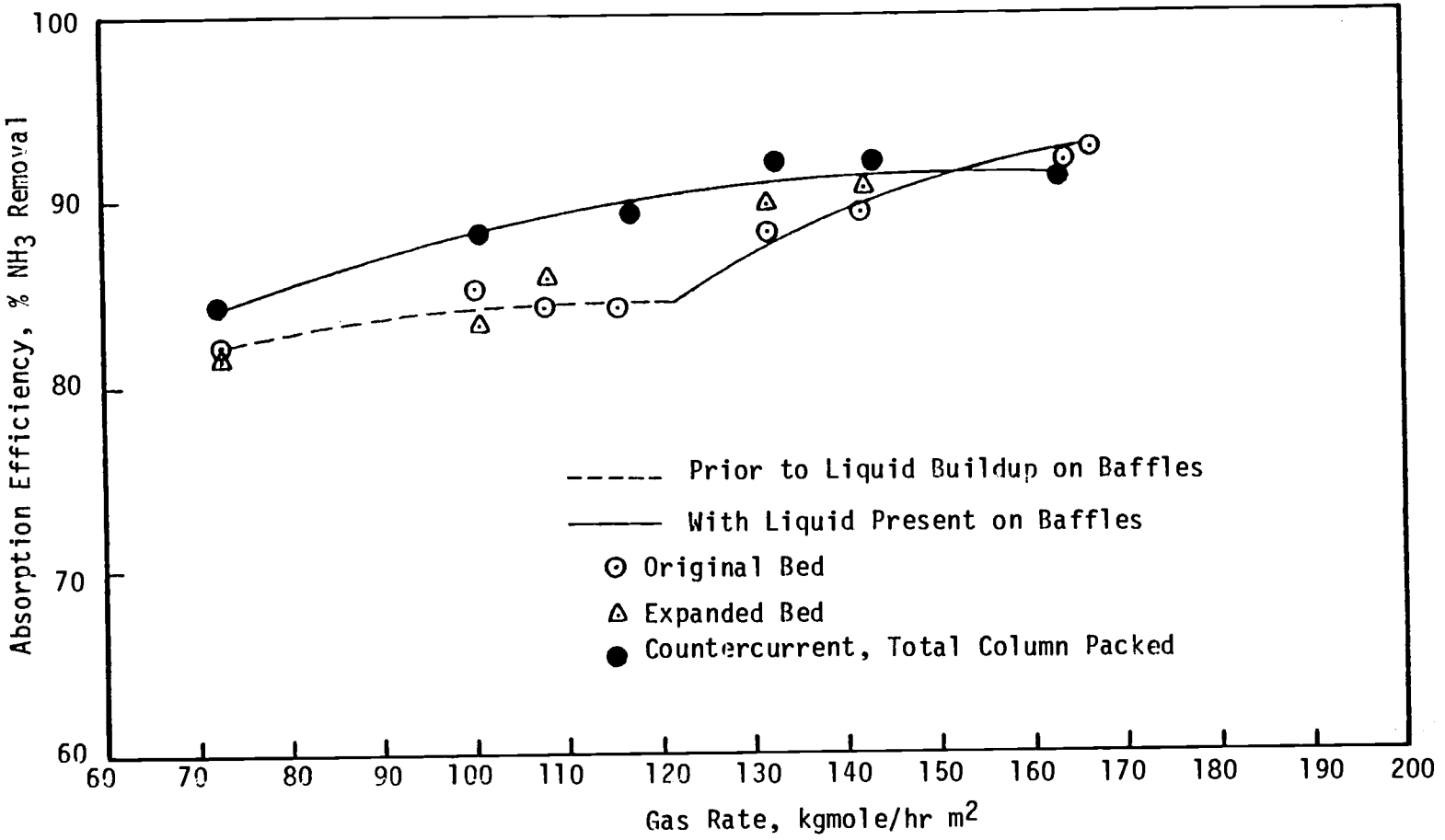

Figure 22. Comparison of Absorption Efficiency Among Various Bed Configurations, for L/G = 4.0.

1. Discussion of Results. By expanding the packing section the column efficiency decreased as shown in Figure 16. It should be mentioned that the dead space was created whenever the criss-crossing behavior of the liquid developed. This phenomenon occurred after passing the transition condition (upper portion of the curve). Therefore, by expanding the packing section, more dead space was generated and the absorption efficiency decreased.

To further investigate the phenomenon, the number of baffles was reduced from 12 to 6. The results are illustrated in Figure 20. This reduction in the number of baffles in the expanded bed obviously created larger dead space, thus a substantially lower absorption efficiency was obtained. These two cases showed that the dead space played an important role in the mass transfer efficiency of the crosscurrent column. However, it was believed that the bubbling action on the baffles might compensate for the loss of efficiency due to the existence of the dead space. The mixing activity on the baffles will be discussed in the next section.

By taking all the baffles out and filling the entire cross section of the column with the packing material (keeping the same packing height) a countercurrent column with twice as large packing volume as the cross-current unit was created. With a uniform liquid distribution over the packing section the dead space was essentially eliminated.

The efficiency of the column increased compared to the crosscurrent unit as shown in Figures 21 and 22 for L/G ratios of 3.0 and 4.0, respectively. The lower curves represent the original and the expanded bed as designated on the plot and the upper curve represent the column

with no dead space. The increase in the mass transfer efficiency is accounted by successfully eliminating the dead space existed in the crosscurrent configuration.

F. Effect on the Mass Transfer Efficiency Due to the Mixing Activity on the Baffles

As mentioned previously, when the crossflow pattern is developed liquid starts to accumulate on the baffles. As the gas rate increases, the mixing activity is observed in the packing section as well as on the baffles. In order to investigate whether the mixing compensated for the loss of efficiency due to the dead space created by the crossflow pattern, the results of the previous section were consulted. A careful evaluation of Figures 21 and 22 revealed an interesting result. The mass transfer efficiency of the countercurrent column (the column with no dead space due to liquid criss-crossing from one baffle to the other) was higher compared to the crosscurrent column as long as there existed the conditions of neither bubbling activity nor vigorous mixing on the baffles. However, when the column reached the condition where vigorous mixing activity was taking place, the crosscurrent column was advantageous. This rather interesting result was observed with both L/G of 3.0 and 4.0 as can be seen in the upper end of the curves in Figures 21 and 22. Although the countercurrent column had twice the packing volume as the crosscurrent column, the mixing activity made the latter more attractive.

VI. CONCEPTUAL MODEL FOR THE CASCADE CROSSCURRENT PACKED COLUMN

The experimental results presented and discussed in the previous chapter helped to better understand the general behavior of the cross-flow columns. The following section will attempt to combine the visual observations with the experimental findings to establish a model to describe the behavior of the crosscurrent column.

A. Presentation of Conceptual Model

Two regions were distinguished in the crosscurrent column. Prior to the liquid buildup on the baffles and after the transition where the liquid was present on the baffles. The liquid accumulation on the baffles ranged from stagnant to vigorous mixing with spray action in the void space. The detailed fluid behavior is shown by sketches in Figure 23. It was proven by the visual observation as well as by the tracer study that at low gas rates (Figure 23a) the liquid was not deflected and moved straight down the column, all of it remaining in the packing section. After the transition point, at intermediate gas rates (Figure 23b) the liquid was deflected into the void space and accumulated on the baffles. Although mixing was not very appreciable on the baffles, the gas-liquid contact within the packing was vigorous. At still higher gas rates (Figure 23c) the vigorous mixing was pronounced on the baffles as well as within the packing section.

As mentioned in the experimental presentation of this work, prior to the transition where the liquid and gas rates were low, portions of the gas found it more convenient to bypass the liquid thus flowed around the baffles. This bypassing phenomenon is pictured in Figure 24. The

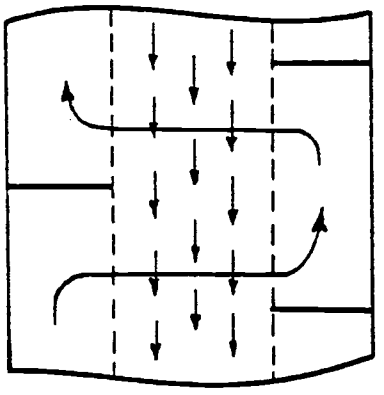

(a) Low Gas Rate

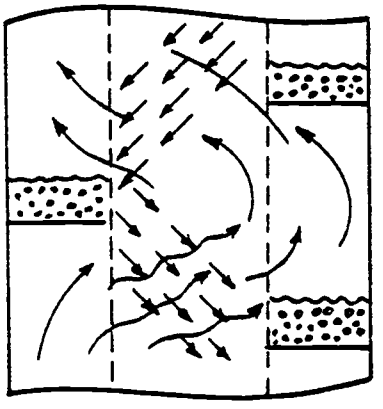

(b) Intermediate Gas Rate

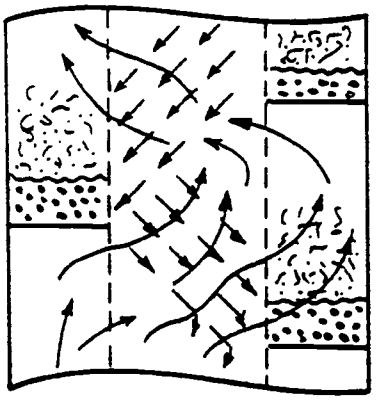

(c) High Gas Rate

Figure 23. Flow Regimes in the Crossflow Column.

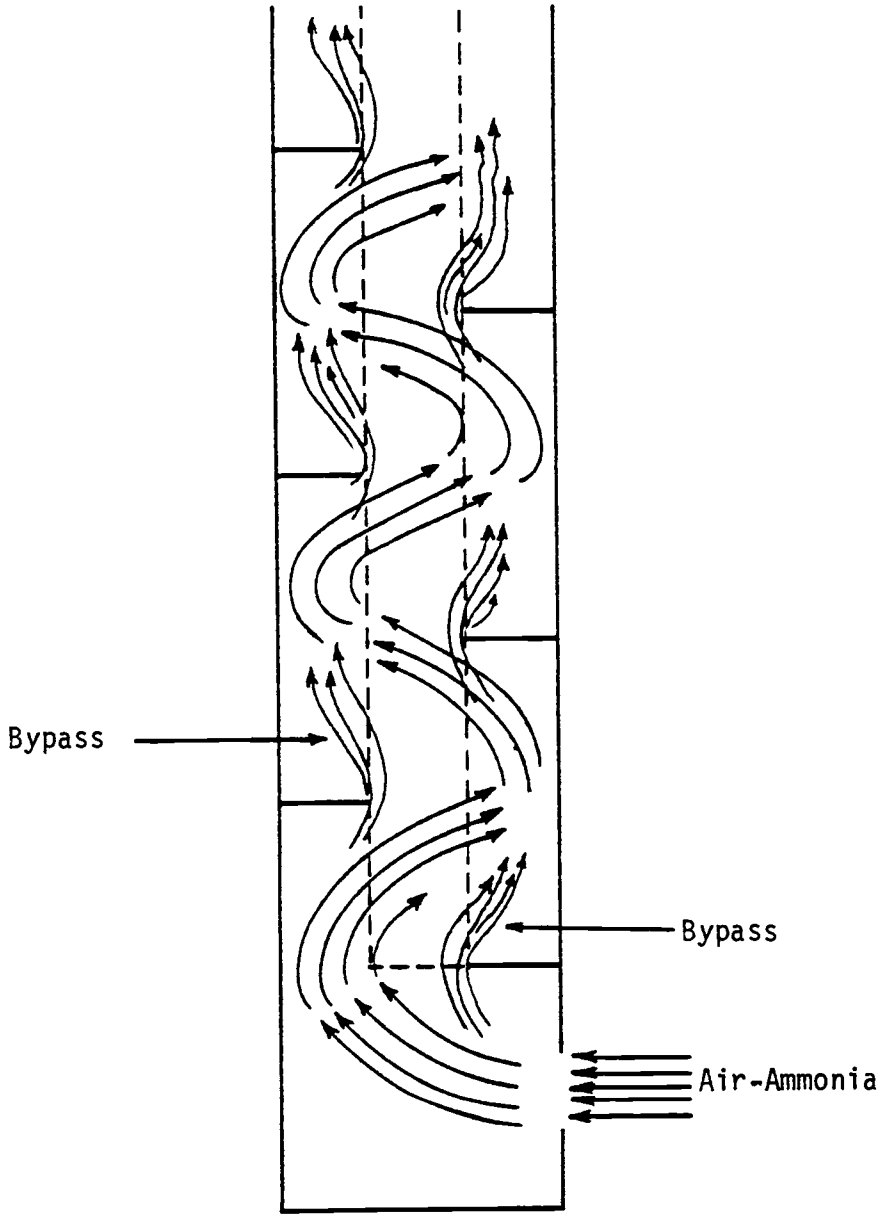

Figure 24. Gas Bypassing Phenomenon in the Crosscurrent Column.

single-stage crossflow was represented as the section between two baffles. In other words, the cascade crossflow column can be generated by placing several single-stage crossflow columns on top of each other. The flow diagram representing the cascade is shown in Figure 25. Since the concentrations of the entering gas and the exit liquid were known, calculations were started from the bottom stage. By the mathematical development shown in the next section, concentration of the entering liquid and the exit gas for the first stage (bottom stage) were obtained. These concentrations, in turn, were used as the entrance gas and the leaving liquid concentrations for the next stage until the top of the column was reached. Since the percent bypass in the column was not known, a trial and error procedure was adopted.

B. Mathematical Development for the Crossflow Column

The following mathematical presentation has been developed for the single-stage crossflow column with the dimensions of X_0, Y_0 and Z_0 as shown in Figure 26. The exact definition of each symbol will be given in the nomenclature.

Well mixed gas enters the tower at the left with a flow rate of W_G (kgmole/hr) and leaves the column at the right. The liquid also enters uniformly distributed at the top at the rate of W_L (kgmole/hr) and exits at the bottom. The concentration of the components in the entering gas and the leaving liquid streams are designated as $\bar{y}$ and $\bar{x}$, mole fractions, respectively. To formulate and solve the problem the following simplifying assumptions have been made to ease the complexity of the equations:

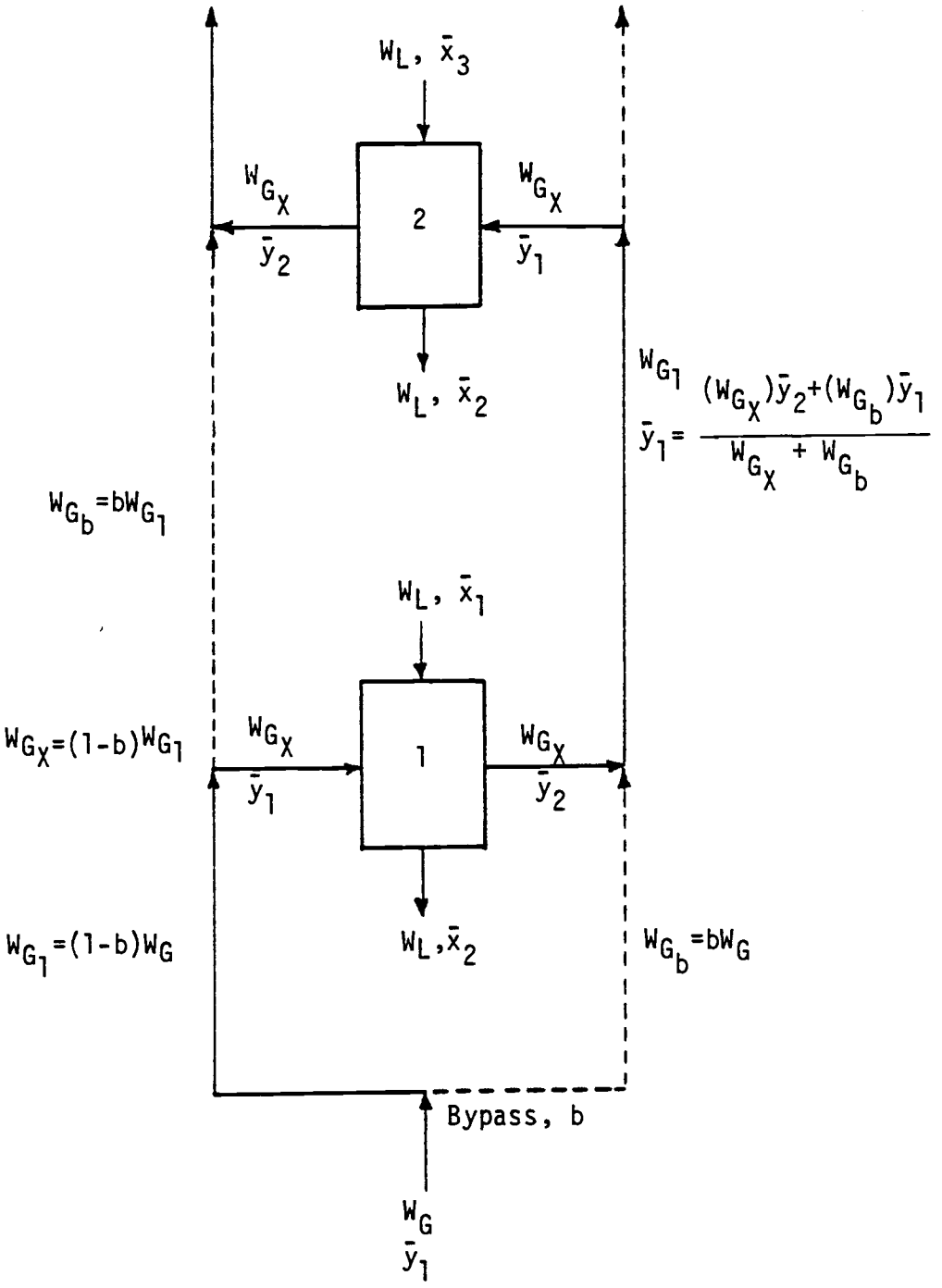

Figure 25. Flow Diagram of the Conceptual Model for the Cascade Crosscurrent Column.

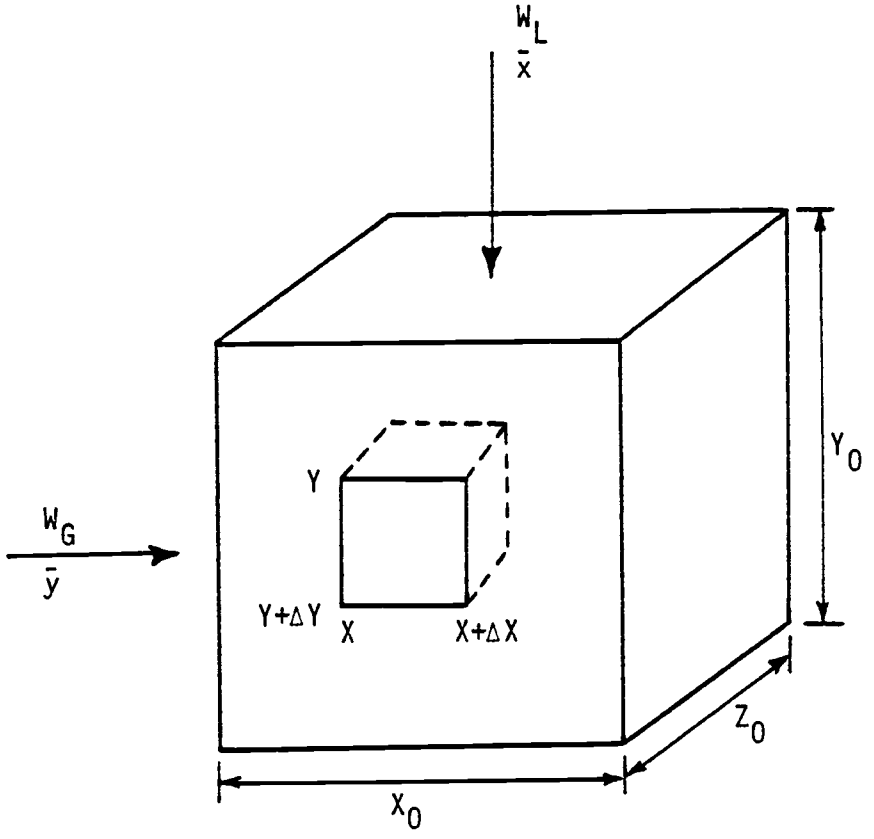

Figure 26. Schematic Representation of Single-Stage Crossflow.

1. Dilute solutions of solute in both phases (ammonia, in this case).
2. Linear equilibrium relationship (good assumption since the ammonia concentration was maintained below 5% in the gas phase).
3. Isothermal operation with uniform flow distribution.
4. Neglecting the solute concentration change along the direction of the tower width (Z direction).
5. Constant overall mass transfer coefficient for a given column condition.

With these simplifying assumptions, the mathematical analysis for the crossflow column can be developed.

The mass balance over a small element of volume of the tower, $\Delta X \Delta Y Z_0$, as shown in Figure 27, yields

$$\text{Input-Output} = \text{Accumulation} \tag{21}$$

$$\text{Input} = \left(W_G \frac{dY}{\bar{Y}_0}\right)\bar{y}\Big|_X + \left(W_L \frac{dX}{\bar{X}_0}\right)\bar{x}_Y \tag{22}$$

fraction of the gas entering the element at position X

fraction of the liquid entering the element at position Y

$$\text{Output} = \left(W_G \frac{dY}{\bar{Y}_0}\right)\bar{y}\Big|_{X+\Delta X} + \left(W_L \frac{dX}{\bar{X}_0}\right)\bar{x}\Big|_{Y+\Delta Y} \tag{23}$$

fraction of the gas leaving the element at position X+ΔX

fraction of the liquid leaving the element at position Y+ΔY

$$\text{Accumulation} = 0 \tag{24}$$

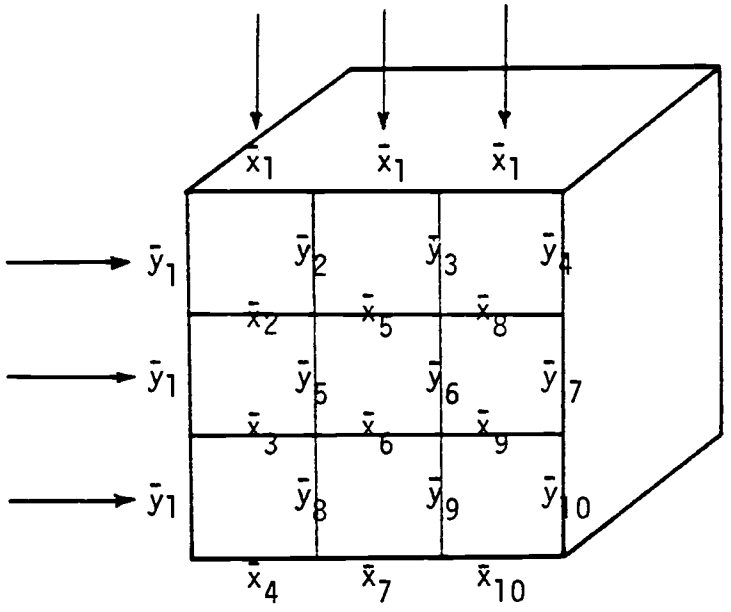

Figure 27. Concentration Distribution in the Single-Stage Crossflow Column.

By substituting Equations 22, 23 and 24 into 21, the following expression is obtained.

$$(W_G\frac{dY}{Y_0})\bar{y}|_X + (W_L\frac{dX}{X_0})\bar{x}|_Y - (W_G\frac{dY}{Y_0})\bar{y}|_{X+\Delta X} - (W_L\frac{dX}{X_0})\bar{x}|_{Y+\Delta Y} = 0 \qquad (25)$$

The quantities evaluated at $X+\Delta X$ and $Y+\Delta Y$ can be expanded in the Taylor series. Assuming W_G and W_L remain essentially constant throughout the element,

$$(W_G\frac{dY}{Y_0})\bar{y}|_{X+\Delta X} = (W_G\frac{dY}{Y_0})\bar{y}|_X + (W_G\frac{dY}{Y_0})\frac{\partial\bar{y}}{\partial X}dX \qquad (26)$$

$$(W_L\frac{dX}{X_0})\bar{x}|_{Y+\Delta Y} = (W_L\frac{dX}{X_0})\bar{x}|_Y + (W_L\frac{dX}{X_0})\frac{\partial\bar{x}}{\partial Y}dY \qquad (27)$$

Substituting Equations 26 and 27 into 25 and simplifying would yield:

$$(W_G\frac{dY}{Y_0})\bar{y}|_X + (W_L\frac{dX}{X_0})\bar{x}|_Y - (W_G\frac{dY}{Y_0})\bar{y}|_X - (W_G\frac{dY}{Y_0})\frac{\partial\bar{y}}{\partial X}dX$$
$$- (W_L\frac{dX}{X_0})\bar{x}|_Y - (W_L\frac{dX}{X_0})\frac{\partial\bar{x}}{\partial Y}dY = 0 \qquad (28)$$

After cancelling some terms, the equation becomes

$$-(W_G\frac{dY}{Y_0})\frac{\partial\bar{y}}{\partial X}dX = (W_L\frac{dX}{X_0})\frac{\partial\bar{x}}{\partial Y}dY \qquad (29)$$

Upon dividing both sides by dXdY, the final form of the equation becomes

$$-\frac{W_G}{Y_0}\frac{\partial\bar{y}}{\partial X} = \frac{W_L}{X_0}\frac{\partial\bar{x}}{\partial Y} \qquad (30)$$

Equation 30 describes the change in the solute concentration in the column.

Component balance in the gas phase yields

$$\text{Input-Output} = \text{Accumulation} \tag{31}$$

$$\text{Input} = \left(W_G \frac{dY}{Y_0}\right)\bar{y}\Big|_X \tag{32}$$

$$\text{Output} = \left(W_G \frac{dY}{Y_0}\right)\bar{y}\Big|_{X+\Delta X} + K_{OG}aP(\bar{y}-\bar{y}^*)dXdYZ_0 \tag{33}$$

$$\text{Accumulation} = 0 \tag{34}$$

By plugging expressions 32, 33 and 34 into 31, the following equation results:

$$\left(W_G \frac{dY}{Y_0}\right)\bar{y}\Big|_X - \left(W_G \frac{dY}{Y_0}\right)\bar{y}\Big|_{X+\Delta X} - K_{OG}aP(\bar{y}-\bar{y}^*)dXdYZ_0 = 0 \tag{35}$$

By expanding the quantity evaluated at $X+\Delta X$ in the Taylor series,

$$\left(W_G \frac{dY}{Y_0}\right)\bar{y}\Big|_{X+\Delta X} = \left(W_G \frac{dY}{Y_0}\right)\bar{y}\Big|_X + \left(W_G \frac{dY}{Y_0}\right)\frac{\partial \bar{y}}{\partial X}dX \tag{36}$$

By substituting (36) into 35 and simplifying, the following equation is obtained:

$$-\left(W_G \frac{dY}{Y_0}\right)\frac{\partial \bar{y}}{\partial X}dX - K_{OG}aP(\bar{y}-\bar{y}^*)dXdYZ_0 = 0 \tag{37}$$

By using Equation 29, the above equation can be written as

$$\left(W_L \frac{dX}{X_0}\right)\frac{\partial \bar{x}}{\partial Y}dY = K_{OG}aP(\bar{y}-\bar{y}^*)dXdYZ_0 \tag{38}$$

Upon dividing both sides of Equation (38) by dXdY,

$$\left(\frac{W_L}{X_0}\right)\frac{\partial \bar{x}}{\partial Y} = K_{OG}aP(\bar{y}-\bar{y}^*)Z_0 \tag{39}$$

where

$$\bar{y}^* = m_H\bar{x} \quad \text{Equilibrium line} \tag{40}$$

The symbols used in the above equation are as follows:

W_G = average gas flow rate, kgmole/hr

W_L = average liquid flow rate, kgmole/hr

$\bar{x}$ = local concentration of solute gas in the liquid phase, mole fraction

$\bar{y}$ = local concentration of solute gas in the gas phase, mole fraction

$\bar{y}^*$ = local concentration of $\bar{y}$ equipibrium with $\bar{x}$, mole fraction

m_H = Henry's law constant

$K_{OG}a$ = overall gas capacity coefficient, kgmole/hr m^3Pa

P = pressure, Pa

X = horizontal coordinate (gas flow direction) , m

Y = vertical coordinate (liquid flow direction), m

X_0 = effective tower depth, m

Y_0 = effective tower height, m

Z_0 = effective tower width, m

1. Solution. In order to solve the equations presented in the previous section the tower was divided into subdivisions as shown in Figure 27. By denoting the number of subdivision in two dimensions of the tower with m and n, the tower dimensions can be written as

$$X_0 = n\Delta X \tag{41}$$

$$Y_0 = m\Delta Y \tag{42}$$

By putting equation 30 in terms of the finite difference and substituting X_0 and Y_0 by equations 41 and 42, respectively, the following equation was obtained:

$$-\frac{W_G}{m\Delta Y}\frac{\Delta\bar{y}}{\Delta X} = \frac{W_L}{n\Delta X}\frac{\Delta\bar{x}}{\Delta Y} \tag{43}$$

Further simplification would yield,

$$\frac{\Delta\bar{y}}{\Delta\bar{x}} = -\frac{W_L m}{W_G n} \tag{44}$$

To simplify the mathematics further, m = n was chosen,

$$\frac{\Delta\bar{y}}{\Delta\bar{x}} = -\frac{W_L}{W_G} \tag{45}$$

Finite difference representation of the tower is shown in Figure 28. If the change in the solute concentration is considered for (i,j)th division of the tower, as shown in Figure 29, then equation 45 could be written as

$$\frac{\bar{y}_{i,j+1} - \bar{y}_{i,j}}{\bar{x}_{i+1,j} - \bar{x}_{i,j}} = -\frac{W_L}{W_G} \tag{46}$$

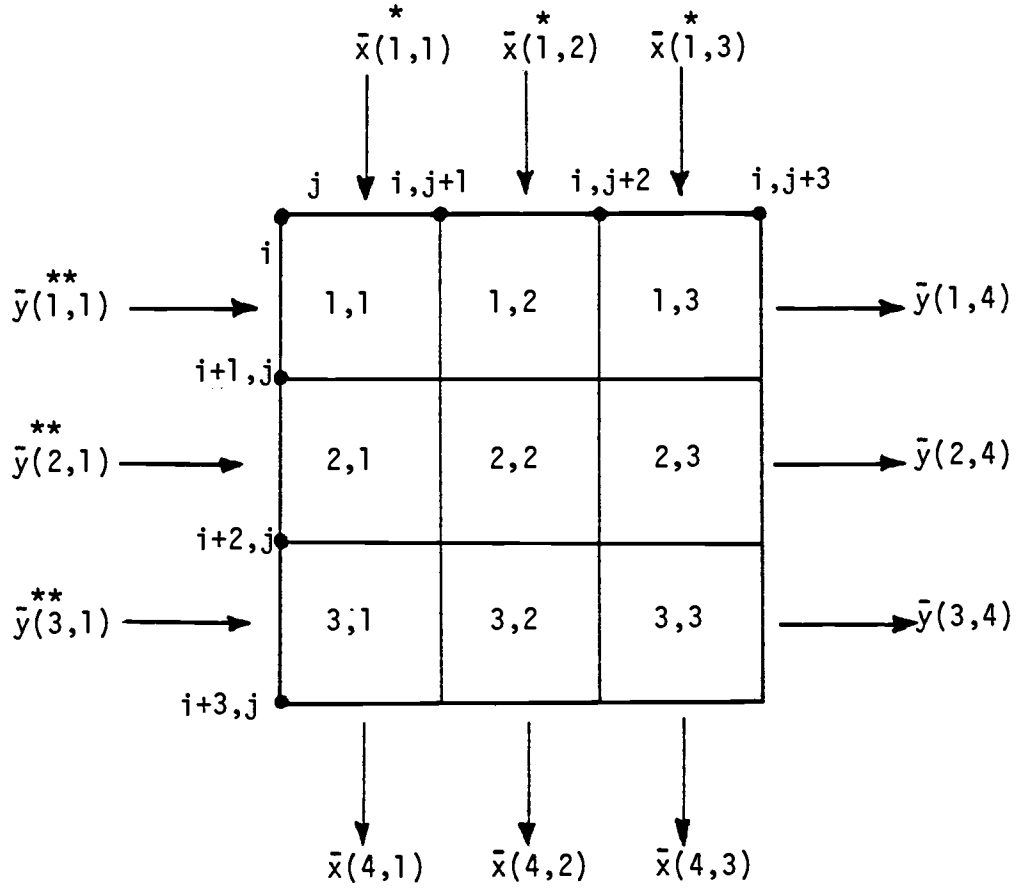

* $\bar{x}(1,1)=\bar{x}(1,2)=\bar{x}(1,3)$

** $\bar{y}(1,1)=\bar{y}(2,1)=\bar{y}(3,1)$

Figure 28. Finite Difference Representation of Each Stage.

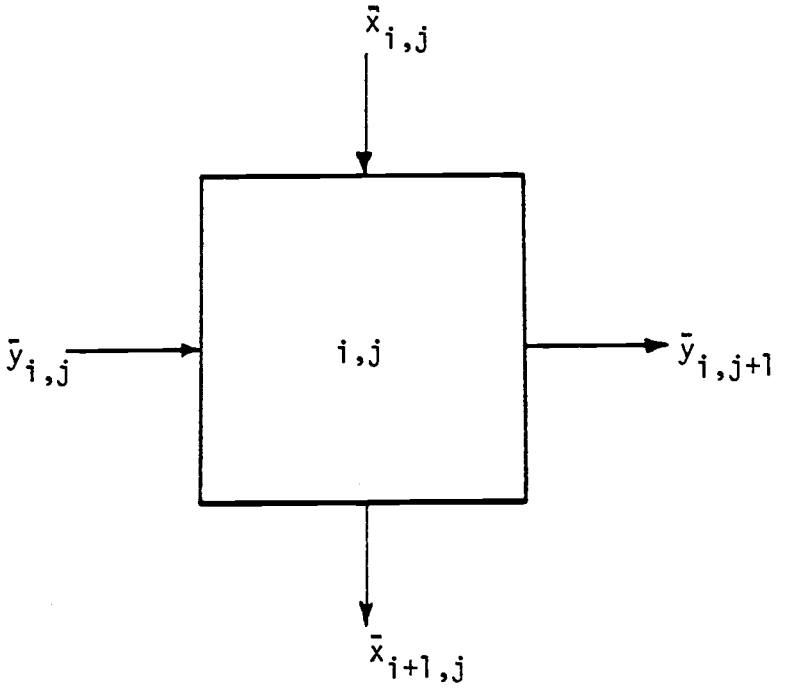

Figure 29. Representation of (i,j)th Division of the Crossflow Column.

Solving for $\bar{y}_{i,j+1}$ would put the above equation in the form of

$$\bar{y}_{i,j+1} = \bar{y}_{i,j} - \frac{W_L}{W_G}(\bar{x}_{i+1,j} - \bar{x}_{i,j}) \tag{47}$$

Equation 47 represents the operating line for the system.

If the finite difference technique is applied, Equation 39 can also be written as,

$$\frac{\Delta\bar{x}}{\Delta Y} = \frac{K_{OG}aP(\bar{y}-\bar{y}^*)}{W_L/X_O Z_O} \tag{48}$$

Again for the (i,j)th division the above equation can be written as

$$\frac{\bar{x}_{i+1,j} - \bar{x}_{i,j}}{\Delta Y} = \frac{K_{OG}aP(\bar{y}-\bar{y}^*)}{W_L/X_O Z_O} \tag{49}$$

In addition, $\bar{y}$ and $\bar{y}^*$ in a small element can be estimated by the following expressions:

$$\bar{y} = 1/2(\bar{y}_{i,j} + \bar{y}_{i,j+1}) \tag{50}$$

$$\bar{y}^* = 1/2(\bar{y}^*_{i,j} + \bar{y}^*_{i,j+1}) \tag{51}$$

By using the equilibrium relationship, Equation 40, $\bar{y}^*$'s can be replaced by the following expressions:

$$\bar{y}^*_{i,j} = m_H \bar{x}_{i,j} \tag{52}$$

$$\bar{y}^*_{i,j+1} = m_H \bar{x}_{i,j+1} \tag{53}$$

Then substituting 52 and 53 into 51 would yield

$$\bar{y}^* = \frac{m_H}{2}(\bar{x}_{i,j} + \bar{x}_{i,j+1}) \tag{54}$$

In equation 49, $\bar{y}$ and $\bar{y}^*$ were replaced by their equivalent expressions from Equations (50) and (54), respectively.

$$\bar{x}_{i+1,j} - \bar{x}_{i,j} = \frac{K_{OG}aP\Delta Y}{2W_L/X_OZ_O}(\bar{y}_{i,j} + \bar{y}_{i,j+1} - m_H\bar{x}_{i,j} - m_H\bar{x}_{i,j+1}) \tag{55}$$

Since the exit liquid and entrance gas concentrations were known from the experimental data, Equation (55) was solved for $x_{i,j}$. If the known parameters on the right hand side of the above equality are lumped together, the following dimensionless parameter would be obtained:

$$B = \frac{K_{OG}aP\Delta Y}{2W_L/X_OZ_O} \tag{56}$$

Upon substituting (56) into (55),

$$\bar{x}_{i,j}(m_HB-1) = -\bar{x}_{i,j+1}(m_HB+1) + B(\bar{y}_{i,j} + \bar{y}_{i,j+1}) \tag{57}$$

or,

$$\bar{x}_{i,j} = \frac{(m_HB+1)\bar{x}_{i,j+1} - B(\bar{y}_{i,j} + \bar{y}_{i,j+1})}{1-m_HB} \tag{58}$$

The unknown quantity $\bar{y}_{i,j+1}$ in Equation (58) can simply be eliminated by using the equation of operating line, Equation (47). Also by assuming $\bar{x}_{i,j+1} \simeq \bar{x}_{i+1,j}$, Equation (58) can be written as

$$\bar{x}_{i,j}(1-Bm_H) = (Bm_H+1)\bar{x}_{i,j+1} - 2B\bar{y}_{i,j} + B\frac{(W_L)}{(W_G)}\bar{x}_{i,j+1} - B\frac{(W_L)}{(W_G)}\bar{x}_{i,j} \tag{59}$$

By factoring out the common terms, the following expression results:

$$\bar{x}_{i,j}(1+B(\frac{W_L}{W_G}-m_H))-\bar{x}_{i,j+1}(1+B(\frac{W_L}{W_G}+m_H))-2B\bar{y}_{i,j} \tag{60}$$

And finally solve for $x_{i,j}$ in terms of known quantities,

$$\bar{x}_{i,j} = \frac{(1+B(\frac{W_L}{W_G}+m_H))\bar{x}_{i,j+1} - 2B\bar{y}_{i,j}}{1+B(\frac{W_L}{W_G}-m_H)} \tag{61}$$

In the above equation all the quantities are known and thus $\bar{x}_{i,j}$ can be calculated. Then knowing $\bar{x}_{i,j}$ and using Equation (47), the operating line, $\bar{y}_{i,j+1}$ (exit gas concentration from (i,j)th division) can be obtained. Information from this division could then be used to calculate the entrance liquid and the exit gas concentration for the next division until the concentration of the gas and liquid are known throughout the single-stage column.

2. Number and Volume of Transfer Units. In studying mass transfer, the concept of a transfer unit is commonly used for interpreting and correlating the experimental data. In this work the idea of the "Volume of a Transfer Unit" (VTU) introduced by Thibodeaux et al. (16), was used. The investigators related the volume of the tower to product of the volume of a transfer unit and square root of the number of overall transfer units as following:

$$V = V_0 N_{0t}^{\frac{1}{2}} \tag{62}$$

where:

V = volume of the tower, m^3

V_0 = volume of a transfer unit, VTU, m^3

N_{0t} = number of overall transfer units, dimensionless

The number of overall transfer units was obtained by integrating the overall and component balance equations. The resulted expression was presented in the form of

$$N_{0t} = \sum_{n=1}^{n} \left[\int_{\bar{y}_{i,j+1}}^{\bar{y}_{i,j}} \frac{d\bar{y}}{\bar{y}-\bar{y}^*} \int_{\bar{x}_{i,j}}^{\bar{x}_{i+1,j}} \frac{d\bar{x}}{\bar{x}^*-\bar{x}} \right] \tag{63}$$

Integration of the above equation and noting that $\bar{x}_{i,j+1} \simeq \bar{x}_{i,j}$ and $\bar{y}_{i+1,j} \simeq \bar{y}_{i,j}$ would yield

$$N_{0t} = \sum_{i=1}^{} \sum_{j=1}^{} \ln\left(\frac{\bar{y}_{i,j}-m\bar{x}_{i,j}}{\bar{y}_{i,j+1}-m\bar{x}_{i,j}}\right) \ln\left(\frac{\bar{y}_{i,j}/m-\bar{x}_{i+1,j}}{\bar{y}_{i,j}/m-\bar{x}_{i,j}}\right) \tag{64}$$

Once the N_{0t} was calculated, Equation (62) was used to evaluate the volume of a transfer unit. V_0, volume of a transfer unit, reflects the efficiency of the mass transfer equipment while $N_{0t}^{\frac{1}{2}}$ reflects the difficulty of the separation.

The cascade calculations were performed stagewise by use of the N_{0t} results of the single stage units.

C. Procedure to Calculate the Percent Bypass in the Cascade Crossflow Column

The conceptual model presented in the previous section illustrated the concept of the bypass in the cascade crossflow column. Since no analytical tool could measure the bypass, the following trial and error procedure was adopted to evaluate the bypass:

1. A percentage bypass was assumed.
2. According to the flow diagram shown in Figure 25, the gas and liquid flow rates were determined.
3. Equations (61) and (47) were used to calculate the entrance liquid and exit gas compositions for the single-stage crossflow column, respectively.
4. New concentration of the gas for entering the next stage was calculated.
5. New flow rates were evaluated (see Figure 25) and were used along with the liquid and gas concentrations to perform the calculations for the next stage.
6. Steps 3 and 4 were repeated until the top of the column was reached.
7. The calculated concentrations of the gas and liquid at the top of the column were compared with the obtained experimental values.
8. If the agreements between these values were satisfactory, the correct bypass was assumed to have been chosen; otherwise, a new bypass was guessed and the steps 2 through 7 were repeated.

D. Testing of the Proposed Model Against the Experimental Data for the Region Before the Transition Point

The multiple stage crosscurrent packed column operates with a combination of contact patterns, as described in the previous section. At various gas and liquid flow rates different contact action exists within the column. At low gas rates the entire gas stream likely does not cross the packed section; fraction of the gas crosses the packing and the rest penetrates the packing only enough to slip around the baffles, as pictured in Figure 24.

The region of the column prior to the transition point was modeled as a crossflow column with a percentage of the gas flow bypassing the baffles. A computer program was developed to perform the trial-and-error procedure presented in Section C of this chapter. Results are shown in Figure 30.

The percent bypass decreased as the column approached the transition point. The gas bypass essentially vanished as the transition was reached. This behavior was observed with the L/G ratios of 1.5, 2.0, 3.0 and 4.0, as shown in Figure 30. At a constant gas rate, the percent bypass decreased with an increase in the L/G ratio. This behavior was anticipated in the column and was pointed out in the presentation of the experimental work. An increase in the L/G ratio meant an increase in the liquid availability in the column, causing the liquid to exert more force to decrease the bypassing phenomenon.

An equation of the form $f(X)=AX^B-C$ was proposed to correlate the percent bypass with the gas rate. In order to find the best values of A, B and C, a "least square" fit through the data points was

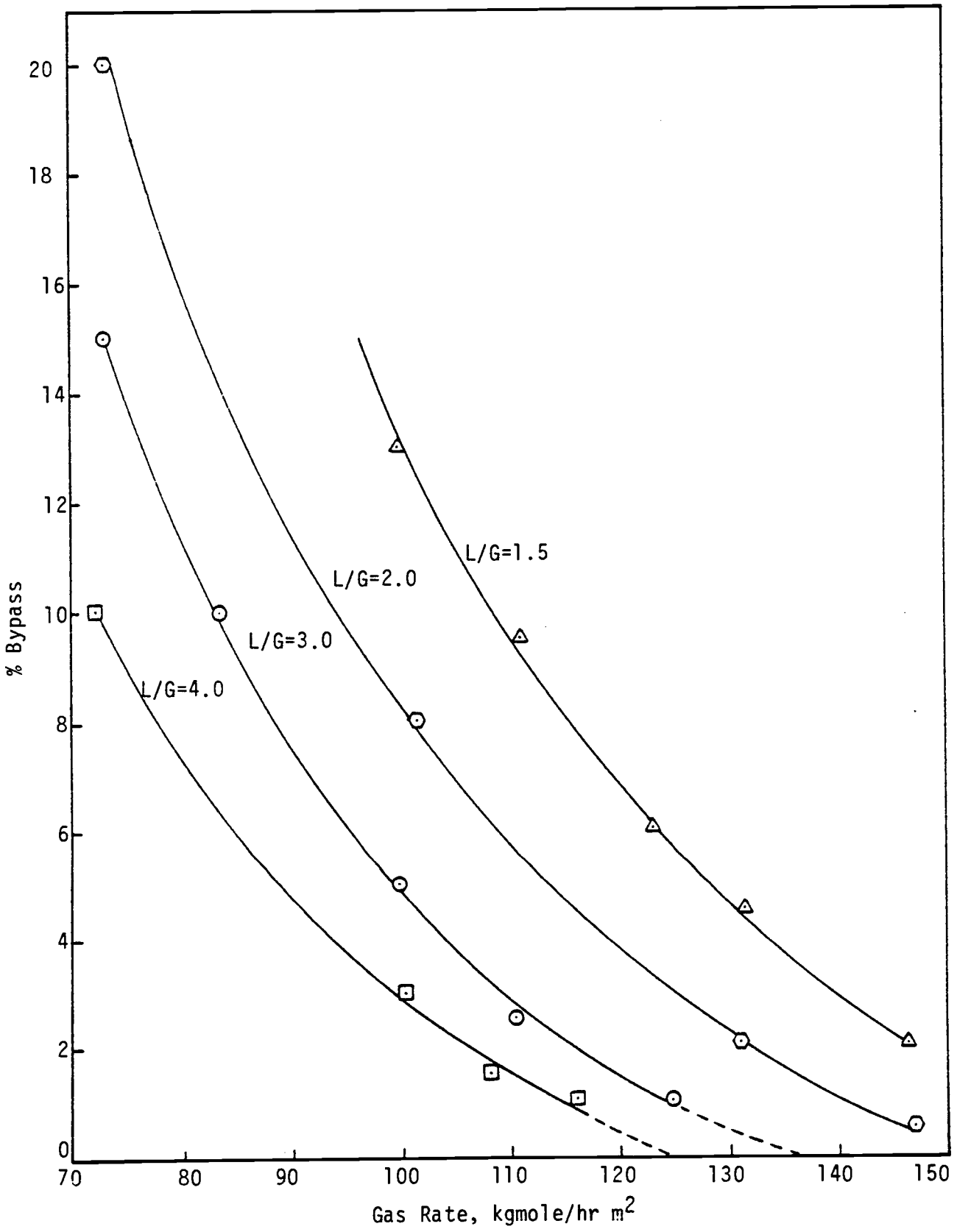

Figure 30. Gas Bypass as a Function of Gas Rate as Predicted by the Proposed Model.

performed and the values of the coefficients were obtained so that the variance of the curve was minimized. The minimization of the variance was achieved by developing a computer program. The procedure incorporated in the program was that an initial value of C was assumed and the least square fit was performed. The value of C was the incremented. Every time C was incremented, the values of A, B, C as well as the variance were printed. By observing the variance going through a minimum, the best values of A, B and C were determined. The obtained values of A, B and C resulted in the following correlations between the percent bypass and the gas rate (kgmole/hr m^2), for the L/G ratios investigated in this work:

$$\% \text{ bypass} = 21721(G)^{-1.466} - 12.50, \text{ for } L/G = 1.5 \quad (65)$$

$$\% \text{ bypass} = 51647(G)^{-1.753} - 7.79, \text{ for } L/G = 2.0 \quad (66)$$

$$\% \text{ bypass} = 218927(G)^{-2.159} - 5.65, \text{ for } L/G = 3.0 \quad (67)$$

$$\% \text{ bypass} = 60638(G)^{-1.937} - 5.18, \text{ for } L/G = 4.0 \quad (68)$$

With standard deviations of 0.2982, 0.2927, 0.3822 and 0.3514 for L/G ratios of 1.5, 2.0, 3.0 and 4.0, respectively.

A different approach was followed to correlate the information given in Figure 30. At a constant gas rate the values of the percent bypass were plotted against the L/G ratios on a log-log paper. As can be seen from Figure 31, these points resulted in a straight line for the gas rate of 100 kgmole/hr m^2. This procedure was repeated for several gas rates between 100 kgmole/hr m^2 and 115 kgmole/hr m^2 since this gas

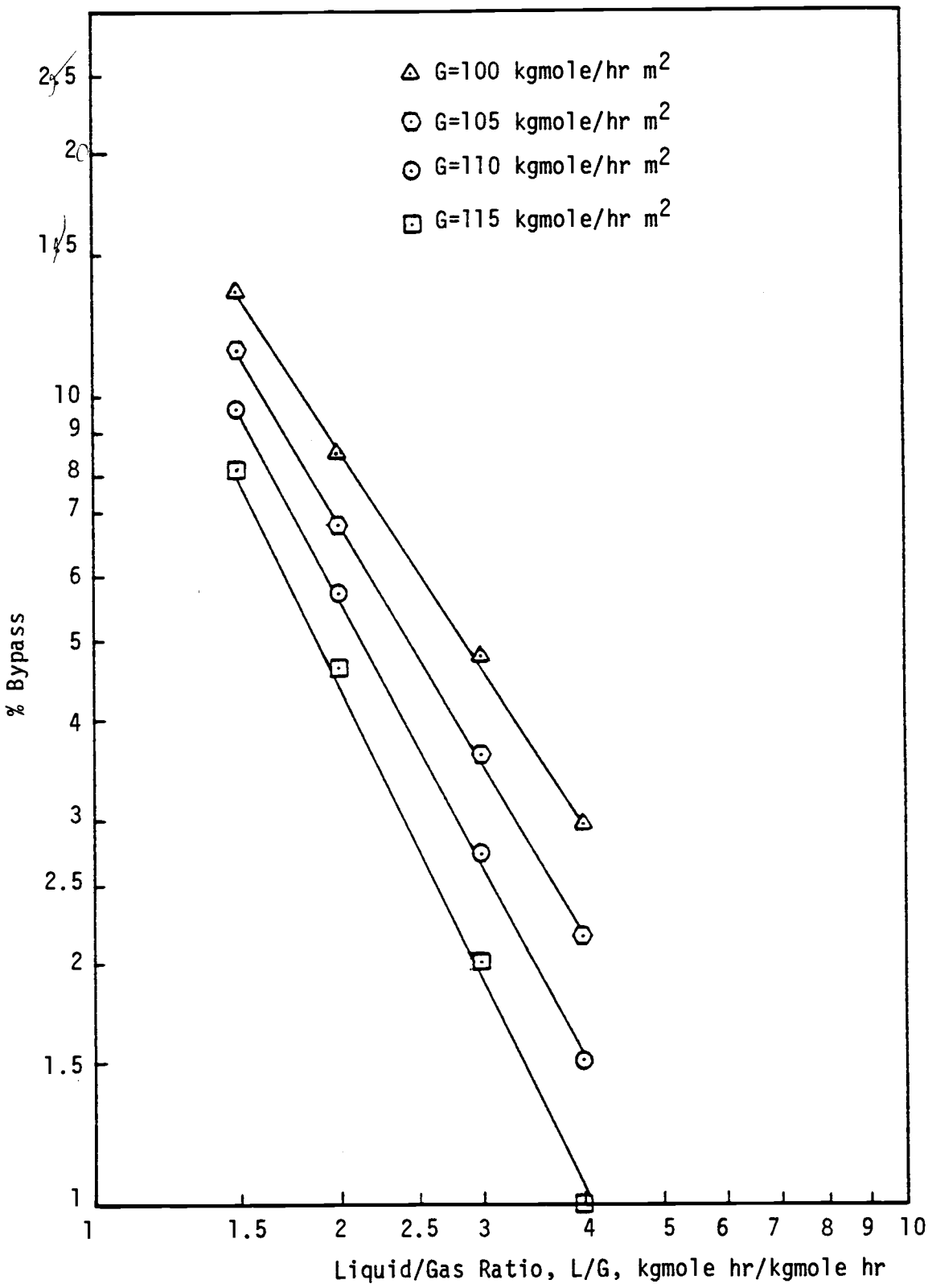

Figure 31. Percent Gas Bypass as a Function of L/G for Various Gas Rates.

range was common among the L/G ratios. Again the functional form of $f(X) = AX^B - C$ was proposed and the "least square" fit resulted in the best values of the coefficients which minimized the variance of the curve. The correlations between the percent bypass and the L/G ratios for the gas rates of 100, 105, 110 and 115 kgmole/hr m^2 are given as:

$$\% \text{ bypass} = 25.10\ (L/G)^{-1.60} + 0.260, \text{ for } G = 100 \text{ kgmole/hr } m^2 \quad (69)$$

$$\% \text{ bypass} = 22.68\ (L/G)^{-1.71} + 0.055, \text{ for } G = 105 \text{ kgmole/hr } m^2 \quad (70)$$

$$\% \text{ bypass} = 20.15\ (L/G)^{-1.75} - 0.275, \text{ for } G = 110 \text{ kgmole/hr } m^2 \quad (71)$$

$$\% \text{ bypass} = 17.82\ (L/G)^{-1.78} - 0.550, \text{ for } G = 115 \text{ kgmole/hr } m^2 \quad (72)$$

with standard deviations of 0.1889, 0.0911, 0.0496 and 0.0487, respectively.

An attempt was made to generate a correlation which would predict the bypass behavior of the column for any gas rate and any L/G ratios (at least for the L/G ratios investigated in this work). It was not easy to find a general correlation which would predict the gas bypass reasonably accurate for the whole range of gas rates. However, for the gas rate between 100 kgmole/hr m^2 to 115 kgmole/hr m^2 the following correlation presented the system's behavior rather accurately:

$$\% \text{ bypass} = A(L/G)^{-B} + C \quad (73)$$

where:

$$A = 75.0 - \frac{G}{2}$$

$$B = 0.65 + \frac{G}{100}$$

$$C = 5.88 - 0.056\ G$$

and the gas rate, G, is in kgmole/hr m^2.

The proposed model agreed well with the experimental values. Tables 4, 5, 6 and 7 along with Figure 32 illustrate how well the proposed model predicts the system's behavior.

The percent error for predicting the absorption efficiency, as shown in the last column of Tables 4, 5, 6 and 7, ranged from .087% to 5.07% with a major function of the points within 1% agreement. This is well within the experimental accuracy, considering the experimental limitation. The calculated values of the entrance liquid concentration were below the limit of detection with the available titration technique and were assumed to be zero which agreed with the experimental values (pure wastes).

In Figure 32, the solid lines are the best fit through the experimental data and the points shown on the curves are the model values. As can be seen the agreement between the experimental and the model values are relatively well for all L/G ratios.

Therefore, it is concluded that the bypass model is an accurate and clear representation of the crossflow column for the region prior to the transition point.

1. Efficiency of the Crosscurrent Column in Terms of the Volume of a Transfer Unit (VTU). The concept of volume of transfer unit and the relevant equations were presented in the theoretical section of this chapter. The experimental and theoretical values of the volume

Table 4. Comparison Between the Experimental Values and the Values Obtained from the Proposed Model, for L/G = 1.5.

Condition: Prior to the Transition Point.

Gas Rate, kgmole/hr m^2	Entrance Liq. Conc., x_1 mole frac.	Entrance Gas Conc., y_1 mole frac.	Exit Gas Concentration, y_2, mole fraction		Absorption Efficiency, %		
	Model*	Experimental	Experimental	Model	Experimental	Model	Error,
99.62	.0005	.00907	.00297	.00303	67.30	66.57	1.10
111.10	.0006	.01559	.00503	.00502	67.70	67.77	0.11
123.33	.0002	.0086	.00265	.00262	69.30	69.61	0.44
131.59	.0004	.01324	.00391	.00341	70.50	74,27	5.07
146.96	.0001	.01304	.00370	.00373	71.60	71.39	0.29

*The values are below limit of detection with the available analytical tools, therefore can be assumed to be zero.

Table 5. Comparison Between the Experimental Values and the Values Obtained from the Proposed Model, for L/G = 2.0.

Condition: Prior to the Transition Point.

Gas Rate, kgmole/hr m^2	Entrance Liq. Conc., x_1 mole frac.	Entrance Gas Conc., y_1 mole frac.	Exit Gas Concentration, y_2, mole fraction		Absorption Efficiency, %		
	Model*	Experimental	Experimental	Model	Experimental	Model	Error,
73.30	.000115	.0202	.00554	.00527	72.90	73.89	1.34
101.58	.000514	.0193	.00464	.00455	76.00	76.43	.569
131.11	.000163	.01978	.00472	.00468	76.10	76.33	.307

*The values are below limit of detection with the available analytical tools, therefore can be assumed to be zero.

Table 6. Comparison Between the Experimental Values and the Values Obtained from the Proposed Model, for L/G = 3.0.

Condition: Prior to the Transition Point.

Gas Rate, kgmole/hr m^2	Entrance Liq. Conc., x_1 mole frac.	Entrance Gas Conc., y_1 mole frac.	Exit Gas Concentration, y_2, mole fraction		Absorption Efficiency, %		
	Model*	Experimental	Experimental	Model	Experimental	Model	Error,
73.05	.000544	.01439	.00338	.00354	76.5	75.39	1.48
83.51	.000417	.01453	.00308	.00324	78.8	77.70	1.41
99.55	.000204	.01387	.00293	.00296	78.9	78.64	0.33
110.46	.000192	.01416	.00272	.00304	80.8	78.53	2.89
124.84	.000126	.01465	.00287	.00309	80.4	78.89	1.91

*The values are below limit of detection with the available analytical tool, therefore can be assumed to be zero.

Table 7. Comparison Between the Experimental Values and the Values Obtained from the Proposed Model, for L/G = 4.0.

Condition: Prior to the Transition Point.

Gas Rate, kgmole/hr m^2	Entrance Liq. Conc., x_1 mole frac.	Entrance Gas Conc., y_1 mole frac.	Exit Gas Concentration, y_2, mole fraction		Absorption Efficiency, %		
	Model*	Experimental	Experimental	Model	Experimental	Model	Error,
72.32	.00035	.0201	.00364	.00349	81.90	82.61	0.86
100.54	.00012	.01965	.00296	.00293	85.00	85.07	0.087
108.13	.000008	.01895	.00307	.00286	84.00	84.92	1.09
116.28	.000005	.01910	.00304	.00293	84.00	84.64	0.75

*The values are below limit of detection with the available analytical tools, therefore can be assumed to be zero.

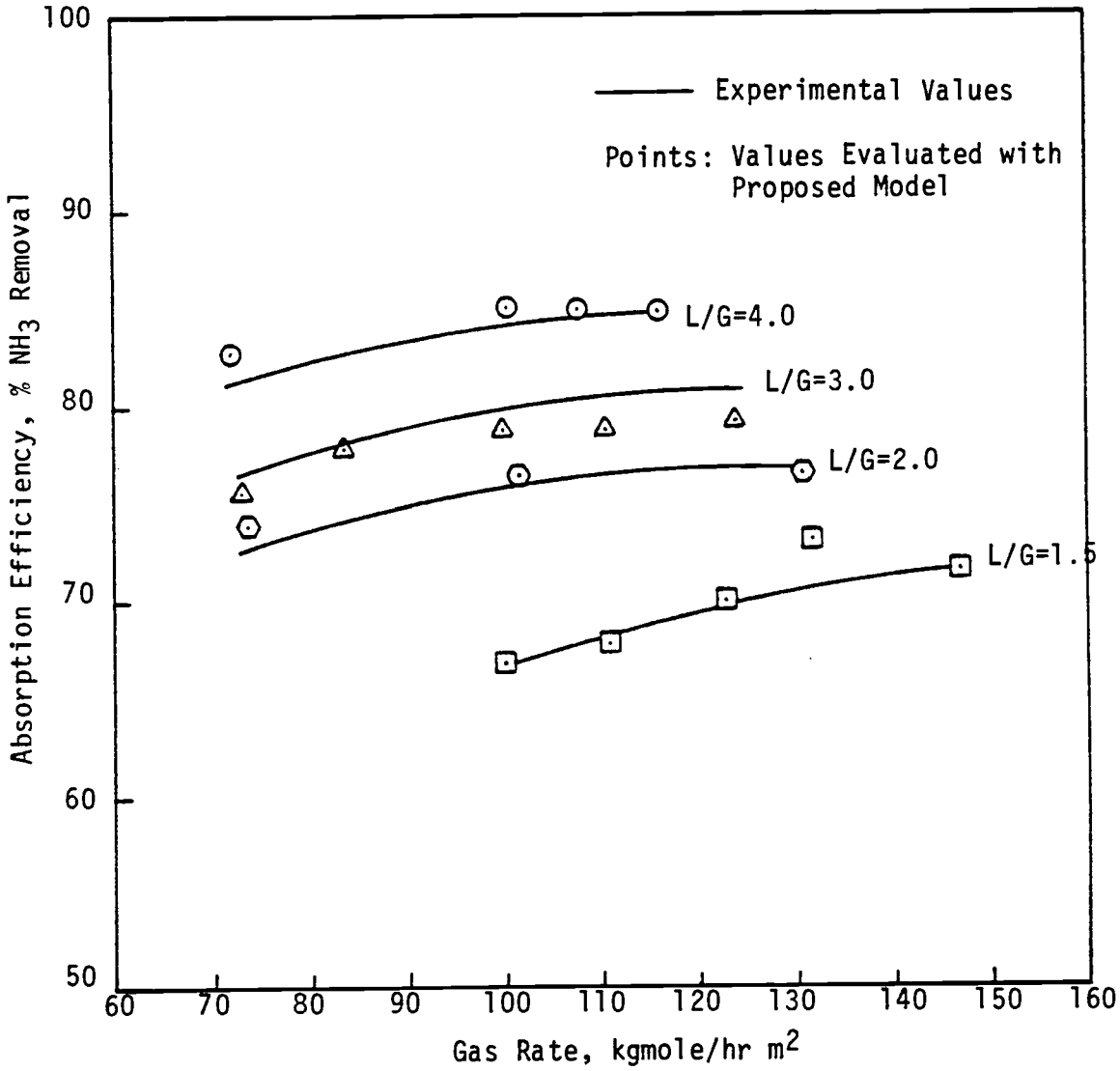

Figure 32. Comparison Between the Experimental and Model Values of Absorption Efficiency for the Region Prior to the Transition.

of a transfer unit were calculated for the region prior to the transition point for the L/G ratios of 1.5, 2.0, 3.0 and 4.0. The experimental "VTU" values were calculated through the definition of the volume of a transfer unit, given by Thibodeaux (16), using the experimental values. The theoretical "VTU" values were obtained by adding up the N_{0t} values from each stage, using the values predicted by the model, and then applying Eq. 62 to calculate VTU values.

The experimental values of the volume of transfer units, as a function of gas rate, are shown in Figure 33 for L/G ratios of 1.5, 2.0, 3.0 and 4.0. The "VTU" decreased as the L/G ratio increased at a constant gas rate. Also for a constant L/G ratio, the VTU decreased as the gas rate increased, as can be seen from Figure 33. A lower VTU value corresponds to better mass transfer efficiency. In other words, a smaller value of VTU means that it takes a smaller column to accomplish the same mass transfer job. As the VTU decreases, the absorption efficiency increases. A careful evaluation of Figures 14 and 33 confirms the above statement.

The same dependency on the L/G ratio was observed with VTU as was observed with the absorption efficiency; the efficiency increased (VTU decreased) with either an increase in the L/G ratio or an increase in the gas rate and flattened as the system approached the transition point. It will be shown in the next section that the efficiency starts increasing (VTU decreasing) again after the system passes the transition. This phenomenon was also observed with the absorption efficiency data.

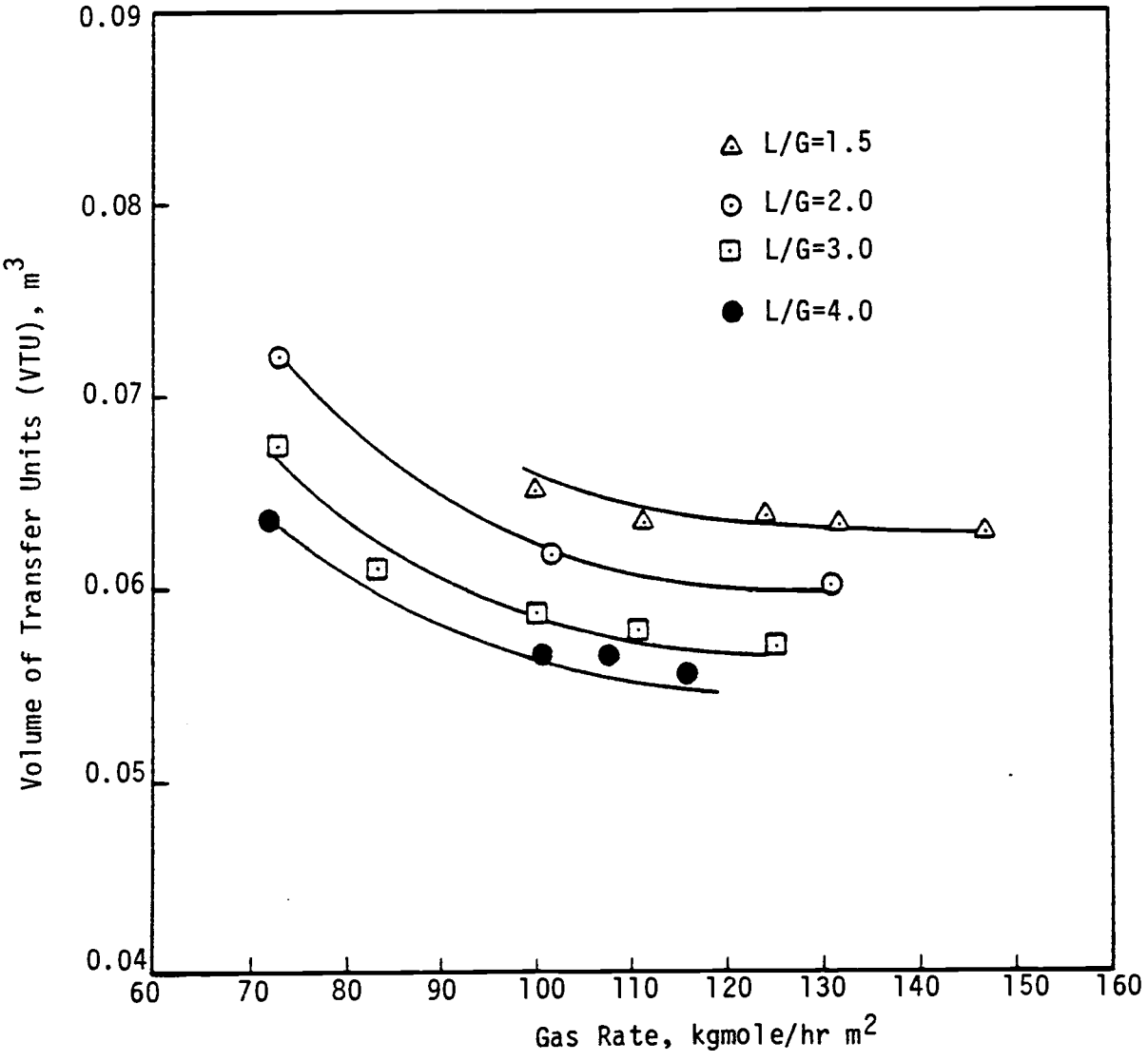

Figure 33. Volume of Transfer Units for Various L/G Ratios for the Region Prior to the Transition Point.

A comparison between the theoretical and the experimental VTU values are presented in Tables 8 and 9 for the L/G ratios investigated in this study. As can be seen from the tables, the agreement is within 10%. Although the percent error indicated a higher degree of deviation between the experimental and the theoretical values than for the absorption efficiency, both methods were good indications of mass transfer efficiency of the crosscurrent column.

E. Testing of the Proposed Model Against the Experimental Data for the Region after the Transition Point

The second distinguished zone in the crosscurrent column was recognized as the region after the transition point. After the transition point was reached, the liquid was deflected into the void space and accumulated on the baffles. The existence of the mixing action in the packing and the baffles was observed and discussed in the presentation of the experimental work. It was mentioned that the mixing action might compensate for the loss of efficiency due to the dead space.

As shown previously, the region of the column prior to the transition was modeled as a crossflow with a certain percentage of the gas flow bypassing the baffles. Once the transition was reached, the bypassing phenomenon essentially vanished. Therefore, the model presented for the region prior to the transition was employed and the bypass was assumed to be zero. This zero bypass model was applied to the physical system and the results are presented in Tables 10, 11, 12 and 13, and Figure 34.

Table 8. Experimental and Theoretical Values of Volume of a Transfer Unit (VTU) for L/G Ratios of 1.5 and 3.0.

Condition: Prior to the Transition Point.

L/G = 1.5				L/G = 3.0			
Gas Rate, kgmole/hr m^2	$(VTU)_{exp.}$, m^3	$(VTU)_{Theo.}$, m^3	Error, %	Gas Rate, kgmole/hr m^2	$(VTU)_{exp.}$, m^3	$(VTU)_{Theo.}$, m^3	Error, %
99.62	0.0651	0.0590	9.37	73.05	0.0674	0.0601	10.83
111.10	0.0634	0.0594	6.31	83.52	0.0609	0.0572	6.07
123.33	0.0637	0.0618	2.98	99.55	0.0586	0.0577	1.54
131.59	0.0631	0.0622	1.43	110.52	0.0578	0.0584	1.04
146.95	0.0628	0.0634	0.95	124.84	0.0569	0.0580	1.94

Table 9. Experimental and Theoretical Values of Volume of a Transfer Unit (VTU) for L/G Ratio of 2.0 and 4.0.

Condition: Prior to the Transition Point.

L/G = 2.0				L/G = 4.0			
Gas Rate, kgmole/hr m^2	$(VTU)_{exp.}$, m^3	$(VTU)_{Theo.}$, m^3	Error, %	Gas Rate, kgmole/hr m^2	$(VTU)_{exp.}$, m^3	$(VTU)_{Theo.}$, m^3	Error, %
73.50	0.0719	0.0609	15.30	72.32	0.0637	0.0598	6.12
101.58	0.0617	0.0589	4.54	100.54	0.0566	0.0571	0.88
131.11	0.060	0.0608	1.33	108.13	0.0566	0.0582	2.82
				116.27	0.0556	0.0590	6.11

Table 10. Comparison Between the Experimental Values and the Values Obtained from the Proposed Model, for L/G = 1.5.

Condition: After the Transition Point.

Gas Rate, kgmole/hr m^2	Entrance Liq. Conc., x_1 mole frac.	Entrance Gas Conc., y_1 mole frac.	Exit Gas Concentration, y_2, mole fraction		Absorption Efficiency, %		
	Model*	Experimental	Experimental	Model	Experimental	Model	Error,
166.20	0.000002	.0131	.00337	.00340	74-0	74.05	0.072
173.77	0.00001	.0130	.00298	.00300	77.0	76.89	0.14
185.64	0.00002	0.0126	.00263	.00266	79.0	78.90	0.13
209.13	0.000006	0.0125	0.00182	0.00183	85.5	85.4	0.11

*The values are below limit of detection with the available analytical tools, therefore can be assumed to be zero.

Table 11. Comparison Between the Experimental Values and the Values Obtained from the Proposed Model, for L/G = 2.0.

Condition: After the Transition Point.

Gas Rate, kgmole/hr m^2	Entrance Liq. Conc., x_1 mole frac.	Entrance, Gas Conc., y_1 mole frac.	Exit Gas Concentration, y_2, mole fraction		Absorption Efficiency, %		
	Model*	Experimental	Experimental	Model	Experimental	Model	Error,
147.52	0.00007	0.0193	0.00433	0.00441	77.50	77.15	0.46
156.86	0.00003	0.0193	0.00377	0.00376	80.44	80.48	0.05
164.52	0.00045	0.0198	0.00305	0.00308	84.60	84.46	0.16
190.0	0.000007	0.0201	0.00236	0.00239	88.20	88.10	0.11

*The values are below limit of detection with the available analytical tools, therefore can be assumed to be zero.

Table 12. Comparison Between the Experimental Values and the Values Obtained from the Proposed Model, for L/G = 3.0.

Condition: After the Transition Point.

Gas Rate, kgmole/hr m^2	Entrance Liq. Conc., x_1 mole frac.	Entrance, Gas Conc., y_1 mole frac.	Exit Gas Concentration, y_2, mole fraction		Absorption Efficiency, %		
	Model*	Experimental	Experimental	Model	Experimental	Model	Error,
131.47	0.00002	0.0151	0.00278	0.00283	81.60	81.29	0.38
149.07	0.00001	0.0151	0.00215	0.00218	85.80	85.57	0.26
164.61	0.00008	0.0148	0.00153	0.00154	89.70	89.6	0.10
170.88	0.000002	0.0143	0.00139	0.00140	90.30	90.2	0.11
186.93	0.000007	0.0151	0.00136	0.00138	90.95	90.83	0.13
207.99	0.000002	0.0148	0.00117	0.00119	92.09	92.00	0.09

*The values are below limit of detection with the available analytical tools, therefore can be assumed to be zero.

Table 13. Comparison Between the Experimental Values and the Values Obtained from the Proposed Model, for L/G = 4.0.

Condition: After the Transition Point.

Gas Rate, kgmole/hr m^2	Entrance Liq. Conc., x_1 mole frac.	Entrance Gas Conc., y_1 mole frac.	Exit Gas Concentration, y_2, mole fraction		Absorption Efficiency, %		
	Model*	Experimental	Experimental	Model	Experimental	Model	Error,
132.17	0.00003	0.0196	0.00235	0.00240	88.00	87.75	0.28
142.18	0.00003	0.020	0.00221	0.00227	89.00	88.66	0.38
163.67	0.00001	0.020	0.00167	0.00170	91.60	91.47	0.14
167.30	0.000004	0.020	0.00156	0.00159	92.40	92.22	0.19

*The values are below limit of detection with the available analytical tools, therefore can be assumed to be zero.

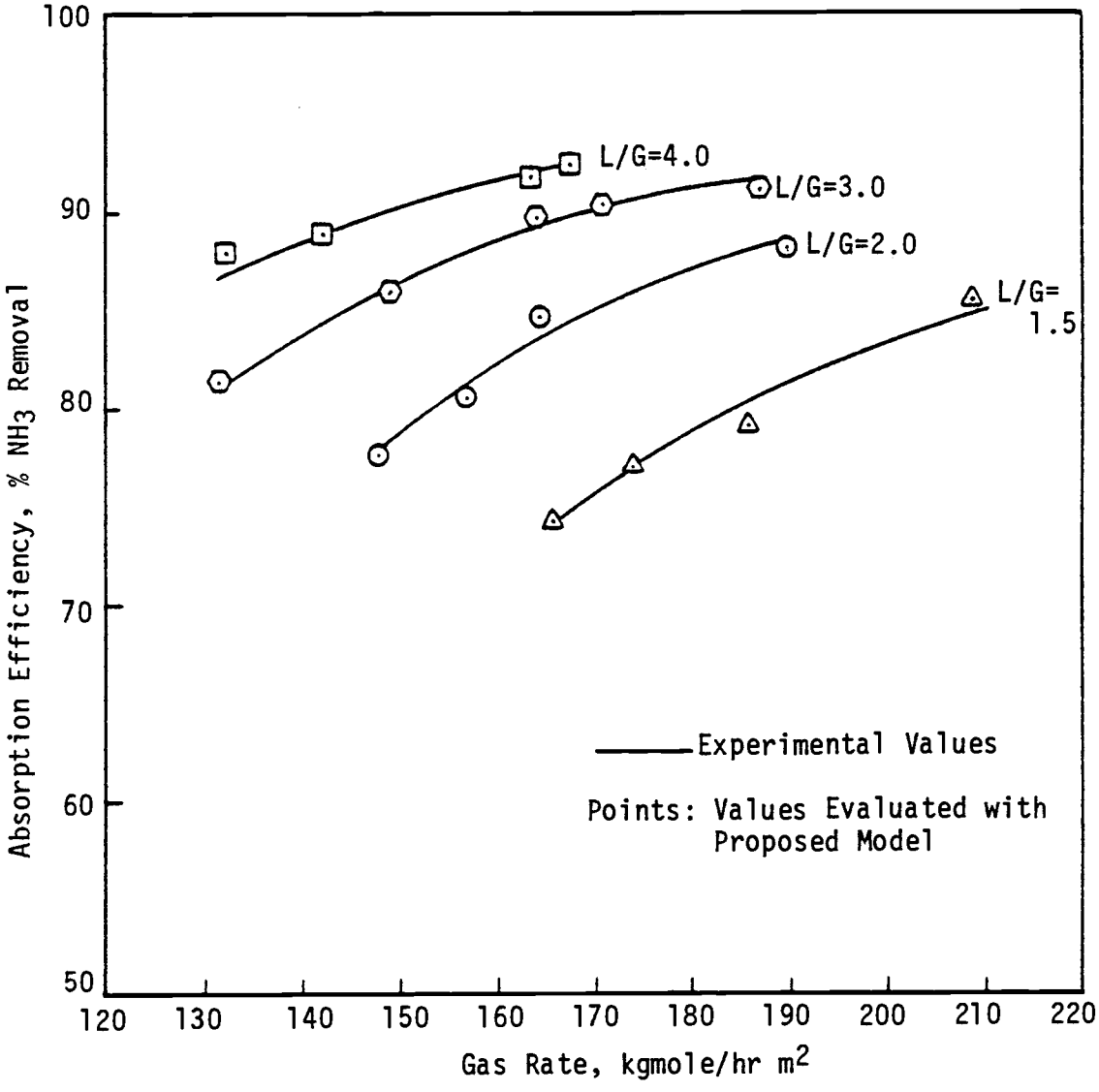

Figure 34. Comparison Between the Experimental and Model Values for the Region After the Transition.

Agreement between the experimental values and the model values for the absorption efficiencies was very good, as shown in Figure 34. Solid curves are the best fit through the experimental values and the points indicated on the curves are the model values. A careful evaluation of Tables 10, 11, 12 and 13 illustrate how well the model predicted the system's behavior. The percent error between the experimental and the model values of the absorption efficiency ranged from .05 to 0.46 which is well within the experimental accuracy. The values of the entrance liquid concentration, shown in the second column of the tables, were definitely below the limit of detection and, accordingly, small enough to be considered zero. It should be mentioned that during the course of modeling this region of the column, the mass transfer coefficients, estimated for the operating conditions of the column, had to be adjusted in order for the entrance liquid concentration to be considered zero. When the mass transfer coefficients for both regions were plotted against the gas rate, an interesting result was obtained. The mass transfer coefficient actually went through a transition. In other words, for the operating conditions of the column, the dotted lines shown in Figure 35 should have been the actual mass transfer coefficient. But these values would have resulted in a non-zero entrance liquid concentration. This indicated that a larger mass transfer coefficient was required when operating above the transition point to account for the mixing action occurring in the column. As the gas rate increased the difference between the adjusted and the actual values increased which accounted for the additional mixing on the baffles. When the system passes through the transition, the liquid accumulation on the baffles are more or less

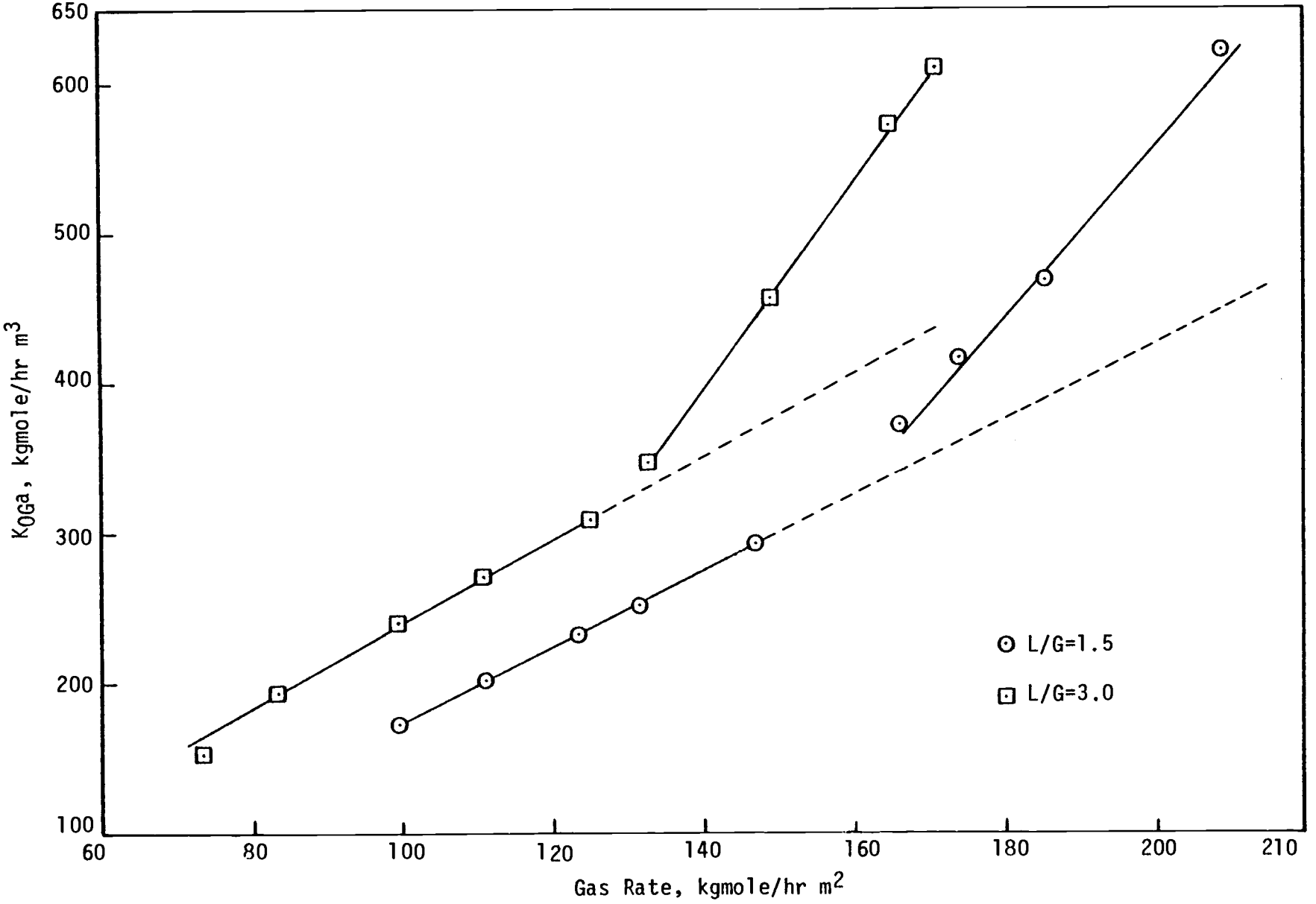

Figure 35. Mass Transfer Capacity as a Function of Gas Rate.

stagnant and mixing is only observed in the packing. However, at higher gas rate the mixing action can be observed on the baffles. For this reason the efficiency of the column increased again after the transition.

1. Efficiency of the Crosscurrent Column in Terms of the Volume of Transfer Units (VTU). The experimental and theoretical values of the VTU were calculated for the L/G ratios of 1.5, 2.0, 3.0 and 4.0. The results are tabulated in Tables 14 and 15.

The experimental values of the volume of transfer units were plotted against the gas rate for various L/G ratios investigated in this work. As shown in Figure 36, the trend observed previously with the absorption efficiency data was observed here as well. For a fixed L/G ratio, the VTU decreased as the gas rate increased. The decrease in VTU is a measure of higher efficiency.

Tables 14 and 15 illustrate a comparison between the experimental VTU values and the values predicted by the model. The agreement is within 5% which is even better than the results obtained for the region prior to the transition point.

Accordingly, the proposed model is capable of predicting the system's behavior before the transition point as well as after the transition point.

F. Testing of the Proposed Model Against the Experimental data for the Expanded Bed

The bypass model, employed for the original bed geometry, was modified for the dimensions of the expanded bed and was used to test the experimental data. In the presentation of the experimental results a

Table 14. Experimental and Theoretical Values of Volume of a Transfer Unit (VTU) for L/G Ratios of 1.5 and 2.0.

Condition: After the Transition Point.

L/G = 1.5				L/G = 2.0			
Gas Rate, kgmole/hr m^2	$(VTU)_{exp.}$, m^3	$(VTU)_{Theo.}$, m^3	Error, %	Gas Rate, kgmole/hr m^2	$(VTU)_{exp.}$, m^3	$(VTU)_{Theo.}$, m^3	Error, %
166.20	.0541	.0559	3.32	147.52	.0535	.0554	3.44
173.77	.0530	.0548	3.47	156.86	.0515	.0534	3.67
185.64	.0524	.0543	3.55	164.52	.0503	.0523	3.97
209.13	.0523	.0543	3.88	190.0	.0490	.0511	4.20

Table 15. Experimental and Theoretical Values of Volume of a Transfer Unit (VTU) for L/G Ratios of 3.0 and 4.0.

Condition: After the Transition Point.

L/G = 3.0				L/G = 4.0			
Gas Rate, kgmole/hr m^2	$(VTU)_{exp.}$, m^3	$(VTU)_{Theo.}$, m^3	Error, %	Gas Rate, kgmole/hr m^2	$(VTU)_{exp.}$, m^3	$(VTU)_{Theo.}$, m^3	Error, %
131.47	.0552	.0571	3.53	132.17	.0498	.0519	4.15
149.07	.0490	.0510	4.04	142.18	.0476	.0497	4.33
164.61	.0476	.0497	4.39	163.67	.0462	.0483	4.64
170.88	.0472	.0493	4.45	167.30	.0458	.0480	4.74
186.93	.0474	.0495	4.54				
207.99	.0465	.0487	4.68				

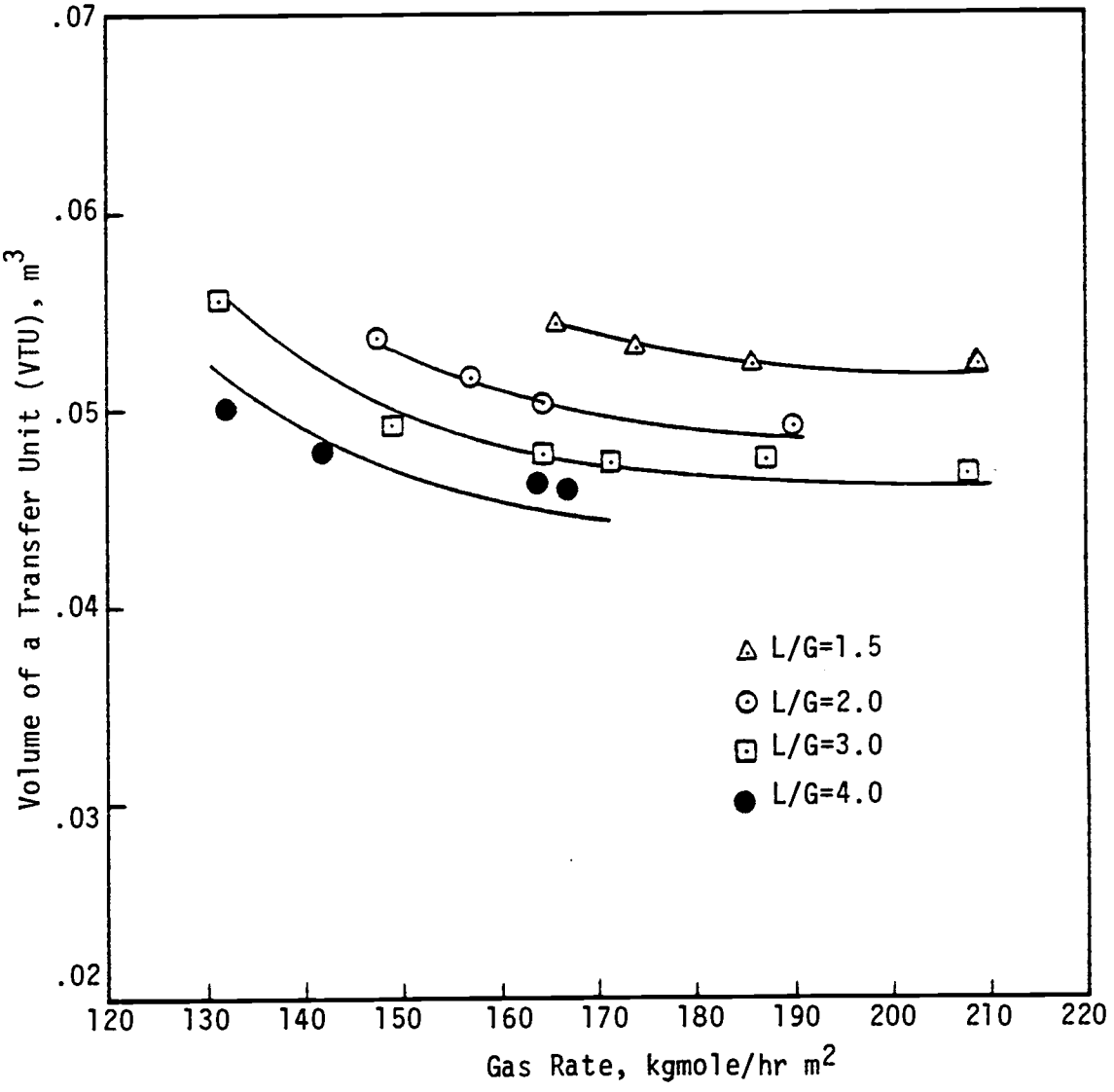

Figure 36. Volume of Transfer Units for Various L/G Ratios for the Region After the Transition Point.

comparison between the two bed configurations was performed. In this section, however, the agreement between the experiment and the proposed model is discussed and proposed correlations are presented.

The percentage of the gas flow bypassing the baffles in the region prior to the transition was obtained by the proposed model for the expanded bed. Results for various L/G ratios are shown in Figure 37.

The percent bypass increased with a decrease in the L/G ratio at a constant gas rate. This confirmed the speculation that at low L/G ratio, a fraction of the gas bypassed the liquid thus causing a decrease in the absorption efficiency. As the flows approached the transition the percentage of the gas flow bypassing the baffles decreased and finally vanished upon further increase in the gas rate.

In order to correlate the percent bypass with the gas rate, the functional form of $F(X) = AX^B+C$ was proposed and the best values of the coefficients were obtained through the least square technique for non-linear equations. The following correlations describe the bypassing phenomenon of the expanded bed as a function of the gas rate for the L/G ratios of 2.0, 3.0 and 4.0:

$$\% \text{ bypass} = 601(G)^{-.4575} - 60.60, \text{ for L/G} = 2.0 \quad (74)$$

$$\% \text{ bypass} = 9300(G)^{-1.346} - 12.53, \text{ for L/G} = 3.0 \quad (75)$$

$$\% \text{ bypass} = 604570(G)^{-2.488} - 3.75, \text{ for L/G} = 4.0 \quad (76)$$

with standard deviations of 1.361, 0.501 and 0.00, respectively.

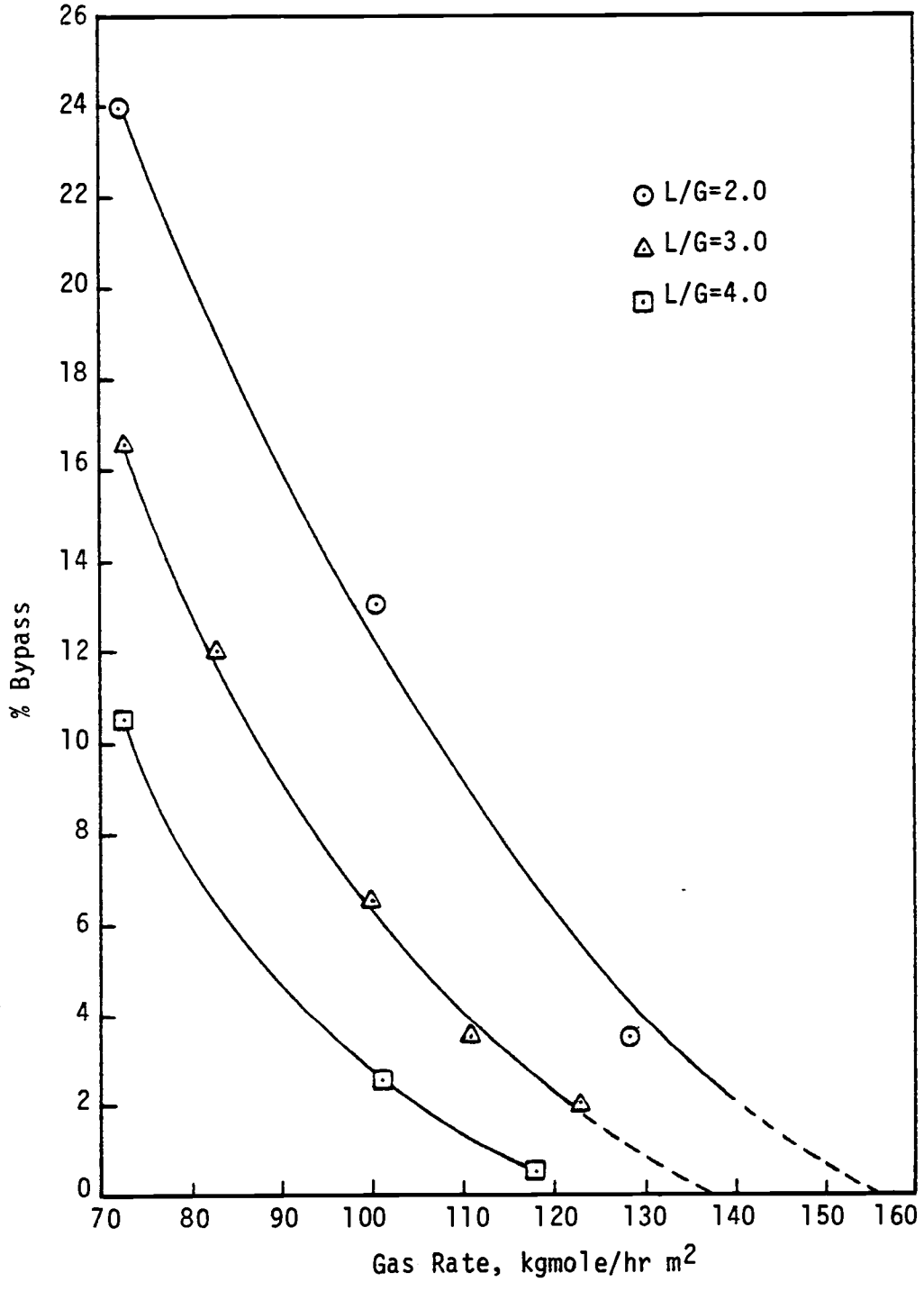

Figure 37. Gas Bypass as a Function of Gas Rate in the Expanded Bed.

The percent bypass was a linear function of L/G at a constant gas rate on a semi-log plot, as presented in Figure 38 for the gas rates of 80, 90, 100 and 110 kgmole/hr m^2. This information was deduced from Figure 37. Since only three L/G ratios were investigated for the expanded bed, a maximum of three points could be read at each constant gas rate from Figure 37. Once again an attempt was made to determine the functional representation of the information shown in Figure 38. The function of the form $f(X) = AX^B - C$ was assumed and the best values of A, B and C were obtained with the variance of the curves at a minimum. The following equations are the results of the least square fit for the gas rates of 80, 90, 100 and 110 kgmole/hr m^2:

$$\% \text{ bypass} = 6000(L/G)^{-0.00312} - 5966.62, \text{ for } G = 80 \text{ kgmole/hr } m^2 \quad (77)$$

$$\% \text{ bypass} = 186(L/G)^{-0.00993} - 162.00, \text{ for } G = 90 \text{ kgmole/hr } m^2 \quad (78)$$

$$\% \text{ bypass} = 51(L/G)^{-0.437} - 25.20, \text{ for } G = 100 \text{ kgmole/hr } m^2 \quad (79)$$

$$\% \text{ bypass} = 33(L/G)^{-0.807} - 9.49, \text{ for } G = 110 \text{ kgmole/hr } m^2 \quad (80)$$

with standard deviations of 0.1953, 0.00265, 0.00224 and 0.0024, respectively. No correlation could be found to represent the gas bypass as a function of G and L/G.

To observe the effect of the bed expansion on the gas bypass phenomenon, comparisons of the gas bypass as a function of the gas rate for the two bed geometries were made. Figures 39, 40 and 41 illustrate the results. The model yielded higher gas bypass at low L/G ratio for the expanded bed configuration. As the L/G ratio increased the difference between the percent bypass for the two bed configurations decreased

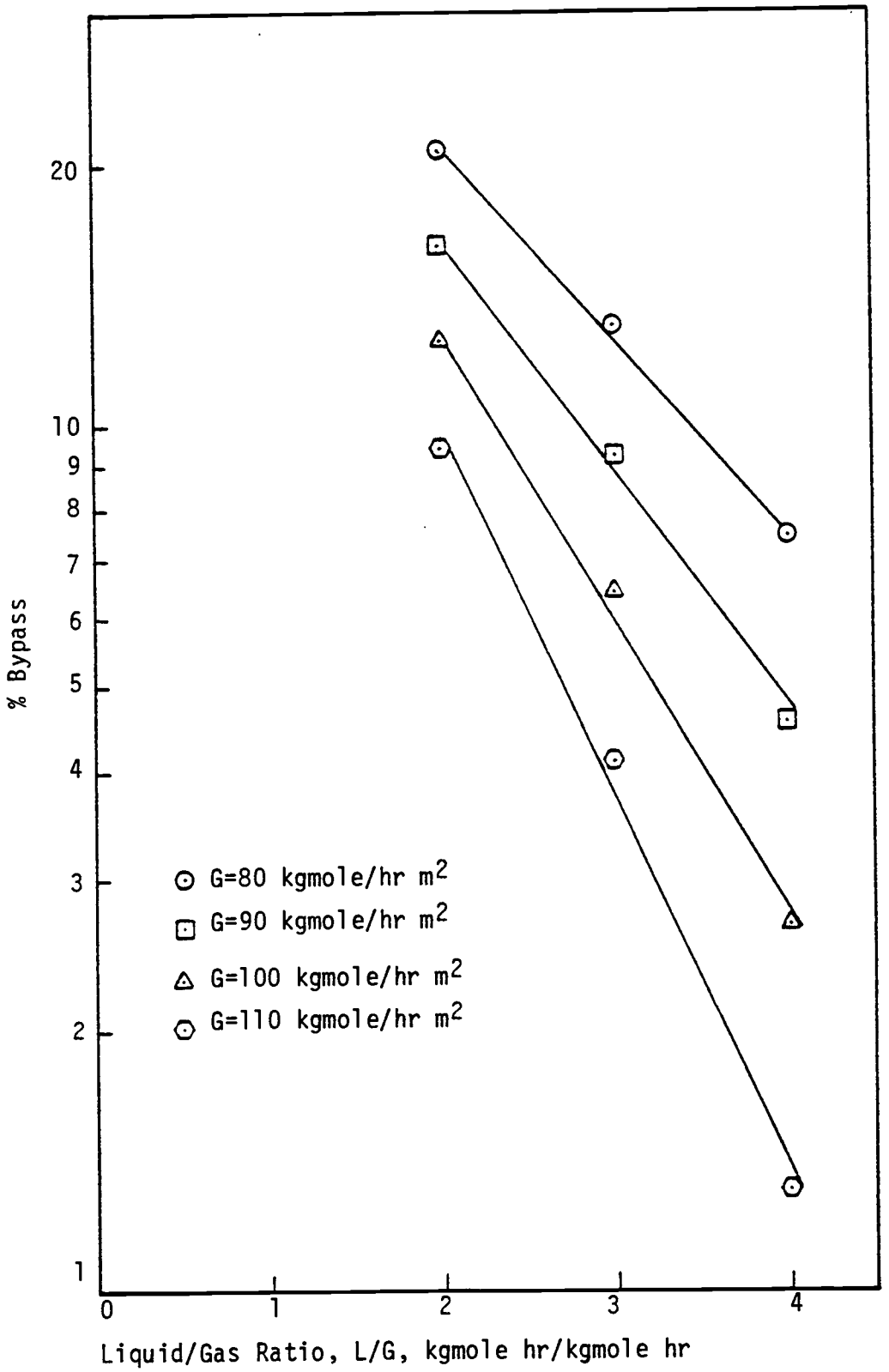

Figure 38. Percentage of Gas Bypass as a Function of L/G for Various Gas Rates.

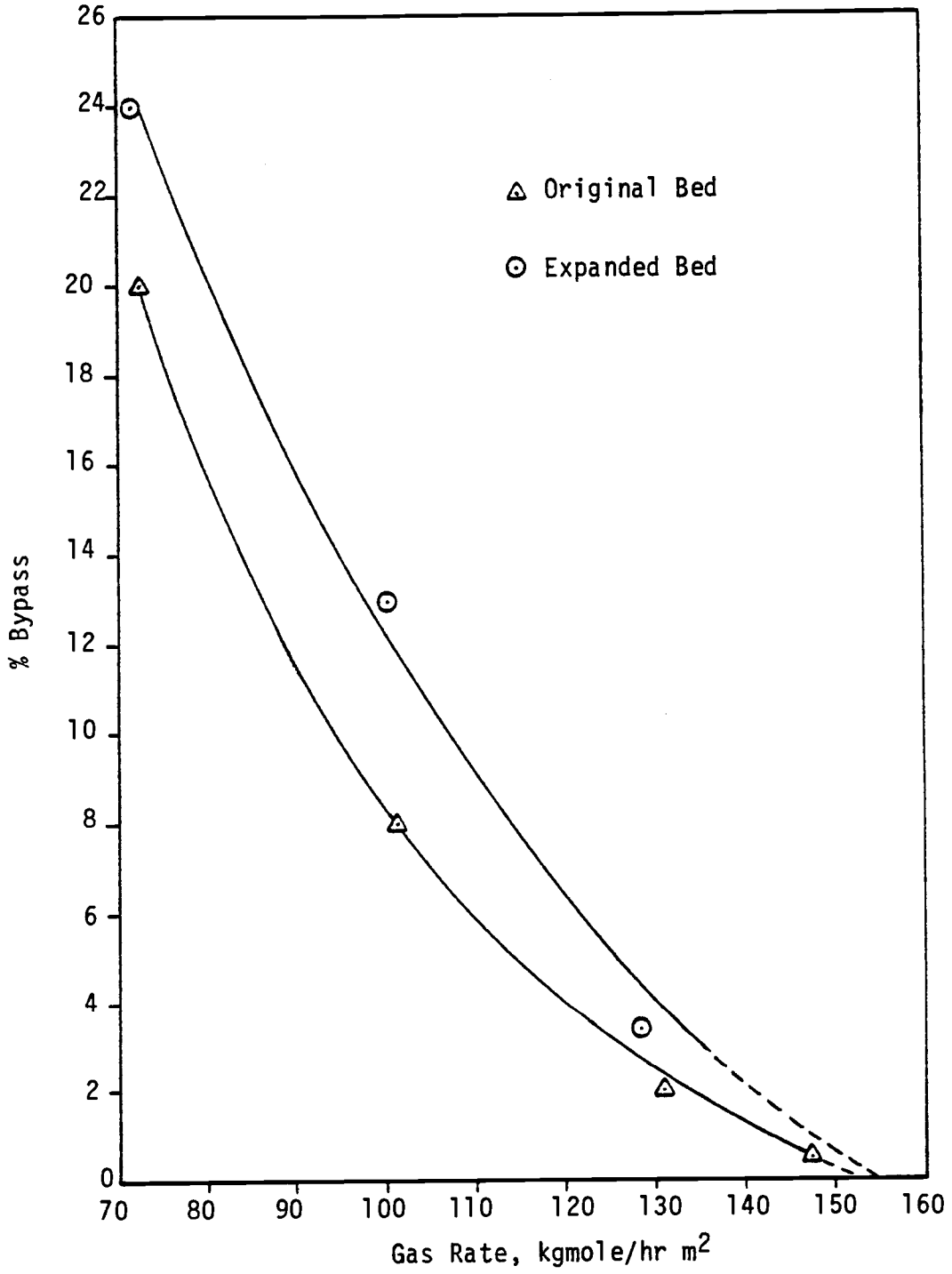

Figure 39. Gas Bypass as a Function of Gas Rate in Original and Expanded Beds, for L/G=2.0.

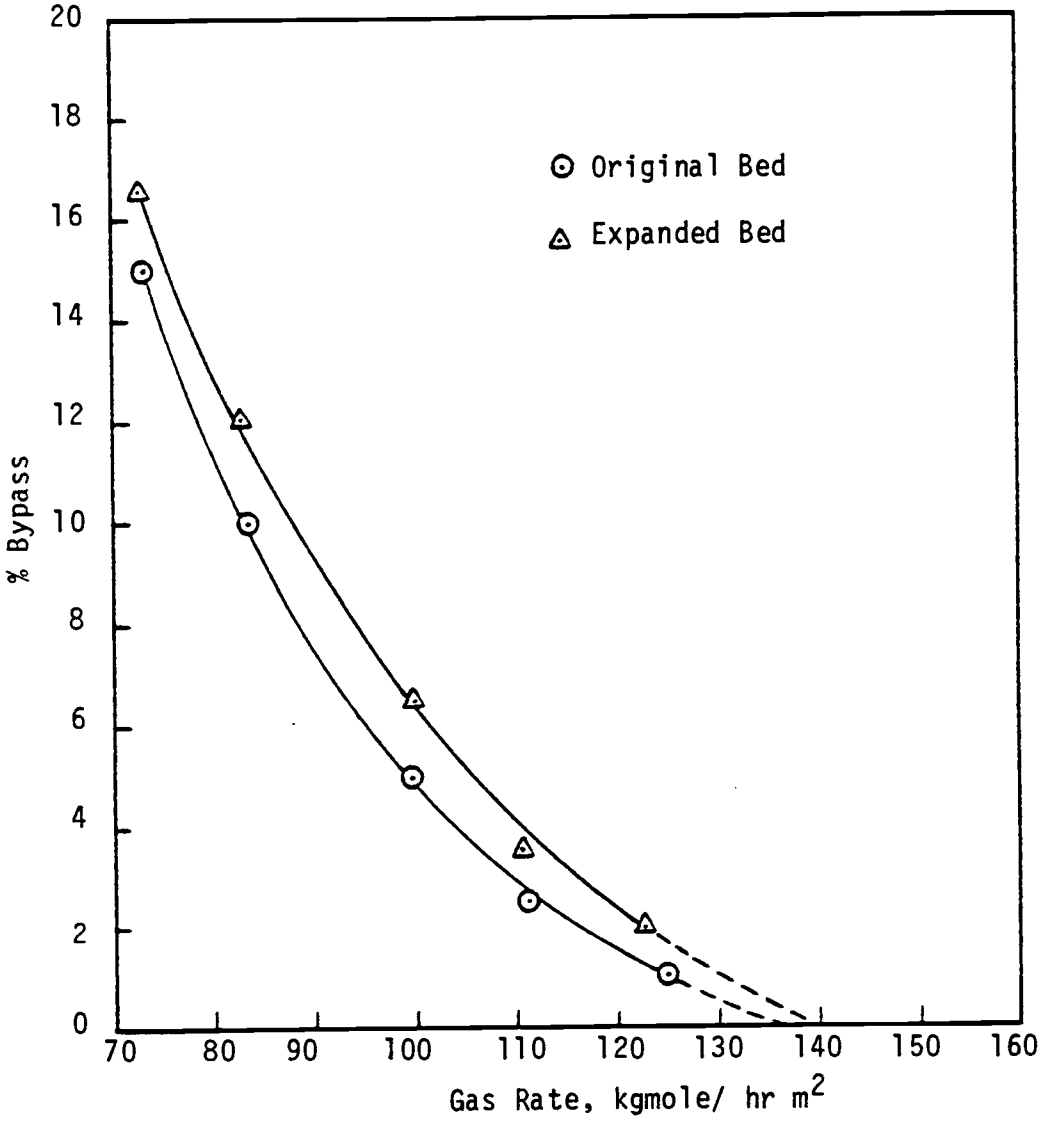

Figure 40. Gas Bypass as a Function of Gas Rate in Original and Expanded Beds, for L/G=3.0.

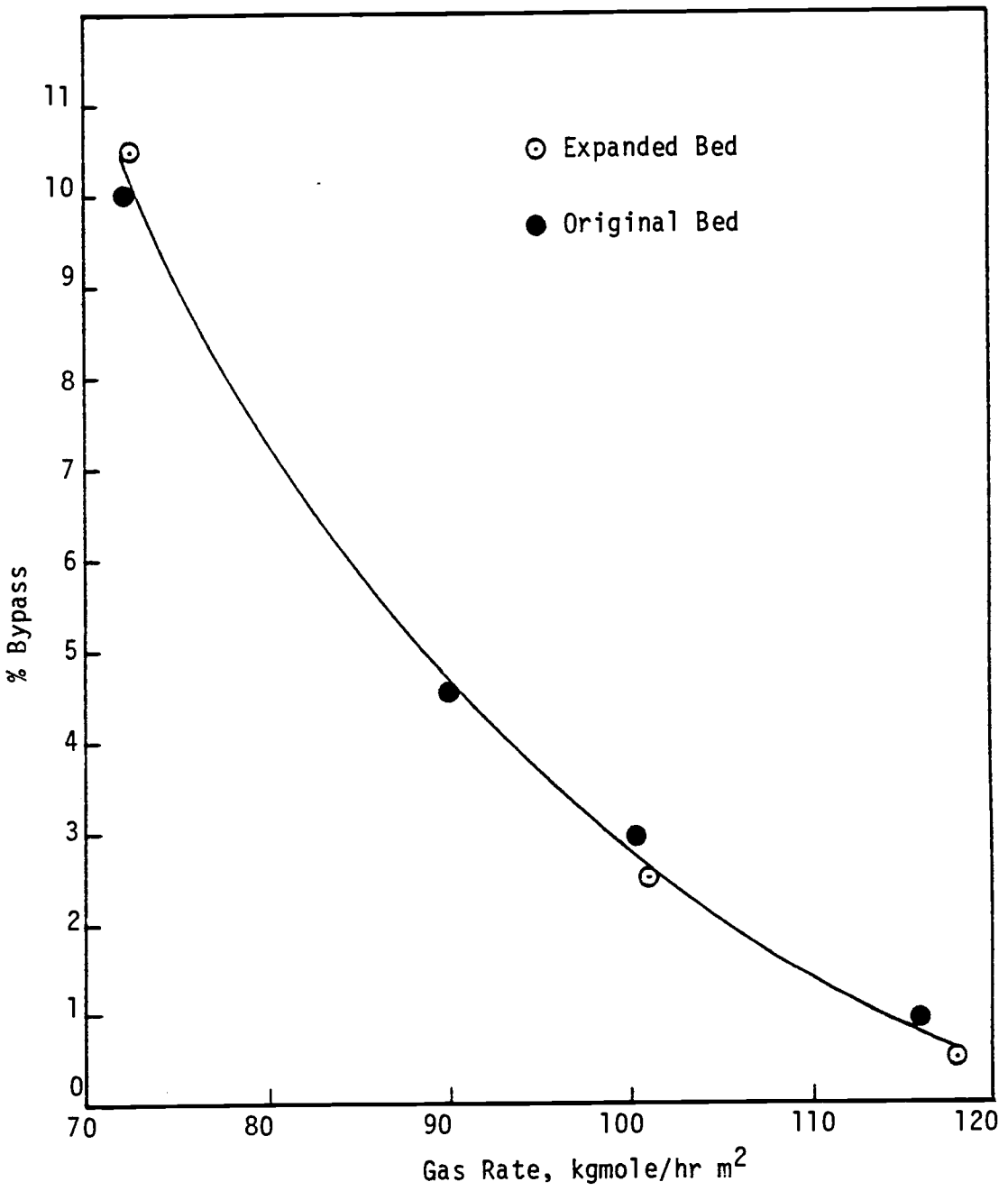

Figure 41. Gas Bypass as a Function of Gas Rate in Original and Expanded Beds, for L/G=4.0.

(see Figure 40). At still higher L/G ratio (L/G = 4.0), the difference in the bypass phenomenon was not appreciable, as shown in Figure 41, thus both configurations were believed to behave identically. It was explained in the presentation of the experimental results that the decrease in the absorption efficiency after the packing expansion was due to the higher gas bypass in the expanded bed. The results of this section confirmed that speculation. In other words, at low L/G ratio (L/G = 2.0) more gas bypassed the liquid, reducing the gas-liquid contact. As a result, the absorption efficiency decreased.

In order to illustrate how well the model agreed with the experimental results for the expanded bed, Tables 16, 17 and 18 as well as Figure 42 were prepared.

The model predicted the absorption efficiency of the expanded bed within 1% in both regions. The agreement can be seen in the last column of Tables 16, 17, and 18 and Figure 42. The dashed lines in Figure 42 represent the experimental results for the region prior to the liquid buildup on the baffles (prior to the transition point) and the solid lines illustrate the behavior of the column after the transition point for the L/G ratios of 2.0, 3.0 and 4.0. The points marked on the curves are the model values. The agreement is excellent.

The results of this section again showed that the proposed model was an accurate presentation of the physical system.

1. Efficiency of the Expanded Bed in Terms of the Volume of a Transfer Units (VTU). The volume of a transfer unit, VTU, was calculated through the procedure described previously and the results are presented in Tables 19 and 20 and Figure 43.

Table 16. Comparison Between the Experimental Values and the Values Obtained from the Proposed Model, for L/G = 2.0.

Conditions: Expanded Bed; Both Regions.

Gas Rate, kgmole/hr m^2	Entrance Liq. Conc., x_1 mole frac.	Entrance Gas Conc., y_1 mole frac.	Exit Gas Concentration, y_2, mole fraction		Absorption Efficiency, %		
	Model*	Experimental	Experimental	Model	Experimental	Model	Error
72.32	.00065	.0206	.00737	.00701	64.00	65.97	3.078
100.40	.00081	.0200	.00639	.00641	68.00	67.95	0.073
128.45	.00027	.0209	.00611	.00612	70.80	70.72	0.113
150.60	.00005	.0193	.005547	.00564	71.30	70.78	0.729
159.54	.00002	.0193	.00476	.00483	75.30	74.97	0.438
170.37	.00004	.0190	.00420	.00426	77.80	77.93	0.167
186.97	.00001	.0189	.00326	.00327	82.75	82.70	0.060

*The values are below limit of detection with the available analytical tools, therefore can be assumed to be zero.

Table 17. Comparison Between the Experimental Values and the Values Obtained from the Proposed Model, for L/G = 3.0.

Conditions: Expanded Bed; Both Regions.

Gas Rate, kgmole/hr m^2	Entrance Liq. Conc., x_1 mole frac.	Entrance Gas Conc., y_1 mole frac.	Exit Gas Concentration, y_2, mole fraction		Absorption Efficiency, %		
	Model*	Experimental	Experimental	Model	Experimental	Model	Error
72.5	.00087	.0240	.00637	.00639	73.50	73.37	0.177
82.78	.00074	.0265	.00625	.00631	76.40	76.19	0.275
99.69	.00049	.0264	.00567	.00587	78.50	77.76	0.943
110.80	.00023	.0253	.00547	.00549	78.40	78.30	0.127
122.85	.00013	.0250	.00529	.00528	78.80	78.88	0.101
134.85	.000003	.0242	.00473	.004733	80.50	80.48	0.022
149.86	.00001	.0236	.00393	.003945	83.30	83.28	0.019
164.02	.00002	.0227	.00294	.00301	87.00	86.74	0.30
186.81	.000006	.0215	.00253	.00255	88.20	88.12	0.087

*The values are below limit of detection with the available analytical tools, therefore can be assumed to be zero.

Table 18. Comparison Between the Experimental Values and the Values Obtained from the Proposed Model, for L/G = 4.0.

Conditions: Expanded Bed; Both Regions.

Gas Rate, kgmole/hr m^2	Entrance Liq. Conc., x_1 mole frac.	Entrance Gas Conc., y_1 mole frac.	Exit Gas Concentration, y_2, mole fraction		Absorption Efficiency, %		
	Model*	Experimental	Experimental	Model	Experimental	Model	Error
72.48	0.00074	.0366	.00664	.00667	81.80	81.78	.024
101.00	.00014	.0263	.00444	.00446	83.00	83.04	.048
117.99	.00003	.0265	.00379	.00378	85.70	85.74	.047
132.15	.00002	.0269	.00279	.00283	89.60	89.48	0.134
142.55	.00001	.0262	.00239	.00241	90.60	90.80	0.221
162.49	.0005	.0238	.00199	.0020	91.60	91.59	0.011

*The values are below limit of detection with the available analytical tools, therefore can be assumed to be zero.

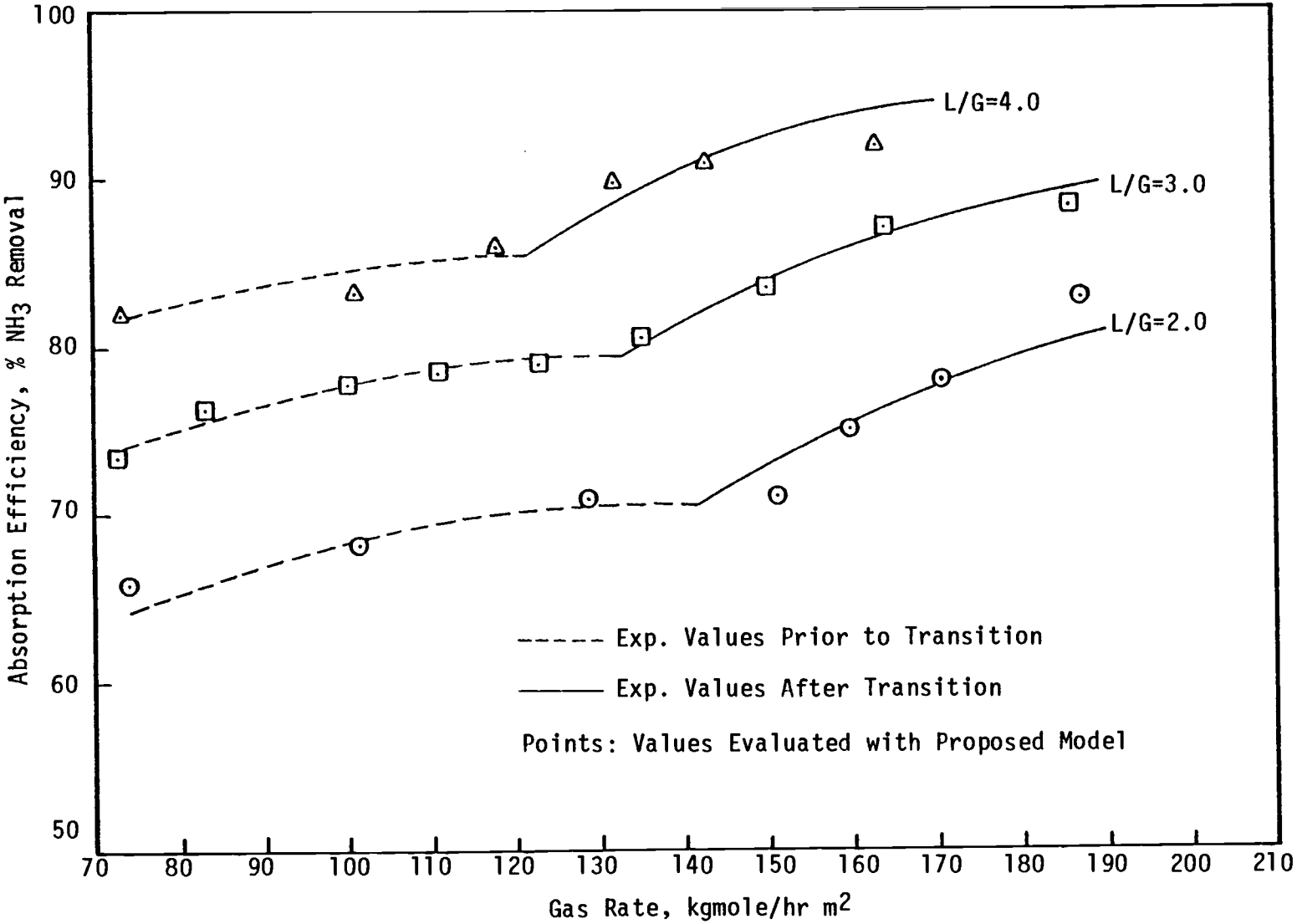

Figure 42. Comparison Between the Experimental and Model Values of the Absorption Efficiency for the Expanded Bed.

The experimental VTUs were plotted against the gas rate for the L/G ratios of 2.0, 3.0 and 4.0, as shown in Figure 43. The dashed and solid lines represented the regions of the column prior to the transition and after the transition, respectively. The transition from one region to the other is clearly shown in the figure. The VTU decreased as the gas rate increased (at a constant L/G ratio) and leveled off as the conditions of the column approached the transition. Once the transition was passed, a decrease in the VTU was observed again. As mentioned previously, a decrease in VTU corresponded to an increase in the absorption efficiency. A comparison of Figures 42 and 43 clarifies this fact further.

The agreement between the experimental and the theoretical VTU values were within 5% for the majority of runs, as shown in Tables 19 and 20. Although the percent error for the VTU values has a higher degree of deviation than the absorption efficiency values, the VTU values are a good representative of the system's efficiency as well.

G. Testing of the Proposed Model Against the Experimental Data for the Expanded Bed with Six Baffles

It was mentioned in the presentation of the experimental results that in order to observe the effect of the dead space in the column the number of baffles was decreased from 12 to 6 to generate more dead space. The results were presented and discussed. However, in order to find out the bypass phenomenon in the expanded bed with only six baffles, the proposed model was modified for the new dimensions. The results are presented in Figure 44.

Table 19. Experimental and Theoretical Values of Volume of a Transfer Unit (VTU) for L/G Ratios of 2.0 and 4.0.

Conditions: Expanded Bed; Both Regions.

L/G = 2.0				L/G = 4.0			
Gas Rate, kgmole/hr m^2	$(VTU)_{exp.}$, m^3	$(VTU)_{Theo.}$, m^3	Error, %	Gas Rate, kgmole/hr m^2	$(VTU)_{exp.}$, m^3	$(VTU)_{Theo.}$, m^3	Error, %
72.32	.0786	.0704	10.43	72.48	.0640	.0600	6.25
100.40	.0648	.0590	8.95	101.00	.0558	.0567	1.61
128.45	.0630	.0629	0.16	117.99	.0567	.0588	3.70
150.60	.0577	.0597	3.47	132.15	.0501	.0524	4.59
159.54	.0549	.0569	3.64	142.55	.0482	.0506	4.98
170.37	.0539	.0561	4.08	162.49	.0460	.0483	5.00
186.97	.0534	.0556	4.12				

Table 20. Experimental and Theoretical Values of Volume of a Transfer Unit (VTU) for L/G Ratio of 3.0.

Conditions: Expanded Bed; Both Regions

L/G = 3.0			
Gas Rate, kgmole/hr m^2	$(VTU)_{exp.}$, m^3	$(VTU)_{Theo.}$ m^3	Error, %
72.50	.0697	.0613	12.05
82.78	.0635	.0586	7.72
99.69	.0601	.0631	4.99
110.80	.0597	.0599	0.33
122.85	.0589	.0599	1.70
134.85	.0566	.0588	3.89
149.86	.0510	.0531	4.12
164.02	.0494	.0517	4.66
186.81	.0486	.0509	4.73
207.29	.0482	.0505	4.77

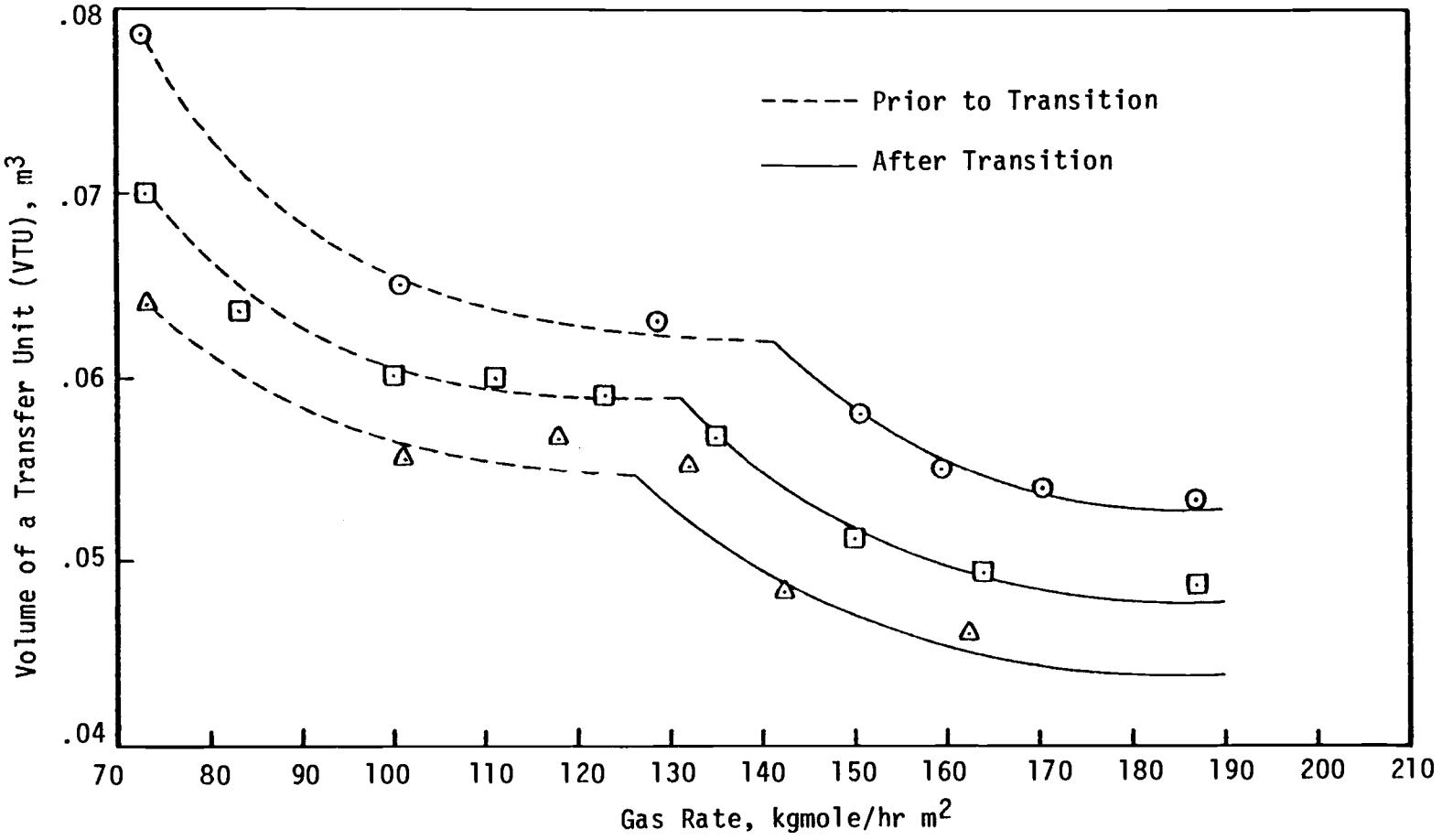

Figure 43. Volume of Transfer Units for Various L/G Ratios for the Expanded Bed.

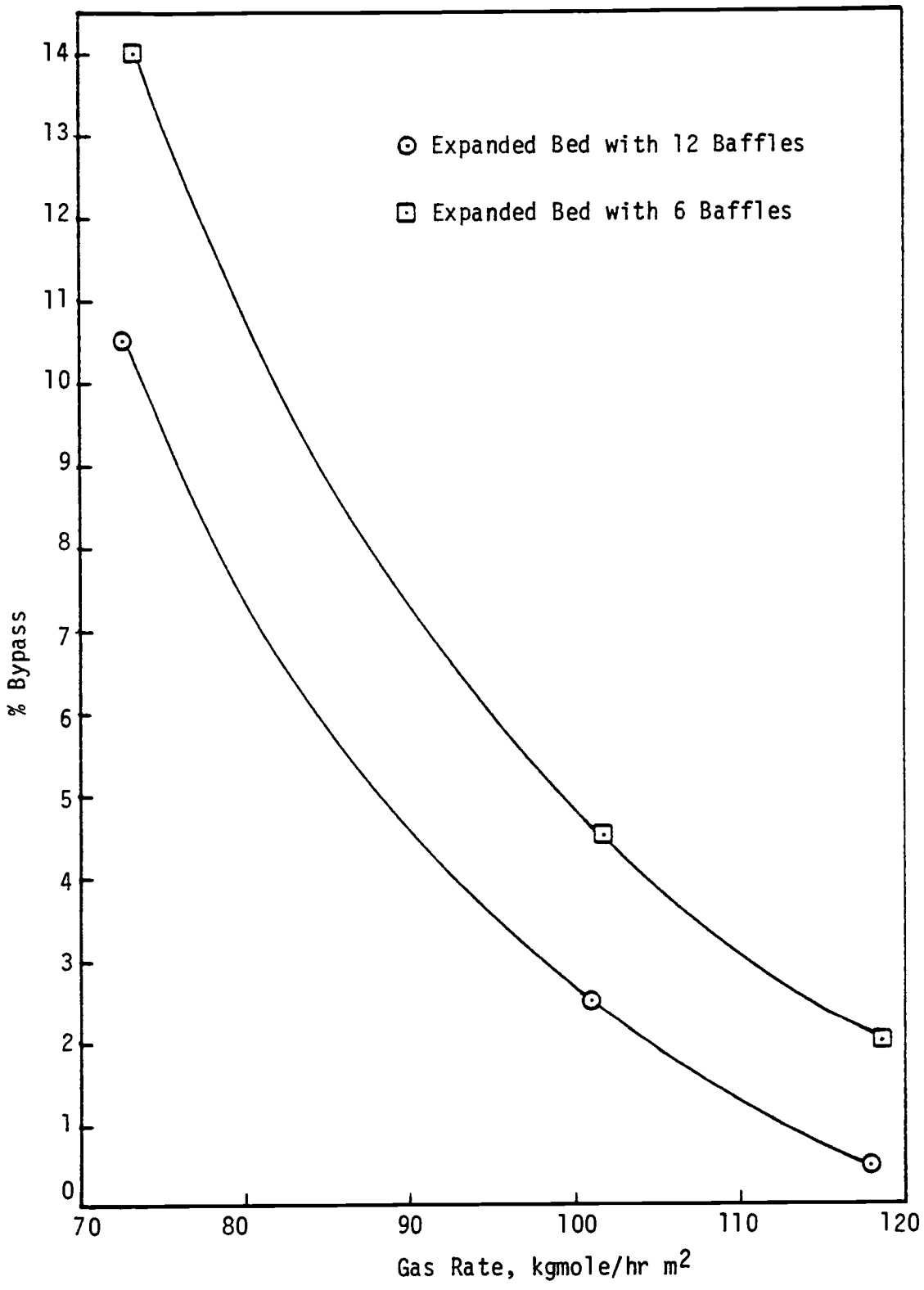

Figure 44. Gas Bypass as a Function of Gas Rate in Expanded Bed with 12 and 6 Baffles; L/G = 4.0.

In order to better understand the bed's bypassing behavior, the results of the expanded bed with 12 baffles are also shown in the same figure. As can be seen from Figure 44, the bypassing phenomenon increased with decreasing the number of baffles. This again explained the reason for the decrease in the column's efficiency due to having larger dead space in the column.

An equation of the form $f(X)=AX^B-C$ was assumed to describe the bypassing phenomenon as a function of the gas rate. After evaluation of the coefficients by the least square technique, mentioned previously, the following equation was obtained:

$$\% \text{ bypass} = 460000(G)^{-2.367} - 3.67, \text{ for } L/G = 4.0 \qquad (81)$$

with standard deviation of 0.002.

For this part of the work, the proposed model also agreed with the experimental results, as shown in Table 21 and Figure 45. The agreement between the experiment and the model values for the absorption efficiency was well within 1% in both regions. As mentioned in other sections, the dashed lines represent the region prior to transition and the solid lines represent the region after the transition where the points indicated on the curves are the model values. Figure 45 also illustrates the absorption efficiency behavior of the expanded bed with 12 and 6 baffles. The bypass model explains the difference between the two curves; the higher the bypass the lower the absorption efficiency.

1. Efficiency of the Expanded Bed with Six Baffles in Terms of the Volume of a Transfer Unit (VTU). The experimental values of the volume of a transfer unit, VTU, for the expanded bed with six baffles, were calculated. The results are summarized in Table 22 and Figure 46.

Table 21. Comparison Between the Experimental Values and the Values Obtained from the Proposed Model, for L/G = 4.0.

Conditions: Expanded Bed, Six Baffles, Both Regions.

Gas Rate, kgmole/hr m^2	Entrance Liq. Conc., x_1 mole frac.	Entrance Gas Conc., y_1 mole frac.	Exit Gas Concentration, y_2, mole fraction		Absorption Efficiency, %		
	Model*	Experimental	Experimental	Model	Experimental	Model	Error
73.40	0.0009	0.0364	0.00945	0.00967	74.00	73.63	0.50
101.68	0.0003	0.0260	0.0050	0.00503	80.80	80.65	0.19
118.66	0.0001	0.0225	0.00426	0.00430	81.00	80.89	0.14
133.19	0.00002	0.0269	0.00484	0.00487	82.00	81.88	0.15
143.70	0.000003	0.0263	0.00362	0.00364	86.00	86.15	0.17
166.46	0.000009	0.0232	0.00263	0.00266	88.60	88.55	0.06

*The values are below limit of detection with the available analytical tools, therefore can be assumed to be zero.

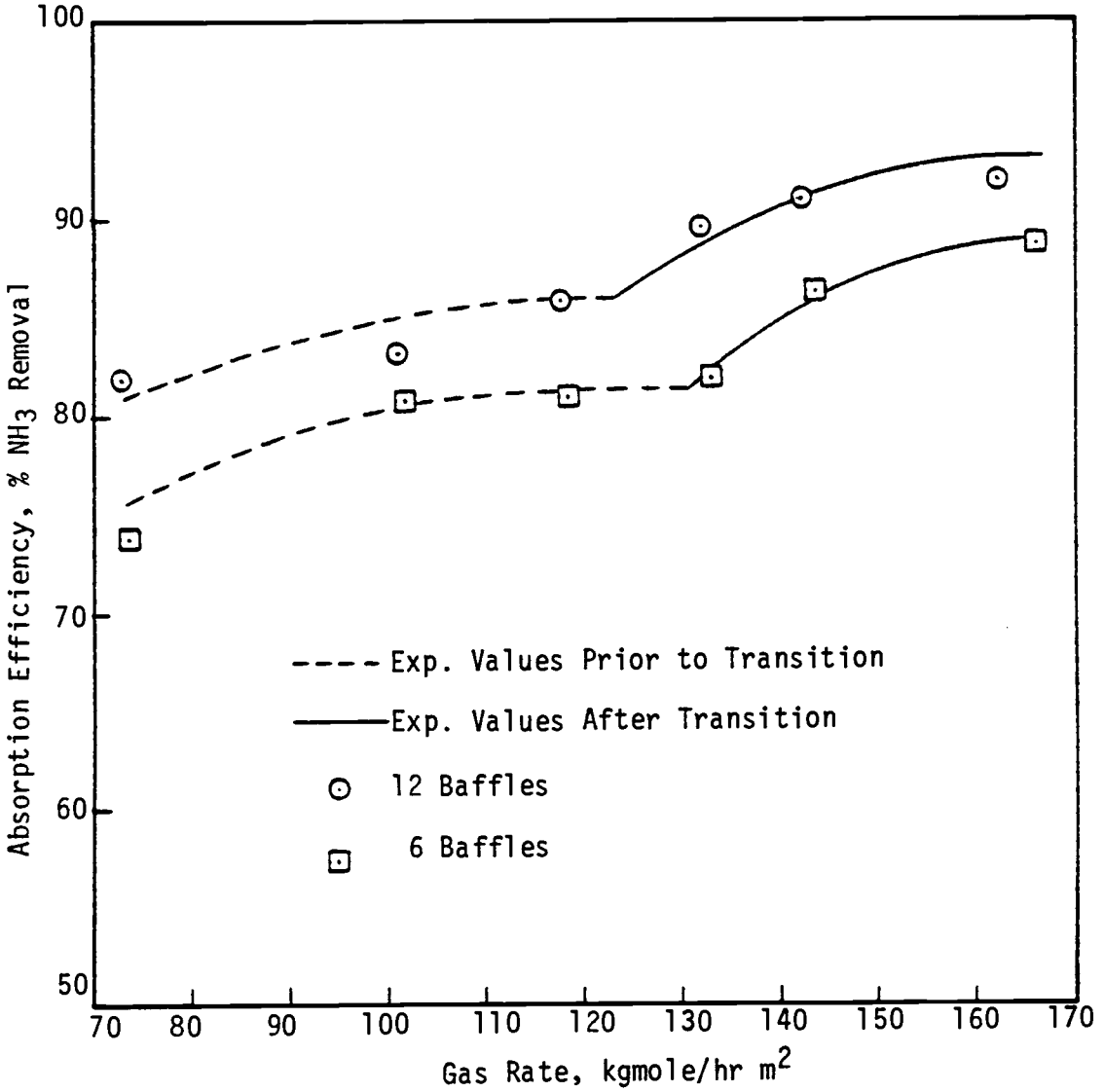

Figure 45. Comparison Between the Experimental and Model Values of the Absorption Efficiency for Expanded Bed with 12 and 6 Baffles; L/G = 4.0.

Table 22. Experimental and Theoretical Values of Volume of a Transfer Unit (VTU)

Conditions: Expanded Bed, Six Baffles, Both Regions

L/G = 4.0			
Gas Rate, kgmole/hr m^2	$(VTU)_{exp.}$ m^3	$(VTU)_{Theo.}$ m^3	Error, %
73.40	0.0664	0.0599	9.79
101.68	0.0581	0.0578	0.52
118.66	0.0573	0.0584	1.92
133.19	0.0570	0.0592	3.86
143.70	0.0512	0.0535	4.49
166.46	0.0478	0.0501	4.81

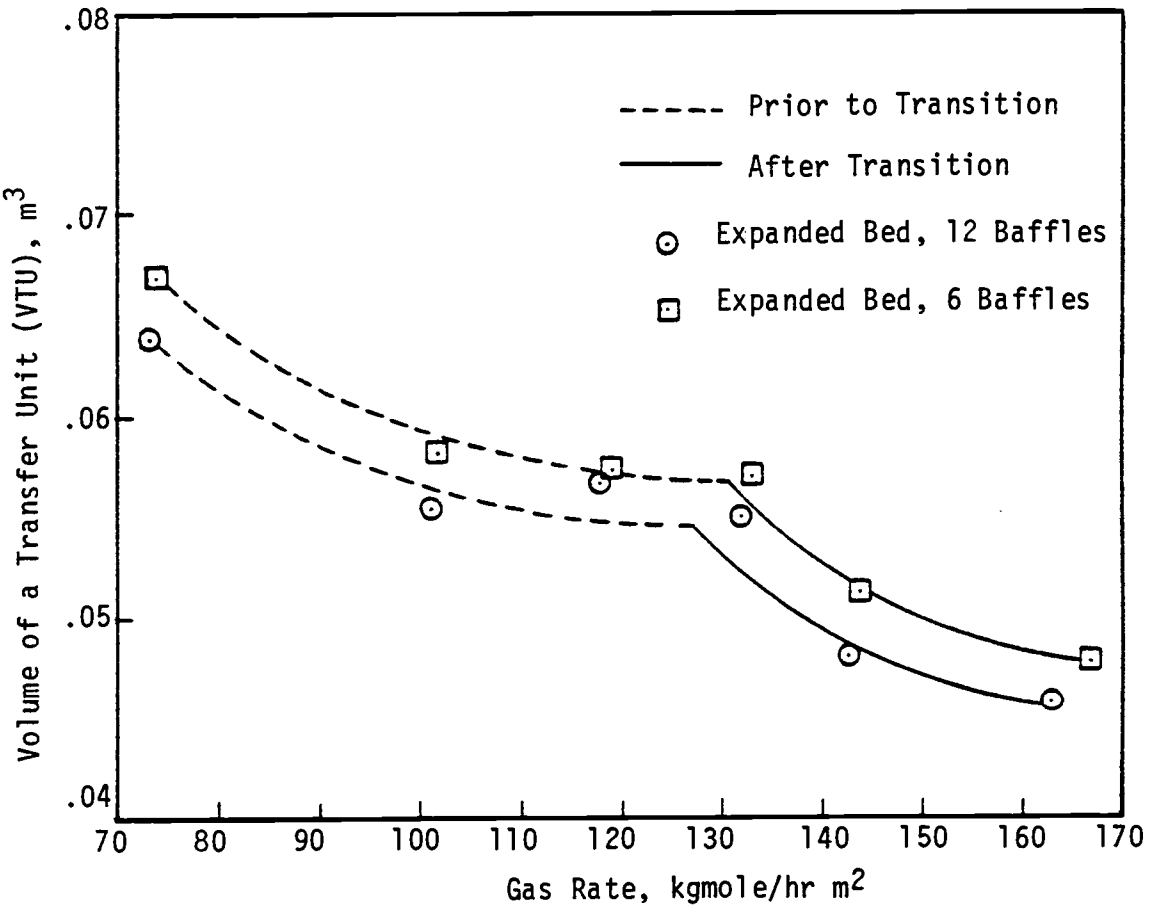

Figure 46. Volume of the Transfer Units for Expanded Bed with 12 and 6 Baffles; L/G = 4.0.

The bed behavior was in agreement with what the absorption efficiency values suggested. In other words, as the gas rate increased, the absorption efficiency increased (see Figure 45) thus a smaller volume of a transfer unit was required to achieve the mass transfer job. This can be seen from Figure 46. For the sake of clarity, the results of the expanded bed with 12 baffles are shown in the same figure. A comparison between Figures 44 and 46 indicated that as the operating conditions in the column approached the transition, a smaller fraction of the gas bypassed the baffles, thus smaller VTU (smaller column) was required. The curve, representing the efficiency in terms of VTU, flattened out near the transition and once the transition was passed, the VTU started to decrease which was an indication of higher absorption efficiency.

As illustrated in different sections of this chapter, the bypass model resulted in an accurate representation of the cascade crossflow packed column. The agreement between the experimental results and the model values further confirmed the validity of the model for both regions in the column for various L/G ratios as well as different bed configurations.

VII. SUMMARY AND CONCLUSIONS

Extensive mass transfer data were collected to quantitatively determine the transition point visually observed in the cascade cross-current packed column. The tracer studies have been incorporated to further confirm the existence of the transition in the column.

The system actually showed a distinct transition. Prior to the transition point, the liquid flowed rather straight down the column while the gas flowed upward in a zig-zag manner. As the system passed the transition point, the liquid deviated its path and a criss-crossing phenomenon was developed. At this point the liquid started to build up on the baffles. The tracer investigation provided a significant step in the improved understanding of the flow behavior as well as the mass transfer efficiency of the cascade crosscurrent column.

Establishment of the system's behavior encouraged further investigation. The same transition behavior was observed with various liquid-to-gas ratios. However, the transition was observed to occur at lower gas rate as the L/G ratio increased. Information deduced from this portion of the work resulted in a development of a graph which would enable the designer to predict the conditions at which the transition occurred, for the range of L/G ratios studied in this work.

The overall mass transfer efficiency was calculated as percent ammonia removed and as volume of a transfer unit for the ammonia-air-water system. Both methods were good indications of the system's mass transfer efficiency. The absorption efficiency increased with an increase in either L/G ratio or the gas rate, keeping the other variable constant.

The effect of intercore to outerwall baffle spacing on the absorption efficiency of the crosscurrent column was also studied. The decrease in the absorption efficiency after the bed expansion, at low L/G ratio, suggested the gas bypassing phenomenon. However, as the L/G ratio increased, the effect of the bed expansion was less pronounced.

The experimental results suggested two distinct regimes in the column. At low gas rates, a fraction of the gas flowed around the baffles without making any contact with the liquid and the rest of the gas crossed the packing section. As the transition was passed, the liquid accumulation on the baffles prevented the gas from bypassing the liquid.

The criss-crossing pattern of the liquid in the column created unirrigated sections of the packing immediately below the baffles. These unirrigated sections, called dead space, were enlarged by either expanding the packing section or decreasing the number of baffles. Lower absorption efficiency was obtained as a result of having larger dead space.

Due to the criss-crossing of the liquid in the column, the liquid accumulated on the baffles. Mixing activities were observed in the packing section as well as on the baffles. The degree of mixing activity increased with an increase in the gas rate. It was concluded that this mixing action compensated for the loss of efficiency due to the dead space, at high gas rate.

The bypass model was proposed based on the experimental results. A trial and error procedure was adopted to determine the percentage of the gas flow bypassing the baffles. The bypass model successfully predicted the system's behavior prior to the transition point.

Correlations were developed that adequately predicted the percent bypass as a function of the gas rate and the L/G ratios, for the operating conditions studied in this work. The theoretical development of the bypass model agreed well with the experimental results.

The zero bypass model was also successful in predicting the system's behavior after the transition point. Agreement between the values calculated by the model with the experimental results confirmed the validity of the proposed model.

The mass transfer results obtained in this work combined with the favorable pressure drop findings, studied by various investigators, suggested that the crosscurrent packed column to be a viable alternative to the conventional towers for the ammonia-air-water system.

VIII. RECOMMENDATIONS FOR FUTURE WORK

Although the results of this study helped to better understand the mass transfer mechanisms in the cascade crosscurrent packed column, further investigation in some areas are required.

The ammonia-air-water system was employed to collect the experimental results. The existing regions in the crosscurrent column may make the cascade even a more efficient mass transfer device for less soluble systems like oxygen or carbon dioxide.

Pall rings were used as the only packing material in this work. Other packing materials for which the mass transfer coefficient is easily available should be examined. This will avoid the estimation of the mass transfer coefficients.

Tracer technique is a powerful tool in studying the types of flow that exist in the packed columns. Extensive tracer experiments should be conducted to determine the types of flow patterns which exist in the column as well as on the baffles. This will help to develop a more accurate presentation of the system's behavior.

Experimental and theoretical studies should be directed to understand the gas absorption accompanied by a chemical reaction (chemical absorption of CO_2 into aqueous solutions of NaOH) in the cascade crosscurrent column.

IX. NOMENCLATURE

A_2 = cross sectional area of orifice, m^2

a = effective surface area per unit volume, m^2/m^3

B = dimensionless parameter defined by Eq. (56)

b = percent gas bypass

C = orifice coefficient

d = diameter of orifice, mm

D = inside diameter of air pipe, 83 mm.

D_f = diameter of float for ammonia rotameter, 0.0127 m.

F = calibration coefficient for water rotameters, mole/s (% of sale)

G = total molar flow rate of gas, kgmole/hr

$K = C/\sqrt{1-\beta^4}$

K_1, K_2 = constants used in orifice equation

$K_{OG}a$ = overall gas capacity coefficient, kgmole/hr m^3Pa

L = total molar flow rate of liquid, kgmole/hr

$\dot{m}_{air,H_2O,NH_3}$ = molar flow rate of air, water and ammonia, mole/s

$\bar{M}$ = average molecular weight of air stream, kg/kgmole

m = number of partition in space along Y

m_H = modified Henry's law constant

N = normality of NaOH and H_2SO_4 solutions, kg·equiv/m^3

N_{Ot} = number of overall transfer units

n = number of partition in space along X

P = total pressure, Pa

P_{atm} = barometric pressure, Pa

P_1 = pressure upstream from orifice, Pa

P_2 = pressure downstream from orifice, Pa

ΔP = pressure drop across orifice, $P_1 - P_2$, Pa

P_{NH_3} = pressure of ammonia gas, Pa

q = volumetric flow rate of ammonia, m^3/S

R_d = percentage change in diameter ratio for the ammonia rotameter

St = Stoke's number

T_w, T_d = wet and dry bulb temperatures of air stream, ^oK

T_1 = orifice upstream air temperature, ^oK

T_{NH_3} = ammonia gas temperature, ^oK

V = volume used in titrations, m^3

v = volume of packing, m^3

V_0 = volume of a transfer unit, VTU, m^3

W = mass flow rate through orifice, kg/s

W_f = weight of float for ammonia rotameter, 2.715×10^{-3} kg

W_G = average gas flow rate, kgmole/hr

W_{G_1} = average gas flow rate after subtraction of the gas bypass flow rate, kgmole/hr

W_{G_b} = gas bypass flow rate, kgmole/hr

W_{G_X} = average gas flow rate through crossflow stage, kgmole/hr

W_L = average liquid flow rate, kgmole/hr

X = horizontal coordinate (gas flow direction), m

X_0 = effective tower depth, m

$X_{in,out}$ = mole fraction of ammonia in the inlet and exit liquid streams; solute free basis

$\bar{x}_1$ = local concentration of solute gas in liquid phase entering crossflow stage (mole fraction)

$\bar{x}_2$ = local concentration of solute gas in liquid phase leaving crossflow stage (mole fraction)

Y = expansion factor through orifice or vertical coordinate (liquid flow direction)

Y_0 = effective tower height, m

$Y_{in,out}$ = mole fraction of ammonia in the inlet and exit gas streams; solute-free basis

$\bar{y}_1$ = local concentration of solute gas in gas phase entering cross-flow stage (mole fraction)

$\bar{y}_2$ = local concentration of solute gas in gas phase leaving cross-flow stage (mole fraction)

$\bar{y}^*$ = local concentration of $\bar{y}$ equilibrium with $\bar{x}$ (mole fraction)

Z = humidity as kg water per kg dry air, kg/kg

Z_0 = effective tower width, m

β = ratio of orifice diameter to pipe diameter, d/D, mm/mm

ρ = density, kg/m^3

ρ_f = density of float for ammonia rotameter, 2530 kg/m^3

μ = ammonia viscosity, Pa.s

Subscripts:

1 = tower inlet

2 = tower outlet

i and j = dual integer notation

Superscript:

* = denotes phase equilibrium

1,2,3,...10 = position number, reference to Figure 27

X. BIBLIOGRAPHY

1. Fordyce, H.E., U.S. Patent No. 2, 776, 121, Official Gazette, p. 97 (1957).

2. Hayashi, Y., Hirai, E., and Ito, N., "An Analysis of Crossflow Cooling Towers," J. of Chem. Eng. of Japan, 9, 458-463 (1976).

3. Pittaway, K.R., and Thibodeaux, L.J., "Measurement of the Oxygen Desorption Rate in a Single-Stage Crossflow Packed Column," Ind. Eng. Chem. Process Des. Dev. 19, 40-46 (1980).

4. Oza, S.B., "Fluid Dynamics of a Crossflow Device," M.S. Thesis, University of Arkansas, Fayetteville, AR (1974).

5. Hanf, E.B., "A Guide to Scrubber Selection," Env. Science and Tech., 4, 110 (1970).

6. National Air Pollution Control Administration, "Control Techniques for Particulate Air Pollutants," U.S. Dept. H.E.W. Bulletin AP-51, Washington, D.C. (1969).

7. Pittaway, K.R., "Liquid-Phase Mass Transfer Coefficient Measurement in a Crosscurrent Packed Tower," Ph.D. Thesis, University of Arkansas, Fayetteville, AR (1976%.

8. Thibodeaux, L.J., "Continuous Crosscurrent Mass Transfer in Towers," Chem. Eng., 76, 165 (1969).

9. Wnek, W.J. and Snow, R.H., "Design of Crossflow Cooling Towers and Ammonia Stripping Towers," Ind. Eng. Chem., Process Des. Dev., 11 (3), 343 (1972).

10. Roesler, J.F., and Smith, R.J., J. Sanit. Eng. Div. ASCE, SA3, 269-86 (1971).

11. Baker, D.R. and Shryock, H.A., "A Comprehensive Approach to the Analysis of Cooling Tower Performance," J. Heat Trans., Trans. AIME, 83, 339 (1961).

12. Inazumi, H. and Kageyama, S., Jo-Chinese Inst. Ch. E., 6, 7-11 (1975).

13. Sherwood, T.K., Pigford, R.L., and Wilke, C.R., Mass Transfer, pp. 291-295, McGraw-Hill, N.Y. (1975).

14. Hayashi, Y., Hirai, E., and Sucyoshi, H., J. Chem. Eng. Jpn., 5(2), 137 (1972).

15. Hayashi, Y., and Hirai, E., Kagaki Kogaku, 35, 214 (1971).

16. Thibodeaux, L.J., Daner, D.R., Kimura, A., Millican, J.D., and Parikh, R.J., "Mass Transfer Units in Single and Multiple Stage Packed Bed, Crossflow Devices," Ind. Eng. Chem., Process Des. Dev., 16, 325 (1977).

17. Gary, M.L., Frankenberger, K., and Glassgow, M., "Cascade Crossflow Packed Column," University of Arkansas, Fayetteville, AR (1974).

18. Thibodeaux, L.J., "Fluid Dynamic Observations on a Packed Crossflow Cascade at High Loadings," University of Arkansas, Fayetteville, AR (1977).

19. Golshani, A., "Dynamics Behavior of a Cascade Crossflow Packed Column," M.S. Thesis, Oregon State University, Corvallis, OR (1977).

20. Zuehlsdorff, D.A., "Absorption of Ammonia in Water Using a Multiple Stage Crosscurrent Packed Column," M.S. Thesis, Oregon State University, Corvallis, OR (1979).

21. Leva, M., Tower Packings and Packed Tower Design, 2nd ed., The United States Stoneware Co., Akron, OH (1953).

22. Treybal, R.E., Mass Transfer Operations, McGraw-Hill Book Co., New York, pp. 153-175, 220-280 (1968).

23. Perry, R.H., Chemical Engineer's Handbook, 5th ed., McGraw-Hill Book Co., New York, pp. 3:96, 211, 14:1-16, 18:19-49 (1973).

24. "Fluid Meters: Their Theory and Applications," ASME Research Report on Fluid Meters, 6th ed., New York, p. 208 (1971).

25. Khang, D.J., "New Scale-up and Design Criteria of Stirrer Agitated Batch and Flow Mixing Vessel," Ph.D. Thesis, Oregon State University, Corvallis, OR (1975).

26. Satvat, B. "Residence Time Distribution in Tubular Flow Vessels with Multiple Baffles," M.S. Thesis, Oregon State University, Corvallis, OR (1976).

27. Ives, D.J., and Janz, G.J., Reference Electrodes, Theory and Practice, Academic Press, NY and London (1961).

28. Van Wylen, G.J. and Sonntag, R.E., Fundamentals of Classical Thermodynamics, 2nd Ed., John Wiley and Sons, Inc., New York p. 666 (1973).

29. Sherwood, T.K. and Reed, C.E., Applied Mathematics in Chemical Engineering, McGraw-Hill Book Co., New York, pp. 344-386 (1939).

XI. APPENDICES

APPENDIX A

CALIBRATION CHARTS

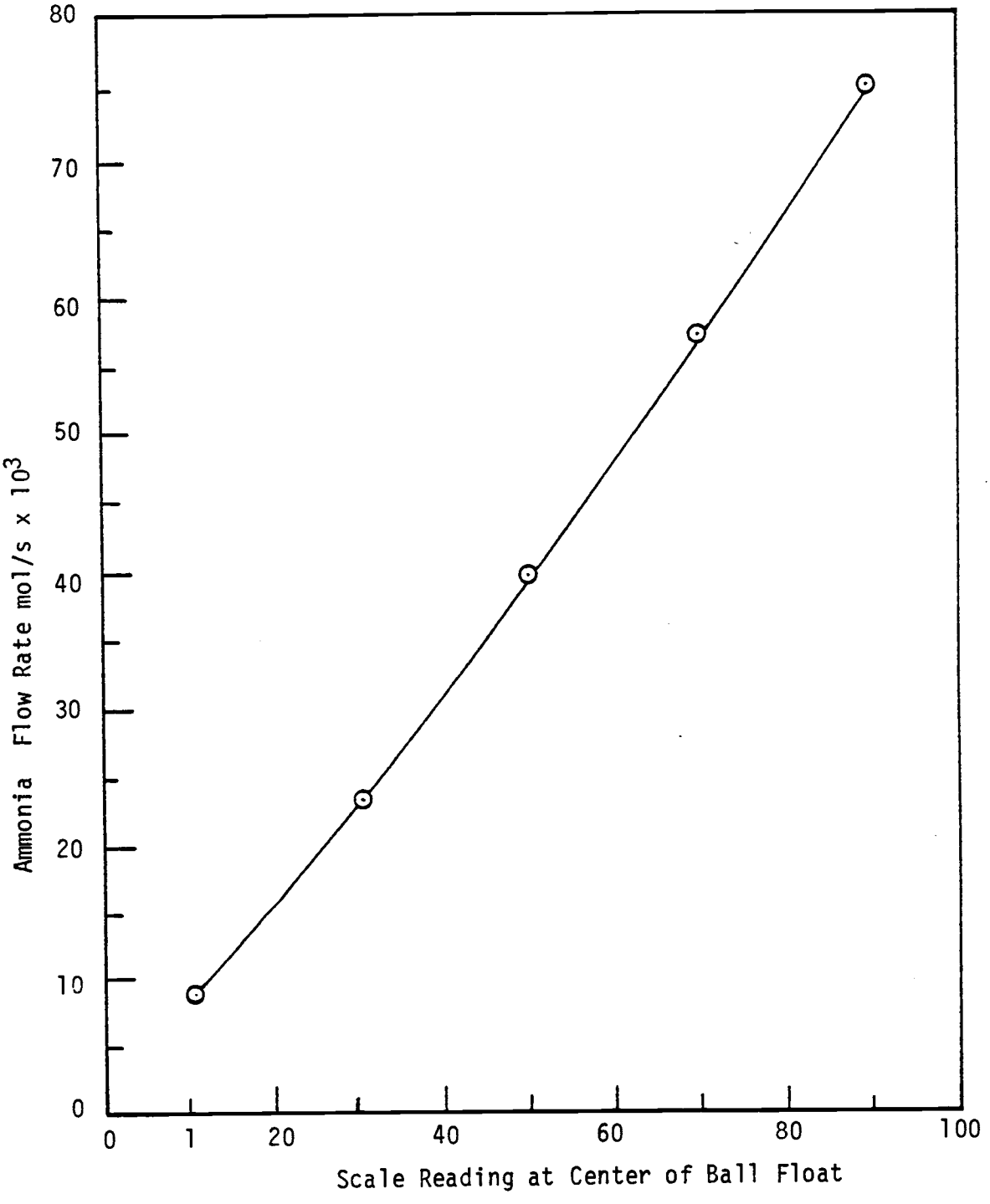

Figure 47. Ammonia Rotameter Calibration at 10°C and 103.4 kPa.

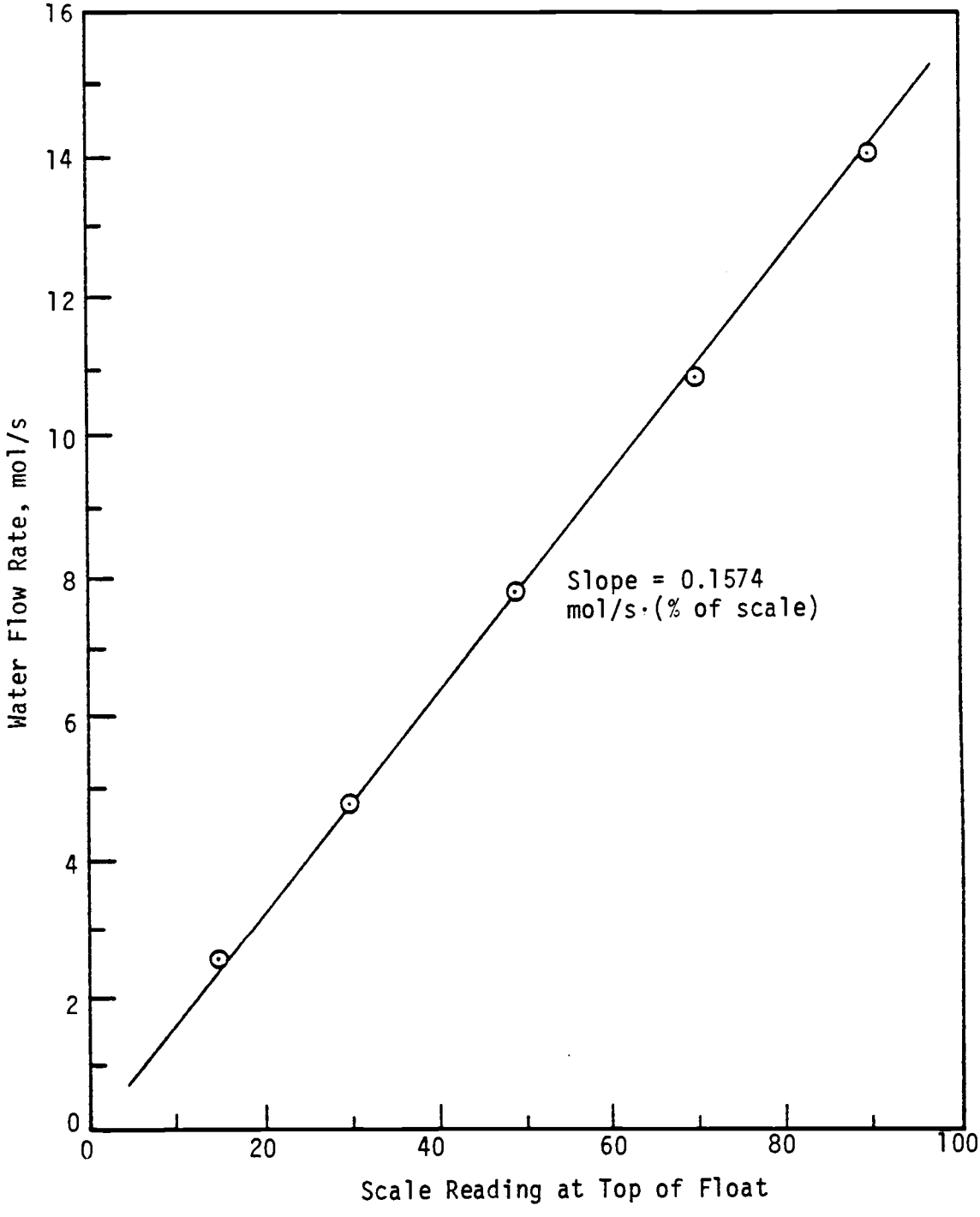

Figure 48. Small Liquid Rotameter Calibration.

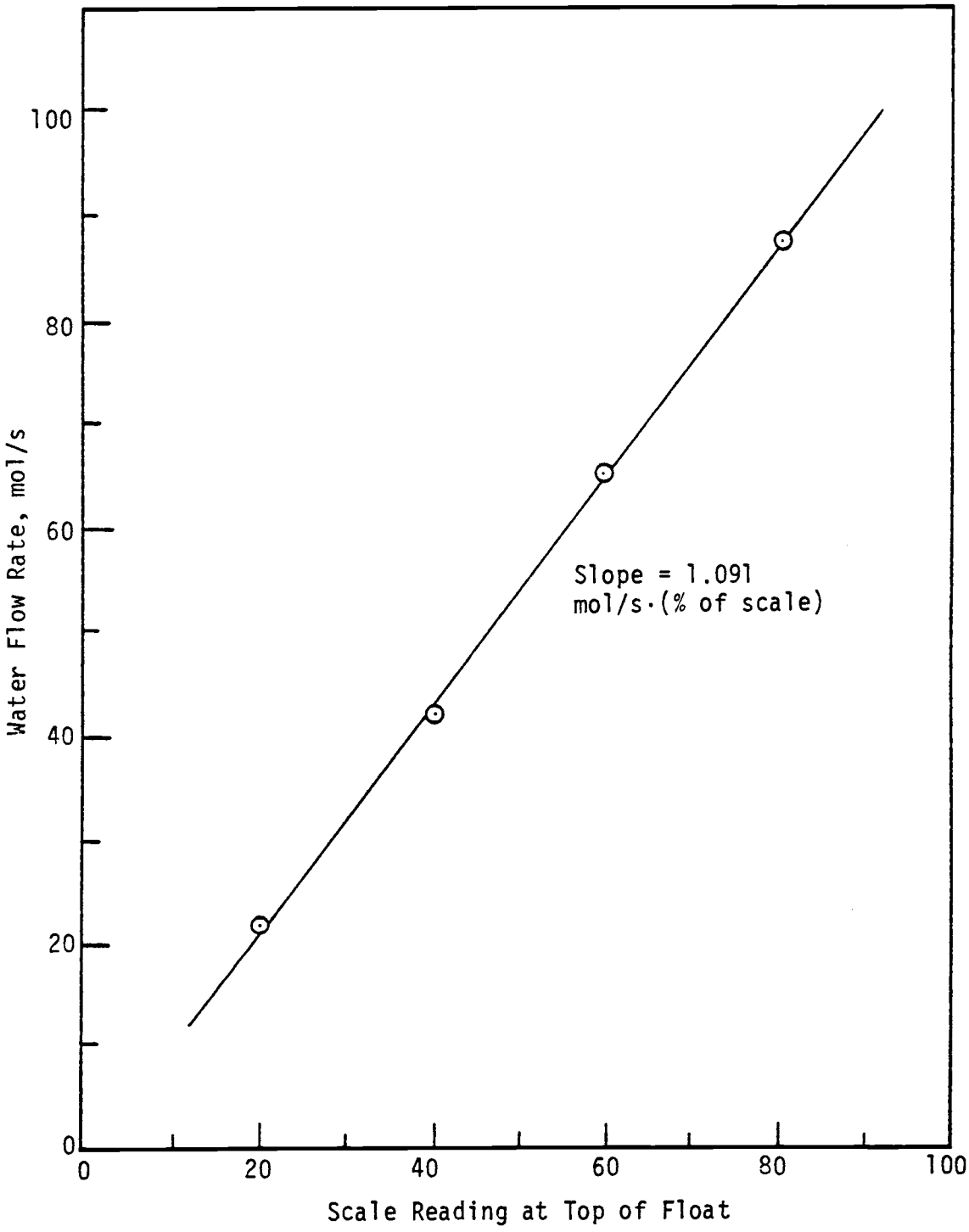

Figure 49. Large Liquid Rotameter Calibration.

APPENDIX B

SAMPLE CALCULATIONS

Run #23 DATA SHEET Date:

No. of baffles - 12 Packing 5/8 in. Pall rings Operation type - Crossflow

Orifice diameter - 2.0 inch

P_{atm},(Hg) - 30.10

$T_{air,in}$(°C) - 54 = 129.2°F

$P1_{(1)} = P_{atm} + \frac{(22.4)-(14.3)}{13.6} = 30.695$"Hg

$\Delta P_{orifice\ (4,5)} = (18.95)-(17.10) = 1.85$"$H_2O$

% of scale 28 for (small) / large rotameter

H_2O holdup on baffles 1"H_2O

Crossflow is observed

	°C	°F	
Air,in T_d =	26,	78.8	Z_{in} = .0087
T_w =	17.2,	63.0	$\bar{M}$ = 28.82
Air,out T_d =	24,	75.2	
T_w =	21.9,	71.5	Z_{out} = .01585

T_{NH_3} = 58°F

$P_{NH_3} = P_{atm} + \frac{(42.15)-(40.35)}{2.54}\frac{14.696}{29.92} =$ 15.13 psia

% of scale = 28

$N_{H_2SO_4}$ = .214 $V_{H_2SO_4}$ = 25 ml

V_{sample} = 10 ml $V_{NaOH,rqd}$ = 14.4 ml, 14.4 ml, 14.4 ml

N_{NaOH} = .20

lb mole/min

$\dot{m}_{air,in}$ = .19511

$\dot{m}_{H_2O,in}$ = .58533

$\dot{m}_{H_2O,out}$ = .58308

$\dot{m}_{NH_3,in}$ = .002891

$\dot{m}_{NH_3,out}$ liquid = .002592

$\dot{m}_{NH_3,out}$ gas = .000299

L/G = 3.0

Y_{in} = .0148 Y_{out} = .00153

X_{out} = .00443 X_{in} = 0.0

ρ_{NH_3} = 7.51 x 10^{-4} gm/ml

μ_{NH_3} = 9.56 x 10^{-3} cp

R = 8.364

St = 13617.28

a = 1.591

b = 2.751

c = 4.030

Cr = 0.9469

$$\% \text{ removal} = 100 \times \frac{NH_{3,in} - NH_{3,out}}{NH_{3,in}} = 89.7\%$$

APPENDIX B

SAMPLE CALCULATIONS

The experimental data were collected in the units that appeared on the instruments and were recorded on data sheets. A sample data sheet is shown in the following pages. Then the data were converted to SI units and calculations were performed. The following sample calculations are for Run #23.

Measurement	Observed Units	S.I. Units
No. of baffles		12
Packing	5/8 inch Pall ring	16.0 mm Pall rings
Orifice Diameter	2.00 inch	50.8 mm
Barometric Pressure	30.10 in Hg	101935 Pa.
T_1	54^oC	327.15^ok
P_1	30.695 in Hg	103946 Pa.
$\Delta P_{orifice}$	1.85 in H_2O	460 Pa.
Small Liquid Rotameters		28% of scale
$T_{d,in}$	26^oC	299.15^ok
$T_{w,in}$	63^oF	290.37^ok
$T_{d,out}$	24^oC	297.15^ok
$T_{w,out}$	71.5^oF	287.59^ok
P_{NH_3}	15.13 psia	104334 Pa.
Ammonia Rotameter		28% of scale
$N_{H_2SO_4}$	0.214 g. equiv/liter	0.214 kg. equiv/m^3

$V_{H_2SO_4}$	25 ml	25×10^{-6} m^3
V_{sample}	10 ml	10×10^{-6} m^3
N_{NaOH}	0.20 g. equiv/liter	0.20 kg. equiv/m^3
$V_{NaOH,required}$	(1) 14.4 ml	14.4×10^{-6} m^3
	(2) 14.4 ml	14.4×10^{-6} m^3
	(3) 14.4 ml	14.4×10^{-6} m^3

The following calculations show the details in obtaining the values shown in the data sheet. The pressure upstream from the orifice plate and the pressure of ammonia gas were calculated from the monameter readings as follows:

$$P_1 = P_{atm} + (\text{Difference in manometer reading})/\frac{\text{in Hg}}{(13.6 \text{ in } H_2O)}$$

$$P_1 = 30.10 \text{ in Hg} + (22.4 - 14.3 \text{ in } H_2O)/(\frac{\text{in Hg}}{13.6 \text{ in } H_2O}) = 30.695 \text{ in Hg}$$

$$P_1 = \frac{30.695 \text{ in Hg} \mid 101325 \text{ Pa}}{\mid 29.92 \text{ in Hg}} = 103946 \text{ Pa}$$

$$P_1 = 103946 \text{ Pa}$$

$$P_{NH_3} = P_{atm} + \frac{\text{manometer reading, Cm Hg}}{2.54 \text{ cm/inch}}$$

$$P_{NH_3} = 30.10 \text{ in Hg} + (\frac{42.15-40.35}{2.54}) \text{ in Hg} = 30.81 \text{ in Hg}$$

$$P_{NH_3} = \frac{30.81 \text{ in Hg} \mid 101325 \text{ Pa}}{\mid 29.92 \text{ in Hg}} = 104334 \text{ Pa}$$

$$P_{NH_3} = 104334 \text{ Pa}$$

The wet and dry bulb temperatures will locate the humidity on the psychometric charts,

$Z_{in} = 0.0087$

$Z_{out} = 0.01585$

then $\bar{M}$ was calculated, using the following equation:

$$\bar{M} = \frac{28.97 + 18.01\ (1.609 \times 0.0087)}{1.00 + (1.609 \times 0.0087)} = 28.82 \text{ kg/kgmole}$$

Since the 50.80 mm orifice diameter was used, the constants K_1 and K_2 were obtained from Table 1 and Equation (2) was used to calculate molar air flow rate,

$$\dot{m}_{air} = 20.721 \times 10^{-3} \left[1.00-0.32871 \frac{460}{103950}\right] \sqrt{\frac{(103950)(460)}{(28.82)(327.15)}}$$

$$\dot{m}_{air} = 1.473 \text{ mole/s}$$

Liquid flow rate was calculated, using Equation (3) for the small rotameter, as follows:

$$\dot{m}_{H_2O} = 0.1574(28) = 4.407 \text{ mole/s}$$

The exit liquid flow rate was calculated by combining Equations 12 and 13, as follows:

$$\dot{m}_{H_2O,out} = \dot{m}_{H_2O,in} - \dot{m}_{air,in}(1.609)(Z_{out}-Z_{in})$$

$$\dot{m}_{H_2O,out} = 4.407-1.473(1.609)(0.01585-0.0087)$$

$$\dot{m}_{H_2O,out} = 4.39 \text{ mole/s}$$

Entering ammonia flow rate was calculated after obtaining the ammonia rotameter readings as follows:

Using Equation (5) and (6), the density was calculated

$$V = 0.6222+8.0\times10^{-5}\ \ 1.8(287.59)-499.67\ \ + 6.0\times10^{-4}(15.0-\frac{104334}{6894.75})$$

$$V = 0.62356$$

$$\rho = 1.291\times10^{-3}(104334)/(287.59)(.62356) = .751$$

$$\rho = .751 \text{ kg/kgmole}$$

Using Equation (10),

$$\mu = 9.2\times10^{-6} + 2.0\times10^{-8}\left[1.8(287.59)-499.67\right]$$

$$\mu = 9.56\times10^{-6} \text{ Pa.s}$$

By using Equation (7), (8) and (9), the quantities R_d, Cr and St were calculated, respectively:

$$R_d = 1.0 + 0.263(28) = 8.364$$

$$St = (2.829 \times 10^{-9})(.751)(8.364)^3/(9.56 \times 10^{-6})^2$$

$$St = 13617$$

$$a = 3.08 \log (8.364)-1.25 = 1.591$$

$$b = 3.83 - 1.17 \log (8.364) = 2.751$$

$$c = \log (13617) - 0.111 \log (8.364) = 4.03$$

then,

$$Cr = (\sqrt{(2.751)^2 + 4(1.591)(4.03)} - 2.751)/(2 \times 1.591)$$

$$Cr = 0.9469$$

With the above quantities, $\dot{m}_{NH_3,in}$ was calculated, using Equation (4):

$$\dot{m}_{NH_3,in} = 1.528x10^{-3}(0.9469)(8.364)\sqrt{.751}\left[2.0 + \frac{8.364}{100}\right]$$

$$\dot{m}_{NH_3,in} = 0.02185 \text{ mole/s}$$

Equation (15) was used to calculate $\dot{m}_{NH_3,out,liquid}$,

$$V_{NaOH} = (14.4+14.4+14.4)(10^{-6})/3.0 = 14.4 \times 10^{-6}$$

$$\dot{m}_{NH_3,out\ liquid} = \frac{(.214)(25x10^{-6})-(0.2)(14.4x10^{-6})}{(1000)(10x10^{-6})}(18.01)(4.39)$$

$$\dot{m}_{NH_3,out\ liquid} = 0.01959 \text{ mole/s}$$

The exit ammonia flow rate was calculated by using Equation (16)

$$\dot{m}_{NH_3,out\ gas} = 0.02185 - 0.0195g = 0.00225 \text{ mole/s}$$

Once the above quantities were calculated, the mole fraction of ammonia in the gas and liquid streams entering and leaving the column were determined as follows:

$$Y_{in} = \dot{m}_{NH_3,in}/\dot{m}_{air} = \frac{0.02185}{1.473} = 0.0148$$

$$Y_{out} = \dot{m}_{NH_3,out\ gas}/\dot{m}_{air} = \frac{0.00225}{1.473} = 0.00153$$

$$X_{out} = \dot{m}_{NH_3,out}/\dot{m}_{H_2O} = \frac{.01959}{4.407} = 0.00443$$
liquid

By using Equation (17) the percent NH_3 removed was calculated,

$$\% \ NH_3 \text{ removed} = \frac{.0148 - .00153}{.0148} \times 100 = 89.7\%$$

The gas flow per total cross sectional area of the column, used in presenting the figures in this work, were calculated as follows:

$$\text{Gas Rate} = \frac{1.473 \text{ gmole}}{\text{sec}} \left| \frac{1 \text{ kgmole}}{1000 \text{ gmole}} \right| \frac{3600 \text{ sec}}{1 \text{ hr}} \Big| \frac{}{0.0322 \text{ m}^2} = 164.6 \frac{\text{kgmole}}{\text{hr m}^2}$$

cross sectional area

Gas Rate = 164.6 kgmole/hr m^2

APPENDIX C

MASS TRANSFER DATA

Table 23. Mass Transfer Data.

Run No.	No. of Baffles	L/G	$\dot{m}_{Air}$ kgmole/hr	$\dot{m}_{H_2O,in}$ kgmole/hr	$\dot{m}_{NH_3,in}$ kgmole/hr	$\dot{m}_{NH_3,out,liq.}$ kgmole/hr
1	12	2.0	2.364	4.725	0.0478	0.0348
2	12	2.0	3.277	6.521	0.0632	0.0480
3	12	2.0	4.229	8.505	0.0837	0.0637
4	12	2.0	4.759	9.525	0.0919	0.0712
5	12	2.0	5.060	10.149	0.0975	0.0785
6	12	2.0	5.307	10.603	0.1053	0.0891
7	12	2.0	6.129	12.247	0.1230	0.1085
8	12	4.0	2.333	9.357	0.0469	0.0384
9	12	4.0	3.243	13.041	0.0637	0.0541
10	12	4.0	3.488	13.948	0.0661	0.0554
11	12	4.0	3.751	15.025	0.0716	0.0602
12	12	4.0	4.264	17.010	0.0837	0.0737
13	12	4.0	4.586	18.314	0.0920	0.0819
14	12	4 0	5.280	21.157	0.1051	0.0963
15	12	4.0	5.397	21.546	0.1105	0.1021
16	12	3.0	2.356	7.087	0.0339	0.0259
17	12	3.0	2.694	8.080	0.0391	0.0308
18	12	3.0	3.211	9.639	0.0445	0.0351
19	12	3.0	3.563	10.773	0.0502	.0406
20	12	3.0	4.027	12.077	0.0590	0.0474
21	12	3.0	4.241	12.757	0.0642	0.0524
22	12	3.0	4.809	14.458	0.0727	0.0624
23	12	3.0	5.310	15.930	0.0787	0.0705

Table 23. (Continued)

Run No.	No. of Baffles	L/G	$\dot{m}_{air}$, kgmole/hr	$\dot{m}_{H_2O,in}$ kgmole/hr	$\dot{m}_{NH_3,in}$ kgmole/hr	$\dot{m}_{NH_3,out,liq}$ kgmole/hr
24	12	3.0	5.512	16.443	0.0787	0.0711
25	12	3.0	6.030	18.144	0.0909	0.0827
26	12	3.0	6.709	20.128	0.0996	0.0917
27	12	1.5	3.213	4.819	0.0291	0.0196
28	12	1.5	3.584	5.386	0.0559	0.0378
29	12	1.5	3.978	5.953	0.0343	0.0238
30	12	1.5	4.245	6.350	0.0562	0.0396
31	12	1.5	4.741	7.144	0.0618	0.0443
32	12	1.5	5.361	8.051	0.0702	0.0522
33	12	1.5	5.605	8.391	0.0727	0.0560
34	12	1.5	5.988	8.958	0.0754	0.0597
35	12	1.5	6.746	10.092	0.0846	0.0723
36	12*	2.0	2.333	4.723	0.0480	0.0354
37	12*	2.0	2.238	6.520	0.0649	0.0442
38	12*	2.0	4.143	8.505	0.0868	0.0614
39	12*	2.0	4.856	9.525	0.0939	0.0669
40	12*	2.0	5.146	10.206	0.0992	0.0747
41	12*	2.0	5.496	10.773	0.1047	0.0815
42	12*	2.0	6.031	12.247	0.1141	0.0945
43	12*	3.0	2.339	7.087	0.0563	0.0414
44	12*	3.0	2.670	8.080	0.0693	0.0540
45	12*	3.0	3.218	9.639	0.0849	0.0667
46	12*	3.0	3.574	10.773	0.0904	0.0709

*Expanded Packing Bed

Table 23. (Continued)

Run No.	No. of Baffles	L/G	$\dot{m}_{air}$, kgmole/hr	$\dot{m}_{H_2O,in}$ kgmole/hr	$\dot{m}_{NH_3,in}$ kgmole/hr	$\dot{m}_{NH_3,out,liq.}$ kgmole/hr
47	12*	3.0	3.963	12.077	0.0991	0.0782
48	12*	3.0	4.350	12.757	0.1055	0.0849
49	12*	3.0	4.834	14.458	0.1142	0.0952
50	12*	3.0	5.291	15.876	0.1201	0.1045
51	12*	3.0	6.026	18.144	0.1294	0.1141
52	12*	3.0	6.687	20.128	0.1294	0.1152
53	12*	4.0	4.263	17.010	0.1148	0.1029
54	12*	4.0	4.599	18.331	0.1206	0.1096
55	12*	4.1	5.242	21.545	0.1246	0.1142
56	12*	4.0	2.338	9.355	0.0855	0.0700
57	12*	4.0	3.258	13.041	0.0857	0.0712
58	12*	4.0	3.806	15.025	0.1010	0.0865
59	None	4.0	2.333	9.355	0.0847	0.0713
60	None	4.0	3.241	13.041	0.0852	0.0749
61	None	4.0	3.791	15.025	0.1003	0.0891
62	None	4.0	4.298	17.010	0.1167	0.1071
63	None	4.0	4.638	18.331	0.1177	0.1080
64	None	4.1	5.273	21.545	0.1163	0.1061
65	None	3.0	2.344	7.087	0.0568	0.0478
66	None	3.0	3.246	9.639	0.0570	0.0503
67	None	3.0	3.981	12.077	0.0799	0.0722
68	None	3.0	4.260	12.757	0.0914	0.0819
69	None	3.0	5.223	15.876	0.1095	0.0972
70	None	3.0	6.761	20.128	0.1313	0.1193

Table 23. (Continued)

Run No.	No. of Baffles	L/G	$\dot{m}_{air}$, kgmole/hr	$\dot{m}_{H_2O,in}$ kgmole/hr	$\dot{m}_{NH_3,in}$ kgmole/hr	$\dot{m}_{NH_3,out,liq.}$ kgmole/hr
71	6*	4.0	2.368	9.355	0.0861	0.0637
72	6*	4.0	2.736	13.041	0.0861	0.0697
73	6*	4.0	3.991	14.999	0.0862	0.0699
74	6*	4.0	4.296	17.010	0.1157	0.0949
75	6*	4.0	4.635	18.711	0.1219	0.1051
76	6*	4.0	5.370	21.545	0.1247	0.1106

APPENDIX D

COMPUTER PROGRAMS

```
      PROGRAM BAYAN(INPUT,OUTPUT,TAPE5=INPUT,TAPE6=OUTPUT)
C
C****                    RUN NO. 23
C****
C**** THIS PROGRAM CALCULATES ENTRANCE LIQUID COMPOSITION,
C**** EXIT GAS COMPOSITION AND NUMBER OF TRANSFER UNITS FOR
C**** EACH STAGE OF THE CORSS-FLOW COLUMN AS WELL AS OVERALL
C**** NUMBER OF TRANSFER UNITS.
C
      DIMENSION X(5,5),Y(5,5)
      REAL LGC,KOGA,NOT,NOTEXP
C
C**** INPUT THE FLOW RATES, EXPERIMENTALLY MEASURED EXIT GAS
C**** COMPOSITION, HENRY'S LAW CONSTANT, MASS TRANSFER COEFFICIENT
C**** GAS BY-PASS AND DIMENSIONS OF ONE STAGE .
C**** COLUMN DIMENSIONS IN FT, UL,LBMOLE/HR; UG,LBMOLE/HR;
C**** KOGA, LBMOLE/HR FT3
C**** ALSO CALCULATE VOLUME OF PACKING FOR EACH STAGE AND THUS
C**** OBTAIN NOT FROM EXPERIMENTAL VALUES
C
      READ(5,5)UL,UG,H,KOGA,YEXIT,XX,X0,Y0,Z0,XAVG,YAVG
    5 FORMAT(1X,5F11.6,/1X,6F11.6)
      DY=Y0/3.0
      V=X0*Y0*Z0
      NOTEXP=6.0*(V**2.0)/(UL*UG/(H*KOGA**2.0))
C
C**** CALCULATE THE BY-PASS GAS FLOW RATE,UGB, AND THE CROSS-FLOW
C**** GAS FLOW RATE,UG1 AND THE DIMENSIONLESS PARAMETER B.
C**** SET INCOMING GAS AND EXIT LIQUID COMPOSITIONS FROM
C**** THE EXPERIMENTAL DATA. CALCULATE LIQUID TO GAS RATIO
C**** AND PERFORM THE CROSS-FLOW CALCULATIONS STARTING FROM
C**** THE BOTTOM OF THE COLUMN.
C
      UG1=(1.0-XX)*UG
      UGB=XX*UG
      B=DY*KOGA/(2.0*UL/(X0*Z0))
      ICOUNT=0
      SUMNT=0.0
    1 UGC=(1.0-XX)*UG1
      LGC=UL/UGC
      DO 10 I=1,3
      Y(I,1)=YAVG
   10 CONTINUE
      DO 20 J=1,3
      X(4,J)=XAVG
   20 CONTINUE
      DO 40 J=1,3
      DO 30 I=1,3
      K=4-I
      X(K,J)=((1.0+B*(LGC+H))*X(K+1,J)-2.0*B*Y(K,J))/(1.0+B*(LGC-H))
      Y(K,J+1)=Y(K,J)-LGC*(X(K+1,J)-X(K,J))
   30 CONTINUE
   40 CONTINUE
```

```
C
C**** CALCULATE " NOT " FROM THE ANALYTICAL CROSS-FLOW CALCULATIONS
C
      SUM=0.0
      DO 44 I=1,3
      DO 33 J=1,3
      PART1=ABS((Y(I,J)-H*X(I,J))/(Y(I,J+1)-H*X(I,J)))
      PART2=ABS((Y(I,J)/H-X(I+1,J))/(Y(I,J)/H-X(I,J)))
      NOT=ALOG(PART1)*ALOG(PART2)
      SUM=SUM+ABS(NOT)
   33 CONTINUE
   44 CONTINUE
C
C**** CALCULATE AVERAGE GAS AND LIQUID COMPOSITIONS AT
C**** THE TOP OF THE COLUMN.
C
      YOUT=(Y(1,4)+Y(2,4)+Y(3,4))/3.0
      XAVG=(X(1,1)+X(1,2)+X(1,3))/3.0
      WG1=WGC+WGB
      WGB=XX*WG1
      YAVG=(WGC*YOUT+WGB*YAVG)/(WGC+WGB)
C
C**** OUTPUT AVERAGE LIQUID AND GAS COMPOSITIONS AT THE TOP OF THE COLUMN
C**** AS WELL AS THE NUMBER OF TRANSFER UNITS AND THE VOLUME OF TRANSFER UNITS.
C
      SUMNT=SUMNT+SUM
      ICOUNT=ICOUNT+1
      IF(ICOUNT.LT.6) GO TO 1
      DIFFN=100.0*ABS(NOTEXP-SUMNT)/NOTEXP
      DIFF=100.0*ABS(YAVG-YEXIT)/YAVG
      VCOL=6.0*V
      VTU=VCOL/SQRT(SUMNT)
      VTUEXP=VCOL/SQRT(NOTEXP)
      DIFFV=100.0*ABS(VTU-VTUEXP)/VTU
      WRITE(6,88)XAVG,YAVG,YEXIT,DIFF,NOTEXP,SUMNT,DIFFN,
     1VTUEXP,VTU,DIFFV
   88 FORMAT(////,10X,*ENTRANCE LIQUID COMPOSITION =*,F10.6,
     1//,10X,*EXIT GAS COMPOSITION =*,F10.6,
     2//,10X,*EXP. VALUE OF EXIT GAS COMPOSITION =*,F10.6,
     3//,10X,*% DEVIATION =*,F10.4,
     4////,10X,*" NOT " CAL. FROM EXPERIMENTAL DATA =*,F10.6,
     5//,10X,*" NOT " CAL. FROM NUMERICAL SOLUTION =*,F10.6,
     6//,10X,*% DEVIATION =*,F10.4,
     7////,10X,*" VTU " CAL. FROM EXPERIMENTAL DATA =*,F10.6,
     8//,10X,*" VTU " CAL. FROM NUMERICAL SOLUTION =*,F10.6,
     9//,10X,*% DEVIATION =*,F10.4///)
      STOP
      END
```

```
      PROGRAM FIT(INPUT,OUTPUT,TAPE5=INPUT,TAPE6=OUTPUT,TAPE1)
C
C**** THIS PROGRAM READS IN A SET OF DATA POINTS AND BY
C**** THE METHOD OF "LEAST SQUARE" FOR NON-LINEAR EQUATIONS,
C**** IT WOULD CALCULATE THE BEST VALUES OF THE COEFFICIENTS
C**** TO MINIMIZE THE VARIANCE.
C
      DIMENSION AA(10),BA(10),CA(10),SA(10)
      COMMON /C/N,RN,XL(10),X(10),Y(10),A,B,S
      READ(1,100) N
  100 FORMAT(I1)
      READ(1,101)(X(I),I=1,N)
      READ(1,101)(Y(I),I=1,N)
  101 FORMAT(3F8.2)
      RN=N
      DO 1 I=1,N
    1 XL(I)=ALOG(X(I))
      WRITE(6,102)
  102 FORMAT(//4X,"N",13X,"X(N)",16X,"Y(N)"/)
      DO 2 I=1,N
    2 WRITE(6,103) I,X(I),Y(I)
  103 FORMAT(4X,I1,2(10X,F10.5))
    3 PRINT*,"ENTER INITIAL C VALUE"
      READ*,CI
      PRINT*,"ENTER C INTERVAL"
      READ*,CINT
      C=CI
      NP=10
      DO 5 I=1,NP
      CALL SSQI(C)
      AA(I)=A
      BA(I)=B
      CA(I)=C
      SA(I)=S
      C=C+CINT
    5 CONTINUE
      CALL PRINT(AA,BA,CA,SA,NP)
      PRINT*,"TO CONTINUE, TYPE 1; OTHERWISE, 0"
      READ*,NTEST
      IF(NTEST.EQ.0) STOP
      GO TO 3
      END
C
C**** THIS SUBROUTINE PRINTS OUT THE OUTPUT
C
      SUBROUTINE PRINT(A,B,C,S,N)
      DIMENSION A(N),B(N),C(N),S(N)
      WRITE(6,105)
  105 FORMAT(3X,"N",6X,"A",9X,"B",9X,"C",9X,"S"/)
      DO 9 I=1,N
    9 WRITE(6,109) I,A(I),B(I),C(I),S(I)
  109 FORMAT(2X,I2,1X,4(F11.4))
      RETURN
      END
```

```
C
C**** THIS SUBROUTINE TAKES IN A GIVEN VALUE OF C IN THE EQUATION
C**** Y=A*X**B+C AND ESTIMATES THE BEST VALUE OF A AND B BY THE
C**** METHOD OF LEAST SQUARES
C
      SUBROUTINE SSQI(B1)
      DIMENSION YT(10),YNL(10)
      COMMON /C/N,RN,XL(10),X(10),Y(10),B2,EX,S
      SXY=0.0
      SX2=0.0
      SY=0.0
      SX=0.0
      DO 11 K=1,N
      YT(K)=Y(K)+B1
      YNL(K)=ALOG(YT(K))
      SY=SY+YNL(K)
      SX=SX+XL(K)
      SX2=SX2+XL(K)*XL(K)
   11 SXY=SXY+XL(K)*YNL(K)
      B2L=(SXY-SX2*SY/SX)/(SX-RN*SX2/SX)
      EXZ=(SY-RN*B2L)/SX
      B2Z=EXP(B2L)
      SZ=0.0
      DO 12 K=1,N
   12 SZ=SZ+(YT(K)-B2Z*X(K)**EXZ)**2
   13 T1=0.0
      T2=0.0
      T3=0.0
      T4=0.0
      T5=0.0
      DO 14 K=1,N
      X1=X(K)**EXZ
      X2=X1=X1
      X3=X1*XL(K)
      T1=T1+X3*YT(K)
      T2=T2+X2*XL(K)
      T3=T3+X1*YT(K)
      T4=T4+X2
   14 T5=T5+X3*X3
      BEZ=(T1-T2*T3/T4)/(B2Z*(T2*T2/T4+T5))
      ALZ=T3/T4-B2Z*(1.0-BEZ*T2/T4)
      B21=B2Z+ALZ
      EX1=EXZ+BEZ
      S1=0.0
      DO 15 K=1,N
   15 S1=S1+(YT(K)-B21*X(K)**EX1)**2
      C=ABS((SZ-S1)/S1)
      IF(C.LE.0.01) GO TO 16
      B2Z=B21
      EXZ=EX1
      SZ=S1
      GO TO 13
   16 EX=EX1
      B2=B21
      S=S1
      RETURN
      END
```